RIKAGAKU KENKYUSHO
the Institute of Physical and Chemical Research
Wako-shi, Saitama Pref., JAPAN

'75

IPCR cyclotron Progress Report 1975

Vol. 9

IPCR Cyclotron Progress Report

Vol. 9

The Institute of Physical and Chemical Research
"RIKAGAKU KENKYUSHO" Wako-shi, Saitama, 351 JAPAN
December, 1975

This volume contains recent information of the IPCR Cyclotron, informal reports and abstracts of papers which will be published at scientific meetings or in publications by staff members, guests, and visitors.

CONTENTS

1. INTRODUCTION

The operation of our cyclotron was satisfactorily smooth as before in last year. Several improvements have been made in the machine and its accessory facilities.

A number of experimental studies of nuclear reactions and level structures was continued from previous years. An on-line Bragg crystal spectrometer was installed to study heavy-ion excited X-rays with high energy resolution. Channeling experiments were commenced with high energy alpha particles. Mössbauer studies were made on magnetic oxides and sulfides and also on defective atoms in solid produced by nuclear reactions. Emission spectra of alkali halides were measured under low temperature heavy-ion irradiation to obtain information on initial species produced. Effects of heavy ions on the DNA synthesis in bacterial cells have been investigated, together with the production of radioisotopes and labeled compounds for the medical use.

The first resonator of the heavy-ion linear accelerator is under construction and scheduled to be installed next autumn. The foundation work for the accelerator building will be started at the end of this year and the building is expected to be completed in early autumn next year.

H. Hagihara

Hitosi Hagihara, Chairman
The Cyclotron Board

2. MACHINE OPERATION

K. Ogiwara, S. Fujita, H. Nakajima, K. Ikegami
T. Kageyama, S. Kohara, H. Takebe, and I. Kohno

The cyclotron was operated on the 24h-per-day basis during the period from Oct. 23 1974 to Oct. 22, 1975. Statistics of machine operation time is shown in Table 1. The total working time of 3853h is lower by about 12 % (520h) compared with last year. This decrease in working time is due to the increase of holidays and of the maintenance days of accelerator.

Table 2 shows beam time allotted to various activities in this period. The cyclotron was operated for 124 days with heavy ions because of increasing request for those ions. In addition, $^{11}B^{3+}$ ions were accelerated at 70 MeV for 2 days. Total percentage of the request for heavy ions exceeded 50 % and the machine time for solid state physics increased more than twice.

Serious troubles occurred in this period as follows. The insulation of loading lines of circular trimming coils was broken by R-F leakage, and the circuits of those coils were shorted.

An induction motor of the circulation pump for deionized cooling water was also broken. These troubles brought about a loss of time of about a month.

Facilities for magnet power supply to the beam handling system were moved to an air-conditioned room to prevent hazard due to dust.

Table 1. Machine operation.

Date	Oscillator	Ion source	Beam
Oct. 23, 1974	37715 (h)	40591 (h)	11025 (h)
Oct. 22, 1975	42088.3 (h)	45174.3 (h)	14878.2 (h)
365 days	4373 (h)	4583 (h)	3853 (h)
Percentage of 365 days	50 %	52 %	44 %

Schedule in this period

Beam time	242 (days)
Overhaul and installation work	46 (days)
Periodical inspection and repair	28 (days)
Vacation and holidays	49 (days)

Table 2. Scheduled beam time and subjects of activity in the period VIII.

Subject		Heavy ion	Light particles	Total
Nucl. phys.	Nuclear reaction	1980 (h)	826 (h)	2806 (h)
	In-beam spectroscopy	312	142	454 (h)
	RI production	0	312	312 (h)
Fields other than nucl. phys.	Nuclear chemistry	0	334	334 (h)
	Radiation chemistry	155	22	177 (h)
	Radiation biology	204	66	270 (h)
	Solid state physics	0	463	463 (h)
	Inner atomic shell excitation study	48	15	63 (h)
Outside users	Nuclear medicine	0	102	102
	Nuclear fuel study	0	156	156
	RI production	0	43	43
Development of instruments		7	10	17
Total		2706 (h)	2491 (h)	5197 (h)
Percent in total		52.1 (%)	47.9 (%)	100 (%)

Maintenance operation and engineering	
Exchange of ion sources	68 (h)
Reserved for beam time adjustment and cooling of radiation	435 (h)
Machine inspection and repair	672 (h)
Total	1175 (h)

3. MACHINE DEVELOPMENT AND ACCELERATOR PHYSICS

3-1. Polarized Ion Source for the INS Cyclotron

S. Motonaga, T. Fujisawa, M. Hemmi, and I. Takeshita

The IPCR polarized ion source of a ground-state atomic beam type was successfully operated

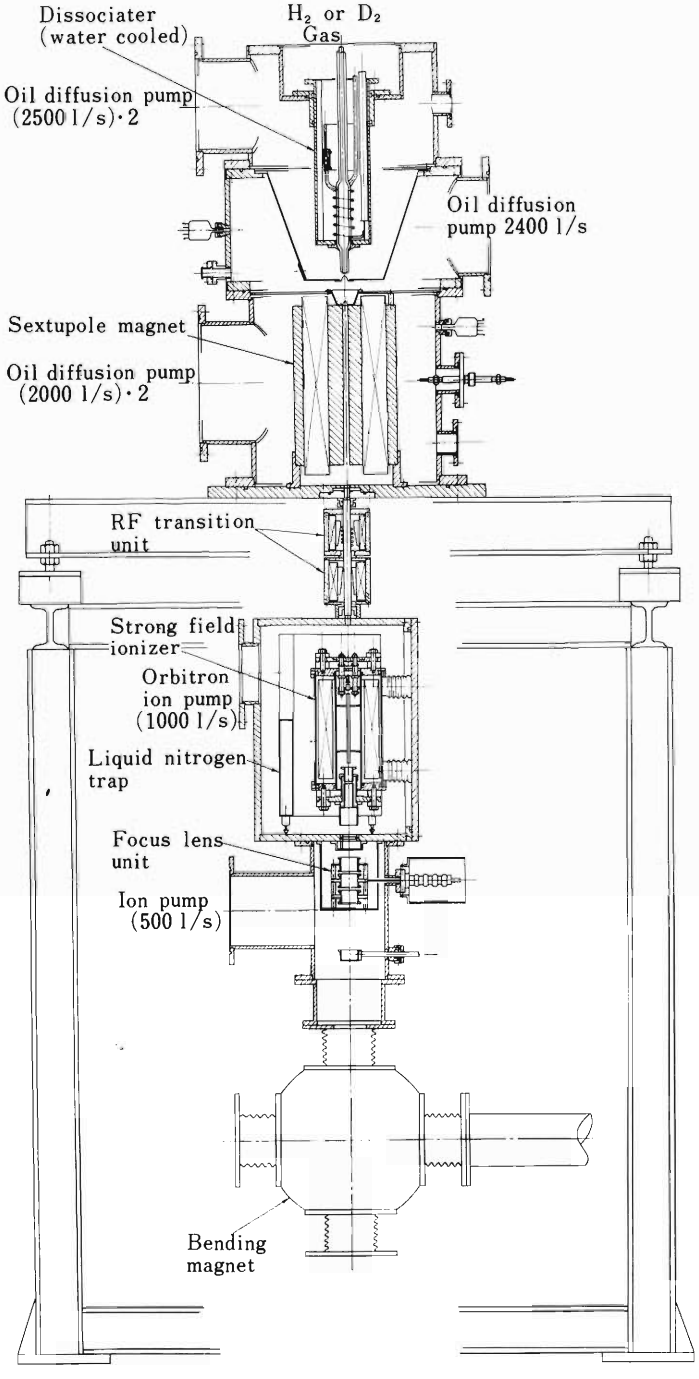

Fig. 1. Schematic view of the polarized ion source for INS cyclotron.

in 1974.[1] Since that time, a number of components of the ion source have been rebuilt for installation in the S-F cyclotron of the Institute for Nuclear Study of Tokyo University.

In order to increase the ion beam intensity and the polarization value, several modifications were made in chamber design, power supply and vacuum system to make dissociation at high pressure of 2 Torr. The ionizer was provided with 20 kV positive potential to the ground. A particular attention was paid to achieve high vacuum in the ionization vacuum chamber. A schematic view of the polarized ion source is shown in Fig. 1, illustrating the major components of the ion source.

The apparatus is now being in test operation and is to be installed in the cyclotron in the spring of 1976.

Reference

1) S. Motonaga, T. Fujisawa, M. Hemmi, H. Takebe, K. Ikegami, and Y. Yamazaki: IPCR Cyclotron Progr. Rep., 8, 84 (1974); S. Motonaga and T. Fujisawa: Proc. 4th Int. Symp. Polarization Phenomena, Zürich, D－1 (1975)

3-2. Improvement of the Central Region Geometry in the Cyclotron

K. Ogiwara, H. Takebe, K. Ikegami, T. Kageyama,
S. Kohara, S. Fujita, and H. Nakajima

Figure 1 shows the performance record of last year. Requirements of heavy ion beam have been increasing year by year, and the cyclotron was operated for about 2700 h with heavy ion source in last year. There was a difficulty to keep the dee voltage stable in the heavy ion accelerations. In August, 1975, the central region was modified as shown in Fig. 2, to increase the transit angle of the first half turn in the west dee so that vertical electrical focusing force becomes to add to that of the magnetic field. The west wing was extended along the path of ions and the east wing was shaped flat as shown in the figure. It was conjectured that this instability came from the following reason: a part of the first turn beam run into the east wing because the axial magnetic focusing force is weaker than the electric defocusing force at the central region. Many electrons were emitted from the east wing by collision of these ions. These electrons were accelerated by r-f field along the line of magnetic field and bombarded the stems of the ion source. This collision eroded the ion source stems. Moreover, spark discharge

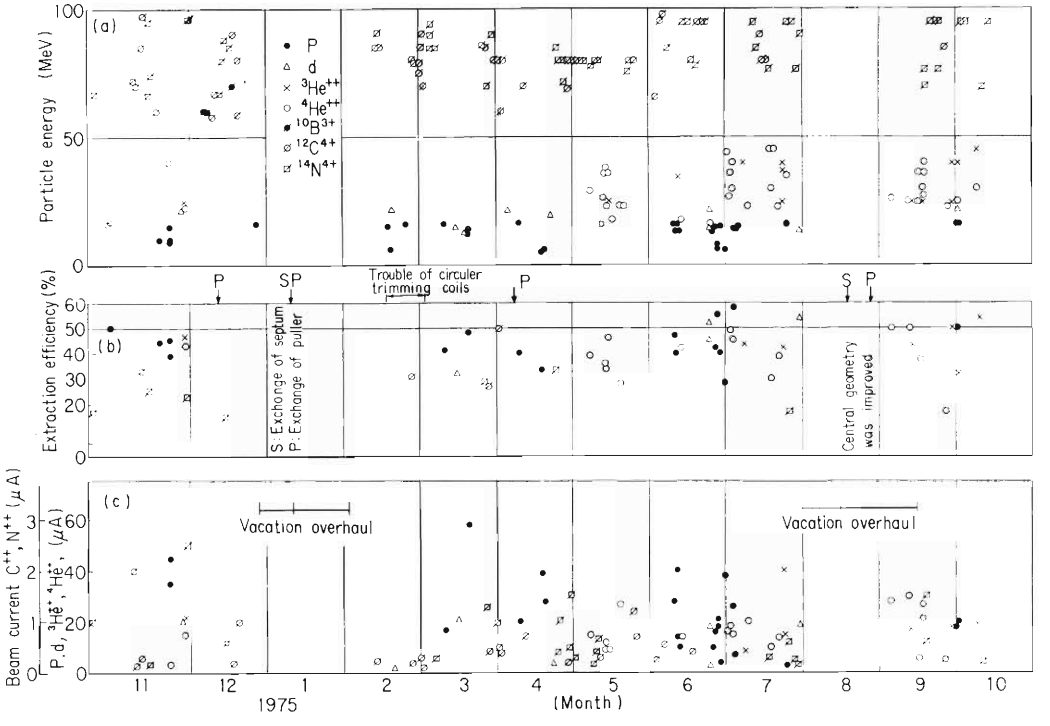

Fig. 1 Operation record of the cyclotron. Arrows represent the repair of septum entrance and puller.
(a) Particle energies used.
(b) Beam extraction efficiency.
(c) Extracted beam currents were actually employed in experiments.

occurred at the central region between the dee and earth plate. To maintain same effective energy gain for the first turn beam, the distance between the west and east wings was not changed. Erosion of the ion source stems is now decreasing. Other effects of this improvement will appear in the near future.

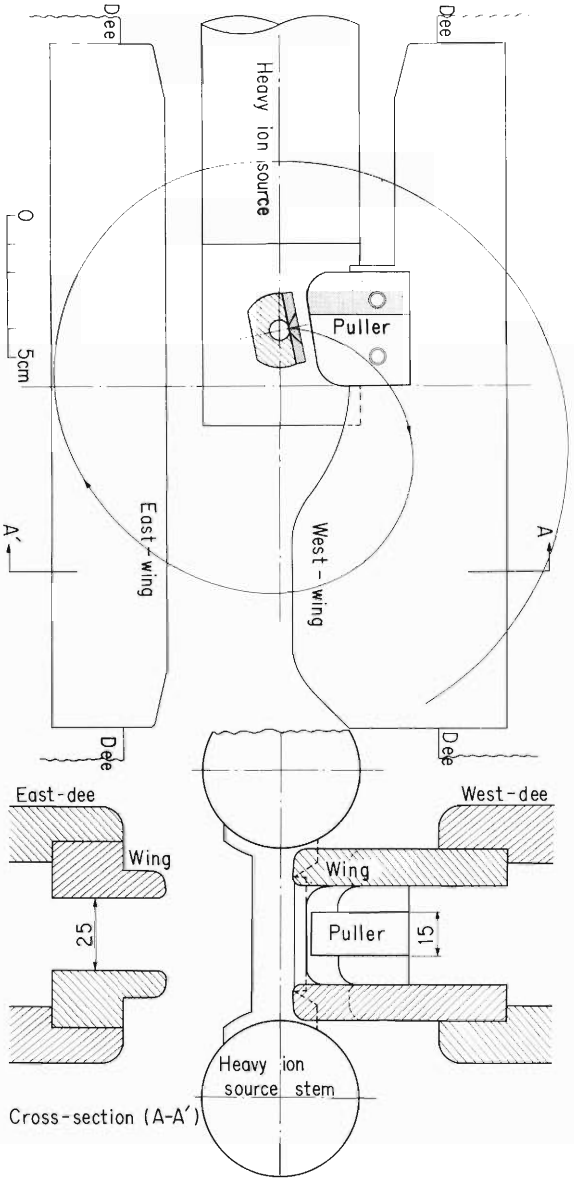

Fig. 2. Schematic drawing of the improved central region geometry.

3-3. Improvement of Power Supply for the Beam Handling System

H. Nakajima, S. Kohara, and K. Ikegami

The beam handling system of the cyclotron consists of four analyzing and/or deflecting magnets and fifteen pairs of quadrupole magnets. In order to combine suitably the ten pairs of stabilized power supplies with the fifteen pairs of quadrupole magnets we prepared a power supply distributor, the design of which was reported previously.[1] This year we have installed the distributor in an air-conditioned room to prevent the distributor from dust. Figures 1 and 2 show the front view of the handling board for the distributor and its main body. We have also moved all power supplies for beam handling magnets from the power supply room to the air-conditioned room mentioned above.

Following improvements of power supply have been made when it was brought into installation.

For power supply of quadrupole magnets, phase control circuits of SCR (silicon controlled rectifier) were improved and the voltage of interlock system of cooling water was lowered from 200 V to 12 V. For power supply of the deflecting magnets except SW II (see Ref. 1), a main control system was replaced by a new circuit system which consisted of large-sized transistors and operational amplifiers. Figure 3 shows the new rack-mounted control system.

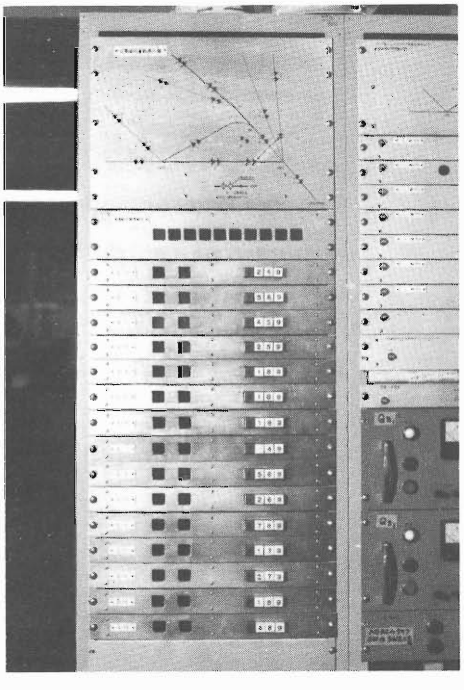

Fig. 1. The handling board for the power supply distributor of quadrupole magnets.

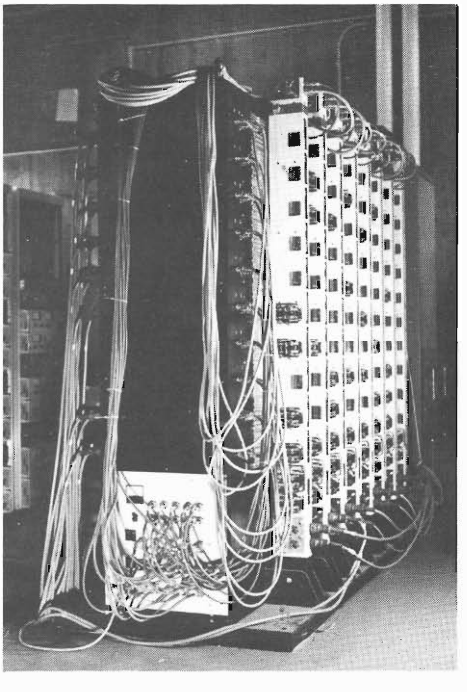

Fig. 2. The main body of power supply distributor of quadrupole magnets.

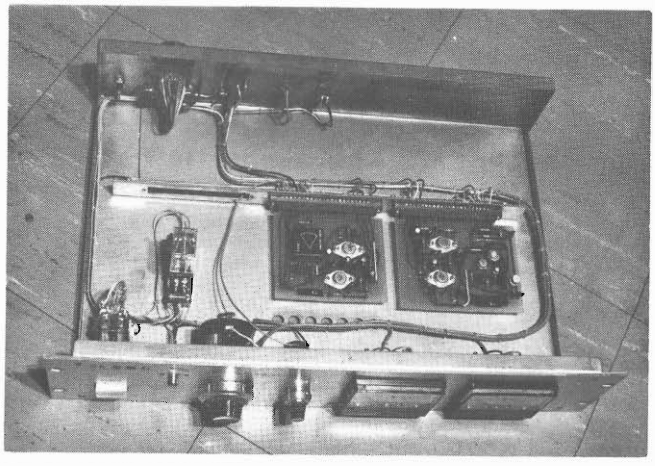

Fig. 3. The new rack-mounted control system.

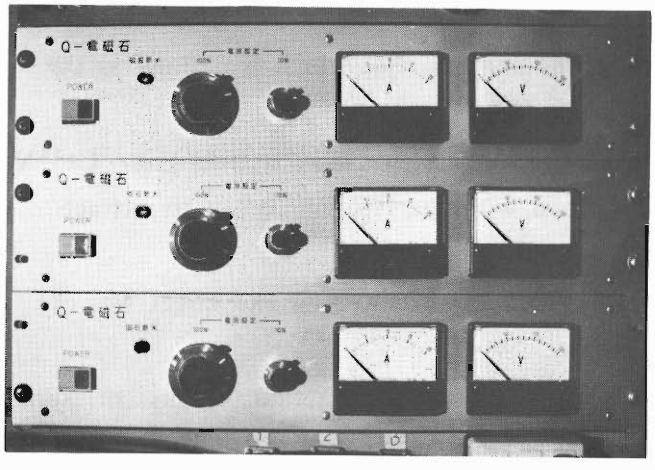

Fig. 4. The controller of power supply for a quadrupole magnet. (installed in the control room)

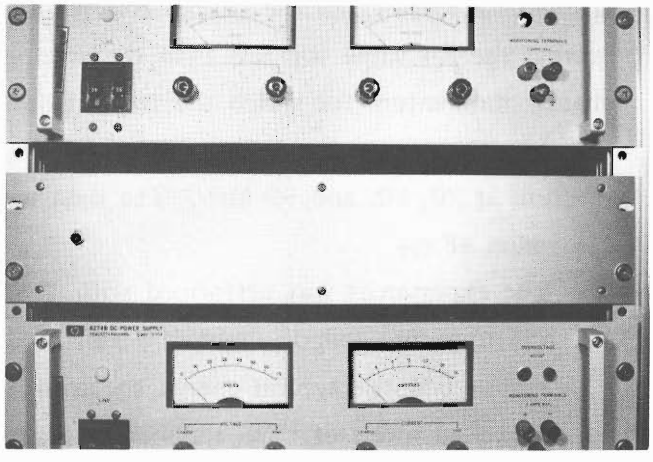

Fig. 5. The auxiliary controller of power supply for a quadrupole magnet. (installed in the power supply room)

All control cables for magnet power supply were replaced with new cables.

Among the stabilized power supplies of quadrupole magnets, three pairs were replaced with those of Hewlett Packard 62 – 74B type and for the DS magnet two series-connected power supplies of Hewlett Packard 62 – 69B type were prepared to obtain stabilized small or medium current. New controllers were attached to these new power supplies. Figures 4 and 5 are photographs of these controllers.

Reference

1) H. Nakajima and M. Hemmi: IPCR Cyclotron Progr. Rep., 5, 19 (1971).

4. NUCLEAR PHYSICS

Scattering and Reactions

4-1. Critical Angular Momentum in $^{12}C + ^{14}N$ Compound Reaction

T. Ooi, T. Motobayashi, I. Kohno, M. Ishihara,
T. Numao, T. Fukuda, and S. M. Lee

According to the studies of $^{12}C(^{14}N,^{6}Li)^{20}Ne$ reaction of Saclay group[1] and Oxford group,[2] the compound nucleus formation is the main process in this reaction at energies between 20 and 76 MeV, and the critical angular momenta (ℓ_{cr}) in the compound formation have been derived from Hauser-Feshbach (HF) analysis of individual level cross sections in the relevant outgoing channel. According to the studies referred to above, it was revealed that at a large incident energy, the ℓ_{cr} value was less than the grazing angular momentum, ℓ_{gr}, which is defined as the angular momentum for which the transmission coefficient is 0.5.

In order to see the behavior of ℓ_{cr} at higher incident energies, we have studied the $^{12}C+^{14}N$ reaction at 70, 80, and 90 MeV. The data were compared with the HF calculation to extract the values of ℓ_{cr}.

The experiment was performed with $^{14}N^{4+}$ beams from the cyclotron. The target was of ^{12}C self-supported foil of about 100 $\mu g/cm^2$ in thickness.

Figure 1 shows typical energy spectrum for the $^{12}C(^{14}N, ^{6}Li)^{20}Ne$ reaction. Peaks corresponding to excited levels of ^{20}Ne are seen evidently. The energy resolution was 350–500 keV at FWHM.

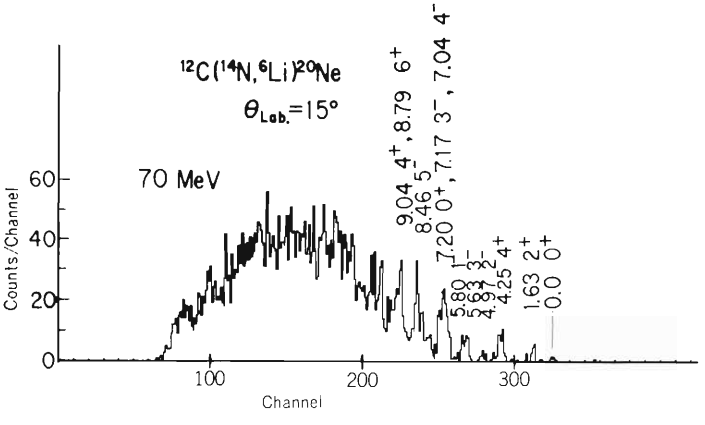

Fig. 1.
^{6}Li energy spectra from the $^{12}C(^{14}N, ^{6}Li)^{20}Ne$ reactions at incident energies of 70, 80, and 90 MeV and 14.7 in the laboratory system.

Excitation functions for some ^{20}Ne levels measured at 14.7° and 10.4° are presented in Fig. 2. Solid curves indicate the HF calculation with ℓ_{cr} values which were chosen to give the best fit to the experimental data. The ℓ_{cr} values are listed in Table 1. Dashed curves are with $\ell_{cr}+1\hbar$. Open circles show data of Saclay group and closed ones are ours. The triangular points are data of Oxford group at 76 MeV. From the present analysis we obtained the ℓ_{cr} values of 17, 18, and 19$\hbar$ at E_{lab} = 70, 80, and 90 MeV, respectively. These ℓ_{cr} values are smaller than

Table 1. ℓ_{gr} and ℓ_{cr} values obtained from experimental data.

Incident energy (MeV)	$\ell_{gr}(\hbar)$	$\ell_{cr}(\hbar)$
20	7	
25	9	
30	11	(11)
35	13	12
40	14	12
45	15	13
50	17	14
52	17	14
55	18	15
60	19	16
70	21	17
80	22	18
90	23	19

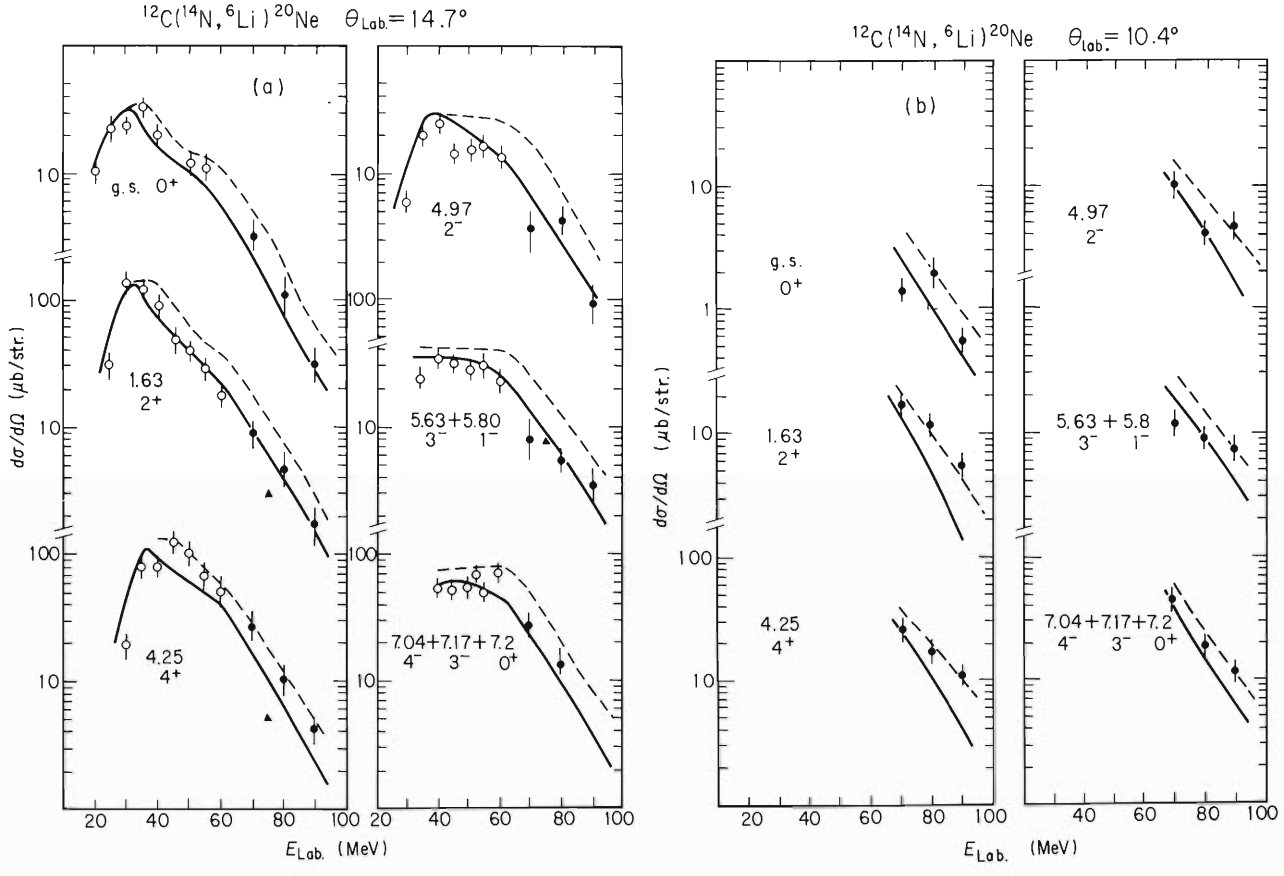

Fig. 2. Excitation functions for some ^{20}Ne states measured at 14.7° and 10.4° in the laboratory system for the $^{12}C(^{14}N, ^{6}Li)^{20}Ne$ reaction.

ℓ_{gr} by 3 or 4ħ.

It can be seen that considerably good fits to the data for all the outgoing channels in the $^{12}C(^{14}N, ^{6}Li)^{20}Ne$ reaction are obtained. This is taken to be a proof of the dominance of the compound process even at these high energies.

Fusion cross section σ_{fus} versus $1/E_{CM}$ plot is shown in Fig. 3. The fusion cross section for $^{14}N+^{12}C$ system at each incident energy has been calculated from the ℓ_{cr} value obtained above. Two straight lines are fitted to the data with the help of Glass and Mosel's formulation:[3]

for large energies: $\sigma_{fus} = \pi R_{cr}^2(1-V_{cr}/E_{CM})$, $\ell_{cr}<\ell_{gr}$,

for small energies: $\sigma_{fus} = \pi R_B^2(1-V_B/E_{CM})$, $\ell_{cr}=\ell_{gr}$.

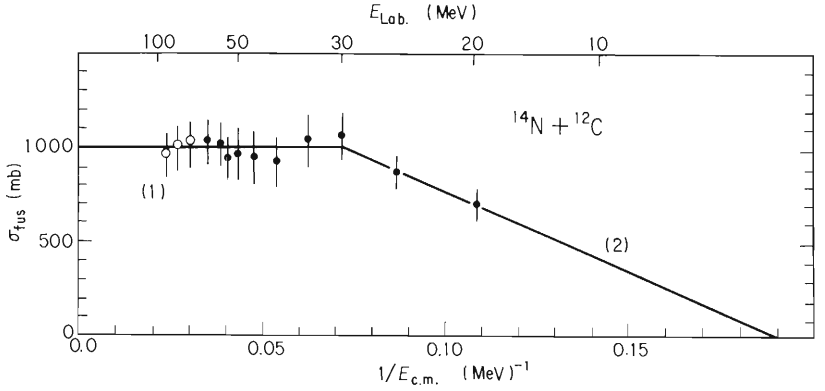

(1) $\sigma_{fus} = \pi R_{cr}^2\left(1-\frac{V_{cr}}{E_{CM}}\right) \approx 1$ barn
$V_{cr} = 0$ $R_{cr} = 5.64$ fm
$r_{cr} = 1.20 \pm 0.06$ fm

(2) $\sigma_{fus} = \pi R_B^2\left(1-\frac{V_B}{E_{CM}}\right)$
$V_B = 5.26$ MeV
$r_B = 1.53$ fm

Fig. 3. Plot of fusion cross for sections σ_{fus} vs. $1/E_{CM}$ $^{12}C + ^{14}N$ reactions.

The line (1) implies

$$\ell_{cr}<\ell_{gr}\ ,\quad \sigma_{fus}<\sigma_{total\ reaction}\ ,$$

and the line (2)

$$\ell_{cr} = \ell_{gr}\ ,\quad \sigma_{fus} = \sigma_{total\ reaction}$$

From the line (1) we obtained $r_{cr} = 1.20 \pm 0.06$ fm, in terms of which the critical distance should be expressed like $R_{cr} = r_{cr}(A_1^{1/3}+A_2^{1/3})$. This r_{cr} value is greater than $r_{cr} = 1.00 \pm 0.07$ determined by Lefort et al.[4] from heavy ion reactions with larger mass systems.

References

1) C. Volant, M. Conjeaud, S. Harar, S. M. Lee, A. Lepine, and E. F. Da Silveira: Nucl. Phys., A238, 120 (1975).
2) T. A. Belote, N. Anyas-Weiss, J. A. Becker, J. C. Cornell, P. S. Fischer, P. N. Hudson, A. Menchaca-Rocha, A. D. Panagistou, and D. K. Scott: Phys. Rev. Lett., 304, 450 (1973).
3) D. Glass and U. Mosel: Nucl. Phys., A237, 429 (1975).
4) M. Lefort: Proc. Int. Conf. on Classical and Quantum Mechanical Aspects of Heavy Ion Collisions, Heidelberg, p. 274 (1974).

4-2. Multiplicity of γ-Rays in Multi-Nucleon Transfer Reactions

T. Numao, M. Ishihara, T. Inamura, and T. Fukuda

It has been shown that the multiplicity of γ-rays, which means an average number of emitted γ-rays in a reaction, gives a good measure of the angular momentum involved in the initial excited states[1),2)] In the present article, this idea was applied to the multi-nucleon transfer reactions induced by heavy ions to study the reaction mechanism through the measurement of transferred angular momentum to the residual nuclei. The multiplicity of γ-rays, M, was deduced from the relation $I_C/I_S = 1-(1-\Omega)^M$, where Ω is the efficiency of γ-ray detector, I_S yields of outgoing particles in singles, and I_C those in coincidence with γ-rays.

The detection system for particles was a counter telescope consisting of 30 μm and 2000 μm Si detectors. A 3" X 3" NaI counter with a 4.5 mm-thick Cu absorber was used for the γ-ray detection and placed at 7 cm from the target. The average efficiency of this system was found to be 2.1 % indicating an accuracy within 10 % in the energy region from 0.2 to 2 MeV. In the coincidence measurement, γ-ray energy, particle identification, and particle energy signals were recorded event-by-event on a disk or a magnetic tape using an on-line computer. To correct the chance coincidence events, the timing spectrum between γ-rays and particles was observed during the coincidence measurement. Contributions from neutrons emitted in the reactions were also observed by putting a 5 cm-thick Pb absorber between the target and the NaI detector and were estimated to be less than 10 %. To see the angular correlation effect of γ-rays, we placed the NaI counter at 30° and 90° in the reaction plane and at the position perpendicular to the reaction plane, and found that the effect was negligibly small if the detector was set at 90° in the reaction plane.

The multiplicities of γ-rays were measured in this way for various particles emitted in the $^{14}N+^{96}Mo$ and $^{14}N+^{181}Ta$ reactions. Figure 1 shows the multiplicity M around the energy of the optimum Q-value versus the number of transferred nucleons, ΔA, observed in the $^{14}N+^{96}Mo$ reaction at $\theta = 30°$ and $E_N = 95$ MeV. The dashed line corresponds to a simple relation $2M = \Delta L = \Delta A \cdot V_{in} \cdot R$,[3)] where V_{in} is defined as $V_{in} = \sqrt{2(E_{in}-E_C)/M_{in}}$ with the incident energy, E_{in}, the Coulomb barrier, E_C, and the incident mass, M_{in}, and R is the sum of two nuclear radii. For small ΔA the observed multiplicity is in good agreement with this prediction, but it differs considerably from the one expected for large ΔA. Figure 2 shows the multiplicity obtained from the $^{14}N + ^{181}Ta$ reaction at $\theta = 50°$ and $E_N = 95$ MeV. A similar character appears in this case, too. Such an attenuation of the multiplicity can be understood as follows: In case of large ΔA, two or more particles are emitted simultaneously or successively, and they also take out large angular momenta.

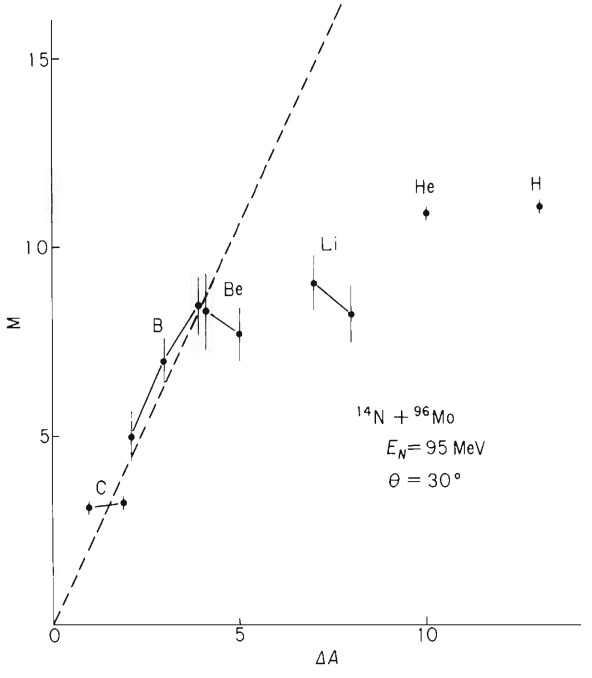

Fig. 1. Multiplicity of γ-rays vs. the number of transferred nucleons observed in the $^{14}N + ^{96}Mo$ reaction.

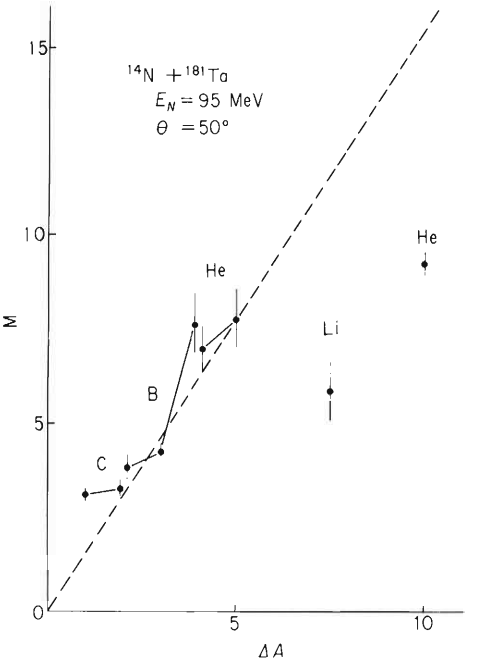

Fig. 2. Multiplicity of γ-rays vs. the number of transferred nucleons observed in the $^{14}N + ^{181}Ta$ reaction.

References

1) P. O. Tjm, F. S. Stephens, R. M. Diamond, J. de Boer, and W. E. Meyerhof: Phys. Rev. Lett., 33, 593 (1974).

2) G. B. Hagemann, R. Broda, B. Herskind, M. Ishihara, and S. Ogaza: Nucl. Phys., A245, 166 (1975).

3) D. M. Brink: Phys. Lett., 40B, 37 (1972).

4-3. Fusion Cross Section Measurement by Beam Attenuation Method

T. Fukuda, M. Ishihara, T. Inamura,
T. Numao, and T. Nomura

In heavy-ion induced reactions, it is important to determine what amount of fraction of the total reaction cross section is attributed to the complete fusion cross section σ_{CF}, since this information may be useful to understand the dynamical properties of reaction mechanism. Although there have been accumulated data of σ_{CF}, the accuracy of the results is rather poor. Moreover, the systematic measurement of σ_{CF} is often limited for the conventional methods used so far. In this note, we report on a new apparatus of the σ_{CF} measurement which has been developed to overcome those defects mentioned above.

A schematic drawing of the set-up is shown in Fig. 1. The collimated beam of heavy ions of reduced intensity (10^5 particles per sec) was introduced into the apparatus and further refined by an entrance slit system of Ta. The incoming particle was identified by the coincident event between two thin detectors C1 and C2. The particles scattered by the detector C2 were rejected by a veto signal coming from a large pulse which was generated by the thick detector CS2 surrounding the C2 detector at the center. The number of outcoming particle was determined by counting the coincident event between the incoming particle and the detector C3. The stopping counter C3 placed behind the target position spanned a large solid angle of forward direction and was designed to detect the unaffected projectile particles through the target as well as the whole charged particles of reaction products, except for fission fragments and heavy recoil fragments due to direct and compound reactions.

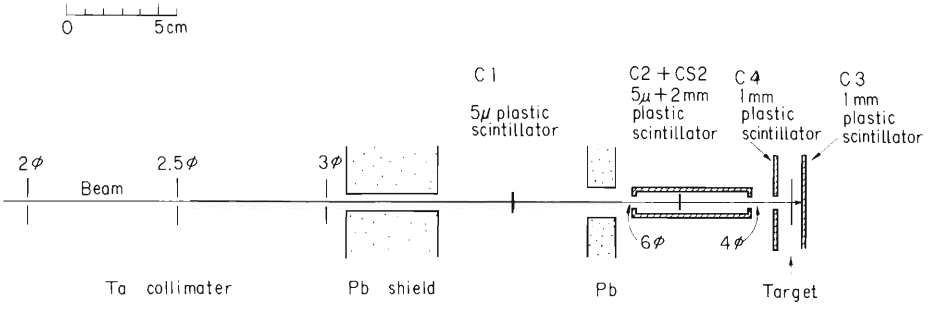

Fig. 1. The schematic experimental set-up. C1, C2, CS2, C3, and C4 are plastic counters.

The numbers of in- and out-coming particles were measured for the cases with the target put on and off the location (these numbers are hereafter denoted as n_{in}, n_{out} and N_{in}, N_{out} for off-and on-target measurements, respectively).

The accuracy of the data from this method is mainly decided by the magnitude of the

difference $n_{in'} - n_{out}$ for the off-target measurement, which has so far been reduced down to 10^{-6} part of n_{in}.

The double difference,

$$\Delta N = (N_{in} - N_{out}) - (n_{in} - n_{out}),$$

gives essentially the total fusion cross section, since the difference corresponds to the cross section of the complete fusion which decays by emission of neutrons alone or by fission process. When the cross section of charged particle emission is appreciable for the fusion reaction, ΔN should be corrected for this process, which is to be measured by the detector C4 placed backward to the target.

Table 1 gives a preliminary result on the $^{14}N(E_{c.m.} = 108$ MeV) + ^{181}Ta reaction. We have also measured the fusion cross section for the $^{14}N(E_{Lab.} = 95, 110, 122$ MeV) + ^{93}Nb and ^{96}Mo reactions, and analysis is now in progress.

Table 1. The target thickness was 2.50 mg/cm^2.
ℓ_{cr} is determined from the relation $\sigma_{CF} = \pi\lambda\!\!\!^{-2}(\ell_{cr} + 1)^2$.
σ_{tot} is the total reaction cross section evaluated for the optical potential.

$(n_{in} - n_{out})/n_{in}$	0.143×10^{-5}
$(N_{in} - N_{out})/N_{in}$	0.934×10^{-5}
σ_{CF}	1040 mb
ℓ_{cr}	46 $\hbar$
σ_{CF}/σ_{tot}	0.57

4-4. Statistical Analysis of Multinucleon Transfer Reactions by Heavy Ions

H. Kamitsubo

A simple relation was found to hold between the most probable Q-value, Q, and the number of transferred nucleons, n, in the heavy ion reactions.[1] In order to explain this relation, a statistical approach was applied to analyze the energy spectra of reaction products. It is assumed that the reaction is induced mainly in a narrow region of nuclear surface so that a very few partial waves in both entrance and exit channels contribute to the reaction. It is also assumed that only the heavier product is highly excited by the reaction and a large part of the transferred angular momentum remains on it. The energy dissipated during the collision is converted into the internal and rotational excitation of the residual system.

The internal excitation energy is given by

$$U = E_i - E_f + Q_{gg} - \Delta(N,P) - E_{rot}.$$

Here E_i and E_f are c.m. energies of the system before and after the reaction, respectively, Q_{gg} is the Q-value of the ground state transition, and $\Delta(N, P)$ is the pairing energy correction for nucleon transfer. The rotational energy, E_{rot}, is a function of the transferred angular momentum L and is written as

$$E_{rot} = \hbar^2 L(L+1)/(2J),$$

J being the moment of inertia of the excited nucleus. The level density of the final system, W_f, is a function of U and by introducing a level density parameter a and a nuclear temperature t, it is written as

$$W_f(U) = \frac{1}{B}\frac{\exp(2\sqrt{aU})}{a^{3/2}\ t^3},\quad U = t^2 - 3t/2.$$

The cross section is proportional to this level density. Then, putting $\partial W_f/\partial E_f = 0$, the most probable Q-value can be calculated as shown in ref. 2. Provided that the only one partial wave contributes to the reaction in the entrance and exit channels, Q_m can be expressed by

$$Q_m = \left(\frac{\mu_i R_i^2 \mu_f R_f^2}{(J+\mu_f R_f^2)^2} - 1\right)(E_i - V_i) - \Delta V_c,$$

$$\Delta V_c = V_i - V_f,$$

where μ and R are the reduced mass and the grazing distance of the system, respectively, and V is the Coulomb barrier. The suffices i and f are used to indicate the initial and final systems, respectively. The moments of inertia can be determined by comparing the calculated values of Q_m with the experimental ones. In Fig. 1 the ratios of the moments of inertia, J_m, to that of the rigid body are shown as a function of n. In case of a few nucleon transfer, J_m is as small as one fifth of J_{rig} and this implies that only a small number of nucleons in the residual nucleus rotates collectively around the core and the moment of inertia of the system is small.

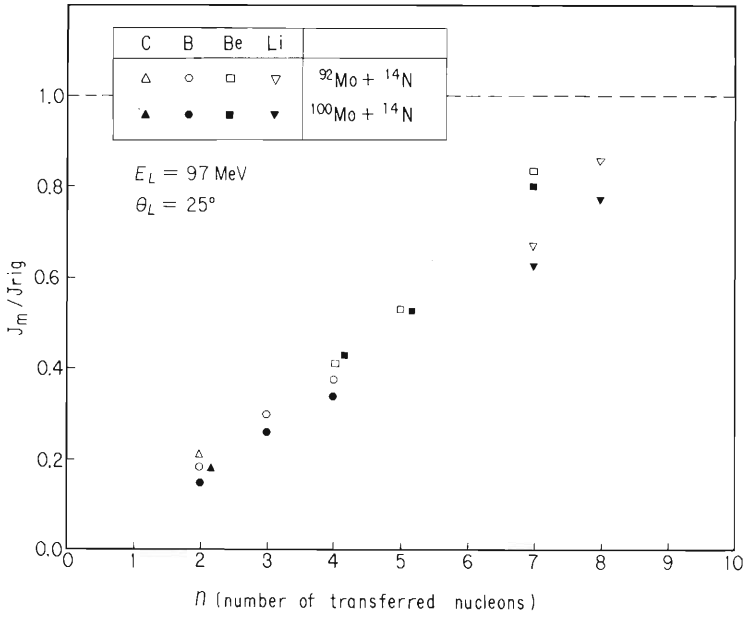

Fig. 1. The ratios of the moment of inertia determined by the present method to the rigid body value.

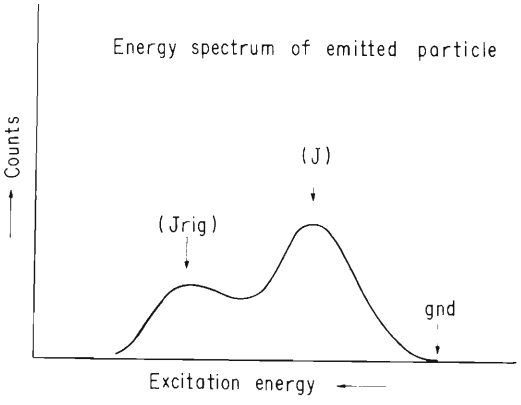

Fig. 2. A typical energy spectrum of emitted particles. Two bumps are observed there, one corresponds to the excitation with J ($<J_{rig}$) and the other corresponds to the excitation with J_{rig}.

However, if many nucleons are transferred, the residual nucleus will be completely excited and have the moment of inertia as large as the rigid body value.

In reactions with a few nucleon transfer, there appears the second bump at excitation energy higher than the first bump discussed above in the energy spectra. As shown in Fig. 2, it is possible to regard the second bump as that which corresponds to the excitation with J_{rig}.

References

1) T. Mikumo: Proc. Int. Symp. on Cluster Structure of Nuclei and Transfer Reactions Induced by Heavy-Ions, Tokyo, p. 617 (1975).
2) H. Kamitsubo: ibid., p. 623.

4-5. Anomalous Angular Distribution in the Transition to the $2s_{1/2}$ State in ^{17}O and ^{13}N

T. Motobayashi, I. Kohno, K. Katori,
M. Yoshie, T. Ooi, and H. Kamitsubo

Recently, an anomaly has been reported in the angular distributions populating $2s_{1/2}$ states of ^{13}C and ^{13}N in studies of the reactions $^{12}C(^{14}N, ^{13}N)^{13}C$[1] and $^{12}C(^{10}B, ^{9}Be)^{13}N$[2] respectively. In these studies it was found that exact finite range DWBA calculations assuming a direct one-step transfer reaction mechanism gave theoretical angular distributions which were oscillating out of phase with the experimental ones. To provide further information on this anomaly, we studied the reaction of $^{16}O(^{14}N, ^{13}N)^{17}O$ leading to the $2s_{1/2}$ state in ^{17}O (E_X = 0.87 MeV), together with the reaction $^{12}C(^{14}N, ^{13}C)^{13}N$ to the $2s_{1/2}$ state in ^{13}N (E_X = 2.37 MeV). A comparison between these two reactions is of interest for two reasons. (i) The $2s_{1/2}$ state in ^{17}O is a better example of the single particle state than that in ^{13}N. (ii) In the ^{14}N + ^{12}C system, strong inelastic scattering channel going to the first 2^+ state of ^{12}C can make some

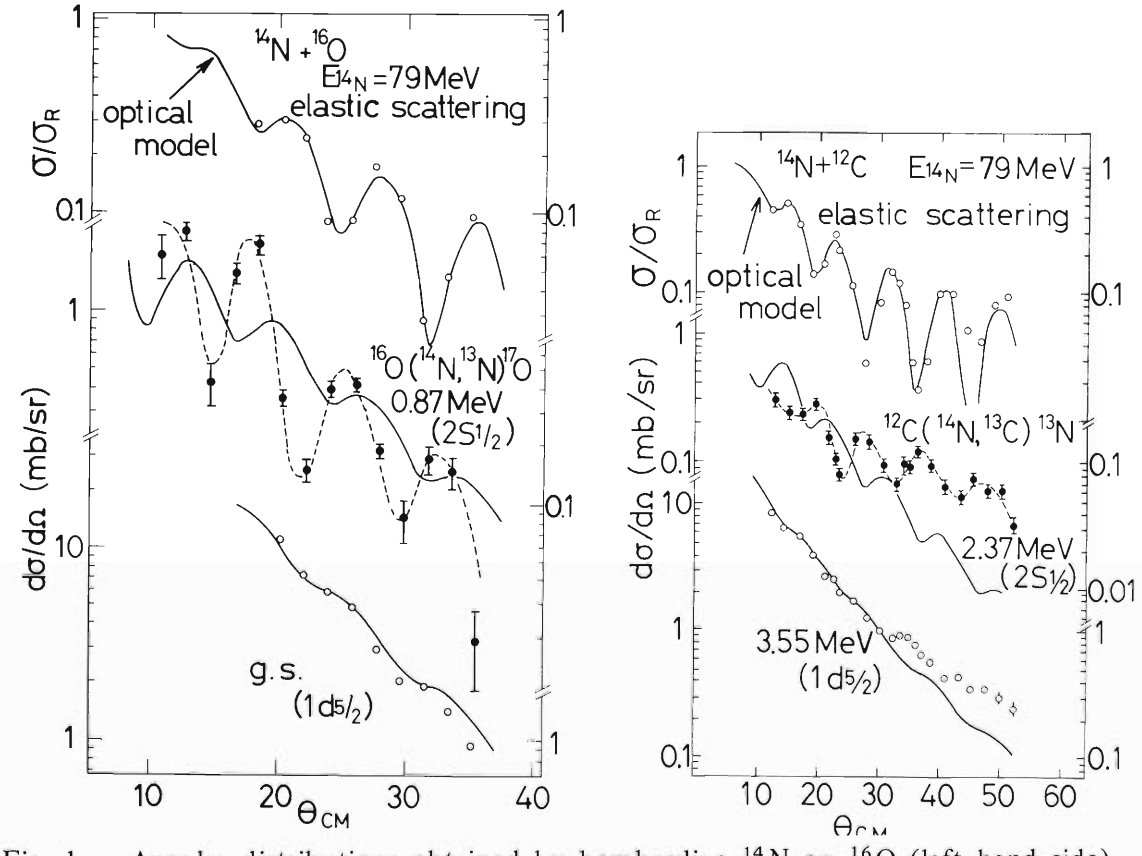

Fig. 1. Angular distributions obtained by bombarding ^{14}N on ^{16}O (left hand side) and ^{12}C (right hand side) at 79 MeV. The solid line in the elastic scattering corresponds to the optical model fit. The solid lines in the transfer reactions correspond to the exact finite range DWBA calculation. The dashed line connecting the experimental points is drawn only to guide the eye.

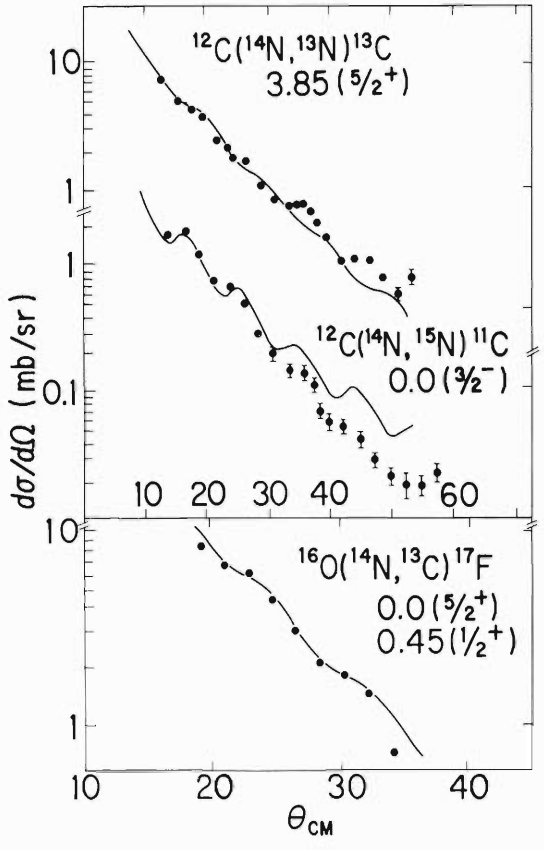

Fig. 2. Angular distributions of the reactions $^{12}C(^{14}N, ^{13}N)^{13}C(5/2^+)$, $^{12}C(^{14}N, ^{15}N)^{11}C(3/2^-)$, and $^{16}O(^{14}N, ^{13}C)^{17}F(5/2^+$ and $1/2^+)$. The solid lines correspond to the exact finite range DWBA calculation.

contribution to the mechanism of the transfer reaction, while in the $^{14}N + ^{16}O$ system there is no such strong inelastic channel.

The angular distributions of other one-nucleon transfer reactions were also studied for comparison.[3),4)]

The angular distributions obtained are shown in Figs. 1 and 2 together with those of the elastic scattering.

Exact finite range DWBA calculations were performed on these angular distributions using the computer code SATURN-MARS 1.[5)] We used the same optical potential parameter set,[6)] V = 65 MeV, W = 20 MeV, r_R = 1.21 fm, r_I = 1.35 fm, a_R = 0.48 fm, a_I = 0.25 fm, and r_C = 1.3 fm, for the entrance and exit channels in both $^{14}N + ^{16}O$ and $^{14}N + ^{12}C$ systems. The solid lines for the elastic data in Figs. 1 and 2 show calculations using this parameter set. The bound state potentials were of Woods-Saxon form with r_0 = 1.2 fm and a = 0.65 fm and the potential depth was adjusted by the separation energy method. For the unbound states of ^{13}N, a small binding energy of 0.05 MeV was assumed. The calculated results are shown by solid lines in Figs. 1 and 2.

The angular distributions for the reactions other than the transitions to the $2s_{1/2}$ states are reasonably fitted by the calculations. The products of two spectroscopic factors $C_1^2S_1 \cdot C_2^2S_2$ and the spectroscopic factor $C_2^2S_2$ are listed in Table 1. To extract the values of $C_2^2S_2$, we used the values of $C_1^2S_1$ predicted for the ground state of ^{14}N by Cohen and Kurath.[7)]

In the case of the $2s_{1/2}$ states of ^{17}O and ^{13}N, the phase of the calculated angular distributions does not agree with that of experimental ones. Based on the result of the full recoil analysis[8)]

Table 1. Spectroscopic factors obtained by comparing the experimental cross sections to the DWBA calculations.

Reaction	J^{π}	$C_1^2S_1 \cdot C_2^2S_2$	$C_2^2S_2$
$^{16}O(^{14}N, ^{13}N)^{17}O$	$5/2^+$	0.71	1.03
	$1/2^+$	0.38	0.55
$^{16}O(^{14}N, ^{13}C)^{17}F$	$5/2^+$	0.49	0.71
$^{12}C(^{14}N, ^{13}N)^{13}C$	$5/2^+$	0.33	0.48
$^{12}C(^{14}N, ^{13}C)^{13}N$	$5/2^+$	0.21	0.30
	$1/2^+$	0.23	0.33
$^{12}C(^{14}N, ^{15}N)^{11}C$	$3/2^-$	3.80	2.70

using a complex-energy eigenstate for the reaction of $^{12}C(^{10}B, ^{9}Be)^{13}N(1/2^+)$, the assumption of small binding energy for the unbound $2s_{1/2}$ state of ^{13}N is expected to give little change in the phase of the angular distribution. Other choice of optical parameter sets affects only the amplitude of the oscillation in the calculated angular distributions, and produces no change in the phase itself. The values of $C_1^2S_1 \cdot C_2^2S_2$ and $C_2^2S_2$ are also listed in Table 1.

A multi-step reaction mechanism can make some contribution to the transition to the $2s_{1/2}$ states as suggested by DeVries et al.[1] If the $[^{12}C(2^+) \otimes d_{5/2}]$ configuration is contained in the $1/2^+$ state of ^{13}N, the process via strong inelastic excitation of the first 2^+ state in ^{12}C is should be important. However, since the anomaly is observed in both ^{13}N and ^{17}O, this process can be excluded to explain these anomalies, since such a strong inelastic scattering channel does not exist in the $^{14}N + ^{16}O$ system.

References

1) R. M. DeVries, M. S. Zisman, J. G. Cramer, K-L. Liu, F. D. Bechetti, H. Homeyer, D. G. Kovar, J. Mahoney, and W. von Oertzen: Phys. Rev. Lett., 32, 680 (1974).
2) K. G. Nair, H. Voit, M. Hamm, C. Towsley, and K. Nagatani: ibid., 33, 1588 (1974).
3) T. Motobayashi, I. Kohno, S. Nakajima, M. Yoshie, K. Katori, T. Mikumo, and H. Kamitsubo: IPCR Cyclotron Progr. Rep., 8, 19 (1974).
4) T. Motobayashi, I. Kohno, T. Ooi, and S. Nakajima: ibid., 9, 65 (1975).
5) T. Tamura and K. S. Low: Comp. Phys. Comm., 8, 349 (1974).
6) I. Kohno, S. Nakajima, T. Tonuma, and M. Odera: J. Phys. Soc. Japan, 30, 910 (1971).
7) S. Cohen and D. Kurath: Nucl. Phys., A101, 37 (1972).
8) L. Ray, W. R. Coker, and T. Udagawa: Phys. Lett., 56B, 318 (1975).

4-6. The (^{14}N, ^{13}C) Reactions on ^{50}Ti, ^{52}Cr, and ^{54}Fe

S. Nakajima, M. Yoshie, T. Motobayashi, and I. Kohno

We measured differential cross sections of the (^{14}N, ^{13}C) reactions on ^{50}Ti, ^{52}Cr, and ^{54}Fe using a ^{14}N (E_{lab} = 70 MeV) beam, and obtained angular distributions for the transitions to the several excited states of the residual nuclei. We also measured angular distributions for the elastic scatterings of ^{14}N by these targets. Analyzing the observed scattering data with the optical model, we deduced the potential parameters as listed in Table 1. They vary smoothly

Table 1. Optical potential parameters used in DWBA calculation.

	V(MeV)	W(MeV)	r_R (fm)	r_I (fm)	a_R (fm)	a_I (fm)
^{14}N + ^{50}Ti	100	10	1.13	1.2	0.5	0.5
^{14}N + ^{52}Cr	100	10	1.135	1.2	0.5	0.5
^{14}N + ^{54}Fe	100	10	1.14	1.2	0.5	0.5

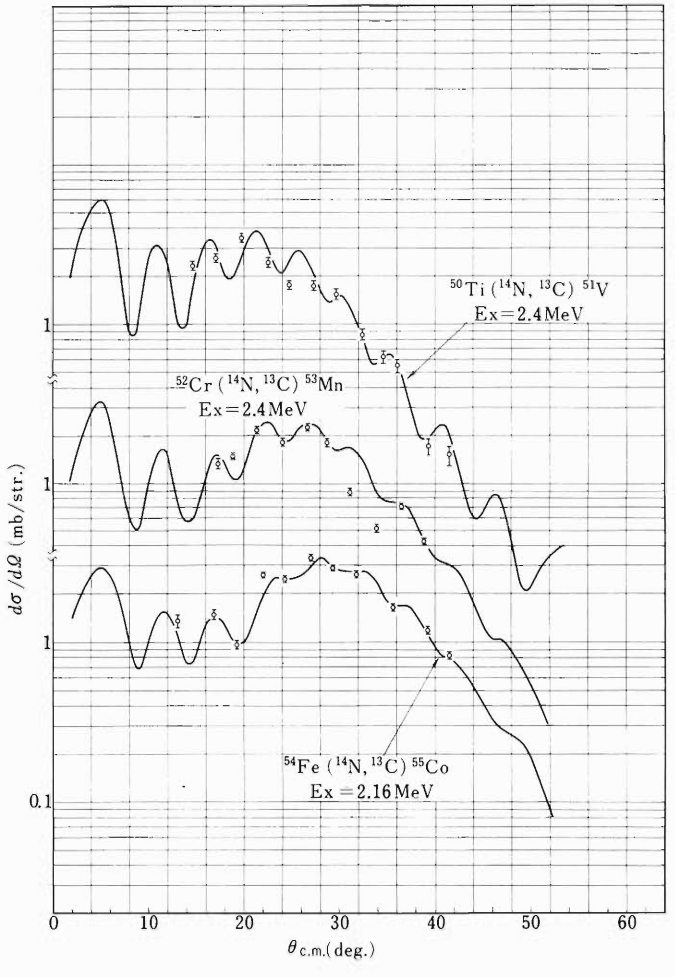

Fig. 1. Angular distributions obtained for the transitions to the $2P_{3/2}$ states in the ^{50}Ti, ^{52}Cr, ^{54}Fe (^{14}N, ^{13}C)^{51}V, ^{53}Mn, ^{55}Co reactions. The solid lines indicate DWBA calculations.

with target mass. We used them in DWBA calculations for the (^{14}N, ^{13}C) reactions. These calculations were performed with the code SATURN-MARS-1 developed by Tamura and Low[1] and compared with the experimental data. The agreement was found to be pretty well for each angular distribution. An example is shown in Fig. 1. To calculate the absolute magnitude, we employed such a normalization factor N as listed in Table 2. The spectroscopic factors for the residual nuclei are also presented in Table 2. It is possible to put N = 1 for every transition to the ground state by adjusting bound state parameters. But for ^{53}Mn the parameters become too small with such an adjustment.

A large N value for the transition to the higher excited state was obtained because our measurement was not good enough to resolve higher excited states.

Table 2. Spectroscopic strengths and the normalization factor N used in the calculation. The normalization factor is defined by $N = (d\sigma/d\Omega)_{exp}/(d\sigma/d\Omega)_{DWBA}$.

Excitation energy (MeV)		Spectroscopic factor $(2J_f+1)C^2S$*	N
^{50}Ti(^{14}N, ^{13}C)^{51}U	0	6.0	0.8
	2.4	1.7	0.8
^{52}Cr(^{14}N, ^{13}C)^{53}Mn	0	3.3	0.6
	2.4	1.7	0.6
	3.7	2.6	1.0
^{54}Fe(^{14}N, ^{13}C)^{55}Co	0	1.9	1.0
	2.2	1.1	1.14
	3.3	2.2	2.0

* Taken from B. Čujec, and I.M. Szöghy: Phys. Rev., 179, 106 (1969); B.J. O'brien, W.E. Dorenbusch, T. A. Belote, and J. Rapaport: Nucl. Phys., A104, 609 (1967).

Reference

1) T. Tamura: Phys. Reports, 14C, 59 (1974).

4-7. Two-Step DWBA Treatment of Heavy Ion Transfer Reactions

T. Kammuri, H. Yoshida, and S. Yamaji

Importance of the multi-step processes in heavy ion reactions is now well recognized. The program code "FRATS" introduced here calculates the two-step DWBA cross section in its full-recoil form. The DWBA amplitude for the process a + A → c + C → b + B is given by

$$T = \langle \chi_b^{(-)}(\mathbf{k}_b,\ \mathbf{r}_b)\ \psi_B \psi_b,\ V_\beta \psi_C \psi_c \mid \frac{1}{E - H_C^0} \mid \psi_C \psi_c,\ V_\alpha \psi_A \psi_a\ \chi_a^{(+)}(\mathbf{k}_a,\ \mathbf{r}_a) \rangle$$

The nuclear matrix element of the first step is decomposed as

$$\int \psi_C^* \psi_c^*\ V_\alpha \psi_A \psi_a\ d\xi = \sum (I_A\ M_A\ j_1\ m_1 | I_C\ M_C)\ (\ell_1\ m_{\ell_1}\ s_1\ m_{s_1} | j_1\ m_1) \times (s_c\ m_c\ s_1\ m_{s1} | s_a\ m_a)\ G^{(\alpha)}_{\ell_1 s_1 j_1 m_{\ell_1}}(\mathbf{r}_c,\ \mathbf{r}_a)$$

in terms of the form factor with specified transferred quantum numbers $(\ell_1 s_1 j_1)$. Here, e.g., $\mathbf{r}_a$ is the relative distance between a and A. Multipole expansion of G was carried out as in the case of one-step DWBA.[1] Defining $G^{(\beta)}_{\ell_2 s_2 j_2}(\mathbf{r}_b,\ \mathbf{r}'_c)$ of the second step and expanding the distorted waves and Green's function in multipole series, we get the four-fold radial integral to be evaluated numerically. With the code "FRATS", we can study the inelastic scattering effect on the one-particle transfer, the successive and simultaneous transfer processes and the non-orthogonality term in the two-particle transfer.

As an example, we present results of calculations on the $^{19}F(^{16}O, ^{15}N)^{20}Ne\ 4^+$ reaction at 68 MeV incident energy.[2] The one-step transition to the lowest 4^+ state in ^{20}Ne is essentially forbidden by the angular momentum conservation. With the aim of comparison with the

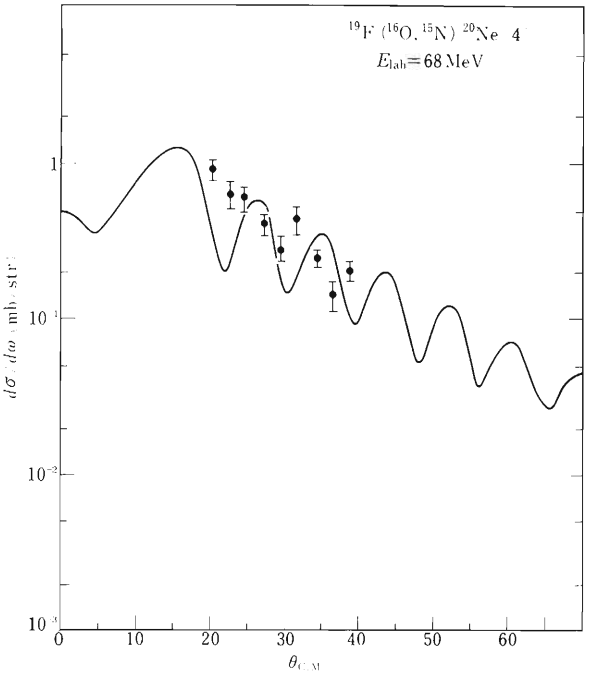

Fig. 1. An example of two-step DWBA calculation. Experimental points are those of Ref. 2.

exact-finite-range CCBA calculation,[3] we have taken account of the one-nucleon transfer to the ^{20}Ne g.s. or the 2^+ state followed by the inelastic excitation to the 4^+ state. The optical parameters used are: V = 100 MeV, r_R = 1.11 fm, a_R = 0.48 fm, W = 27 MeV, r_I = 1.26 fm, and a_I = 0.26 fm. The deformation parameters used for ^{20}Ne were β_2 = 0.45 and β_4 = 0.15. The spectroscopic amplitudes for the ^{19}F $1/2^+ \rightarrow ^{20}$Ne 0^+ and ^{19}F $1/2^+ \rightarrow ^{20}$Ne 2^+ were taken to be 0.58 and -0.58 respectively.[3] The calculated result is compared with experimental data in Fig. 1, where the normalization factor is about 12. The magnitude of the cross section is smaller by a factor of about 3 than the value given in Ref. 3. The difference is probably due to our selection of only one set of the quantum numbers $(\ell_1 s_1 j_1 \ell s j)$.

References

1) H. Yoshida: Private communication.
2) F. Pougheon, G. Rotbard, P. Roussel, and J. Vernotte: Phys. Rev. Lett., 34, 158 (1975).
3) K. S. Low, T. Tamura, and T. Udagawa: Private communication.

4-8. Exact Finite-Range DWBA Calculations for the Reaction $^{60}Ni(^{18}O, ^{16}O)^{62}Ni_{g.s.}$

T. Takemasa

Recently a new attempt[1] was made on a finite-range full-recoil distorted-wave Born-approximation (DWBA) calculation by use of a microscopic form factor for heavy-ion induced two-nucleon transfer reactions. The method utilizes a multipole-series expansion of the two-nucleon overlap as a function of the relative angular momentum $\tilde{\ell}$ of the transferred nucleon pair. This method has been applied to the reaction $^{60}Ni(^{18}O, ^{16}O)^{62}Ni_{g.s.}$ at E = 65 MeV[2] to study the

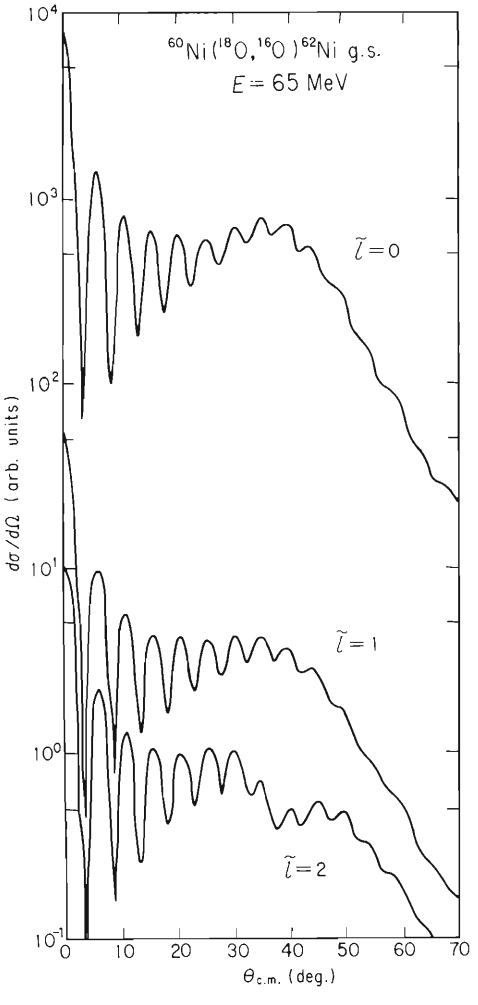

Fig. 1. Plot of the differential cross sections of the reaction $^{60}Ni(^{18}O, ^{16}O)^{62}Ni_{g.s.}$ for each relative angular momentum of a transferred nucleon pair $\tilde{\ell}$.

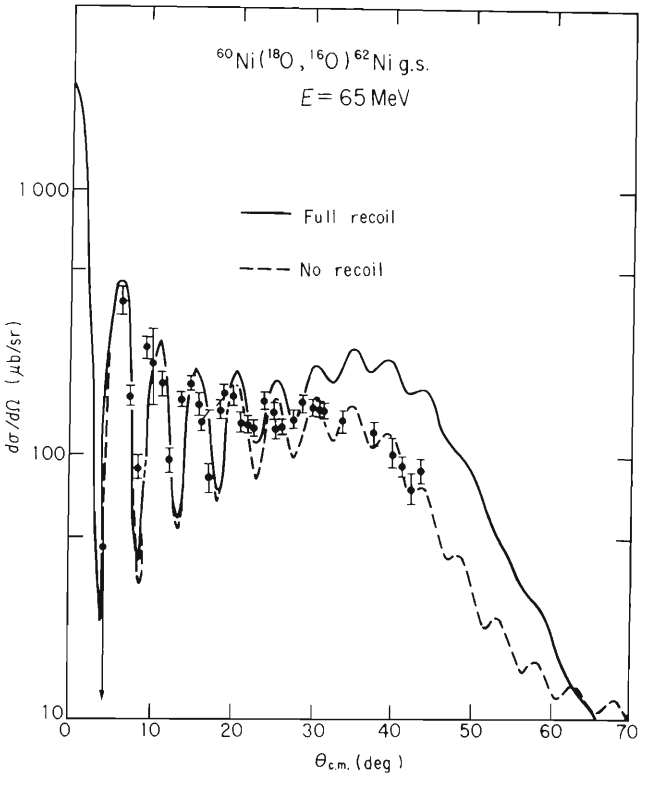

Fig. 2. Comparison of the differential cross sections obtained from no-recoil (Ref. 2) and full-recoil DWBA calculations with experimental data (Ref. 2). Both curves are arbitrarily normalized to the experimental data.

effect of recoil on the shape and magnitude of the differential cross sections employing the surface transparent "Brookhaven" potentials.[2)]

In Fig. 1, we plot the differential cross section for the individual $\tilde{\ell}$ to exhibit the accuracy of our method for the reaction $^{60}Ni(^{18}O, ^{16}O)^{62}Ni_{g.s.}$. As can be seen, the convergence of the $\tilde{\ell}$ series is rapid. The cross section obtained by a coherent superposition of the multipoles $\tilde{\ell}$ = 0, 1, and 2 ensures an accuracy of better than 1 – 2 %. This result indicates that our method is practically suitable for analyzing experimental data. In the followings we present the results calculated taking into account up to the $\tilde{\ell}$ = 3 term.

In Fig. 2, the differential cross sections obtained by the full-recoil and no-recoil calculations are compared with the experimental data.[2)] The normalization constants $N = \sigma(\theta)_{exp}/\sigma(\theta)_{theor}$ are 3.9 and 15.0 for the no-recoil curve and the full-recoil one, respectively. In both calculations use is made of the same two-neutron transfer amplitudes for the oxygen and nickel nuclei. In Ref. 2 the three active single-particle states $2p_{3/2}$, $1f_{5/2}$, and $2p_{1/2}$ were taken into account for the Ni. The no-recoil calculation gives the cross section larger than the full-recoil calculation by a factor of about 3.8. The shape of the angular distribution calculated by use of the full-recoil DWBA is in good agreement with the result of the no-recoil DWBA calculation at forward angles. At larger angles, however, the difference between the no-recoil curve and the full-recoil one becomes larger and, in addition, the recoil effect diminishes oscillations in the angular distribution for angles greater than about 45°. Moreover, the agreement between the experimental data and the full-recoil DWBA curve becomes poorer for angles greater than about 30°.

Finally, we have examined the dependence of the differential cross section upon the

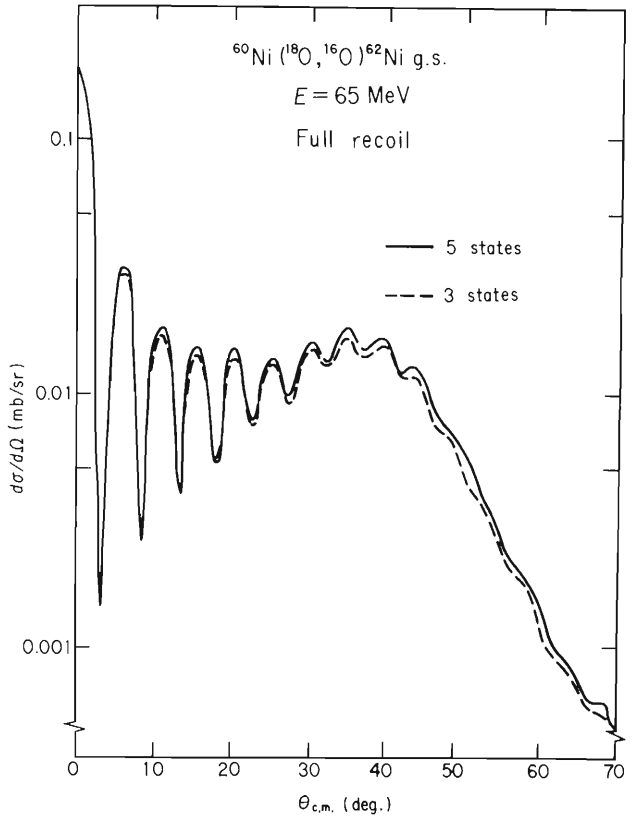

Fig. 3. Comparison of the result of the full-recoil DWBA calculation carried out by taking into account the three active single-particle states in the calculation of the spectroscopic amplitudes for the Ni nuclei with that obtained by taking into account the five active single-particle states. The former corresponds to the dashed line and the latter to the solid line.

configuration mixing. The five active single-particle states, $1f_{7/2}$, $2p_{3/2}$, $1f_{5/2}$, $2p_{1/2}$, and $1g_{9/2}$ are taken into account in calculating the spectroscopic amplitude for the Ni system. Figure 3 shows a comparison between the calculated results based on the three and five single-particle states. The almost complete agreement between two curves is a clear indication that the increase of the amount of the configuration mixing for the Ni nuclei does not give any improvement in both the shape and magnitude of the differential cross section. The discrepancy in magnitude between theory and experiment indicates the need to correctly treat the two-nucleon transfer form factors[3] and also to take into account the two-step (successive) mode[4] in calculation of the transition amplitude.

References

1) T. Takemasa: Phys. Lett., 55B, 28 (1975).
2) M. J. LeVine et al.: Phys. Rev., C10, 1602 (1974).
3) D. H. Feng et al.: Phys. Lett., 47B, 477 (1973).
4) T. Udagawa et al.: Private communication.

4-9. Analysis of Elastic Scattering of ^{16}O by ^{19}F (2)

T. Motobayashi and B. Imanishi

We analyzed elastic scattering of ^{16}O by ^{19}F by the coupled channel method considering an exchange process of ^{16}O-core. The formalism of this method has been discussed previously.[1] Here we report the results in case of the full recoil calculation.

Figures 1 and 2 show the results of the calculations using potentials of type A (r = 2.0 fm and a = 0.65 fm) and type B (r = 1.3 fm and a = 0.7 fm) for ^{16}O-t interaction. The dashed lines in the figures are the results of the calculation of heavy-ion approximation with the same cfp values as in the full recoil calculation. In Fig. 1 (type A potential) the cfp value (0.25) is

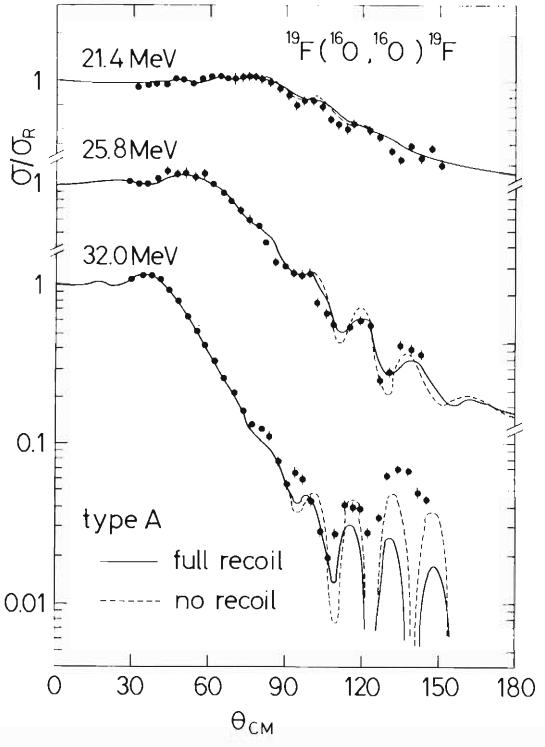

Fig. 1. Angular distributions of elastic scattering of ^{16}O on ^{19}F at three energies calculated by a core-exchange model. The solid lines show the results of the full-recoil calculation and the dotted lines the results of the no-recoil one. Type A potential is used (the parameters are given in the text).

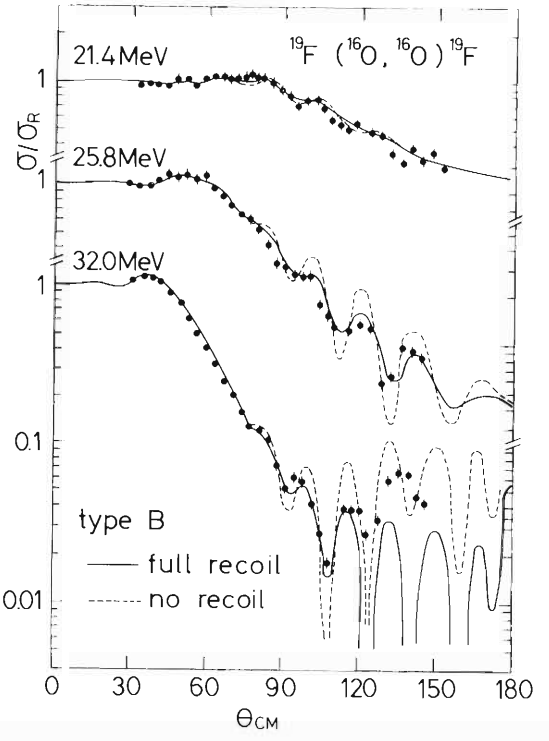

Fig. 2. The same as Fig. 1. Type B potential is used.

taken to be the same as the one used in the full recoil analysis of the reaction $^{19}F(^{3}He,^{6}Li)^{16}O$ by Strohbush et al.[2] In Fig. 2 (type B potential) the cfp value (0.75) is determined so as to give a best fit to the data.

As seen in Figs. 1 and 2 the recoil effect is important in determining the amplitude of oscillation in the angular distributions, while it does not affect the phase of oscillation. The effect presented here is strong even at lower incident energies and appear to be stronger for the short range potential (type B) than for the long range one (type A). Such effects are difficult to understand by a usual criterion[3),4)] on the no-recoil approximation:

$$k \ll M/ma, \qquad (1)$$

where k denotes the wave number of relative motion between two incident nuclei and a the force range of the interaction between ^{16}O and triton. M and m denote the masses of ^{16}O and triton respectively.

In order to understand the recoil effects mentioned above, we consider the adiabatic approximation employed in the PSS method,[5),6)] which is equivalent to the no-recoil approximation. In this method, one may choose the vectors $\vec{R}$ and $\vec{x}$ which represent the system, where $\vec{R}$ and $\vec{x}$ denote the distance between ^{16}O and triton and between two ^{16}O nuclei respectively. In the asymptotic region of $\vec{x}$, the operators $\hbar^2\vec{\Delta}_x\vec{\Delta}_R/M$ and $\hbar^2\vec{\Delta}_x^2/M$ remain in the total Hamiltonian, and in the adiabatic approximation the former may be neglected compared with the latter if the following condition is satisfied:

$$\kappa \ll k, \qquad (2)$$

where κ represents the wave number corresponding to the bound state wave function. This is a new condition[7)] for the validity of the no-recoil approximation, which would be invalidated in decreasing incident energy or in increasing κ. A large value of κ is expected when the force range of the interaction is small. Thus, the relation (2) explains the reason why the no-recoil approximation is invalid in the present case even if the relation (1) fails, and this can be understood from Table 1.

Table 1. Values of κ, k, and M/ma (fm^{-1}).

	Pot. A			Pot. B		
E_{lab} (MeV)	κ	k	M/ma	κ	k	M/ma
21.4	2.2	0.21	1.1	3.0	0.21	1.6
25.8	2.2	0.97	1.1	3.0	0.97	1.6
32.0	2.2	1.53	1.1	3.0	1.53	1.6

The values of k are calculated at r = 8.8 fm for the respective bombarding energies.

References

1) T. Motobayashi and B. Imanishi: IPCR Cyclotron Progr. Rep., 8, 24 (1974).
2) U. Strohbush, W. Schnidt, and G. Huber: Nucl. Phys., A163, 453 (1971).
3) P. J. A. Buttle and L. J. B. Goldfarb: ibid., 78, 409 (1966); A176, 299 (1971).
4) R. M. DeVries and K. I. Kubo: Phys. Rev. Lett., 30, 325 (1973).
5) W. Von Oertzen and W. Nörenberg: Nucl. Phys., A207, 113 (1973).
6) See, for example, N. F. Mott, and H. S. Massey: "Theory of Atomic Collisions", Clarendon Press, Oxford, p. 153 (1953).
7) B. Imanishi: Proc. INS-IPCR Symposium on Cluster Structure of Nuclei and Transfer Reactions Induced by Heavy Ions, Tokyo, 1975, Ed. H. Kamitsubo, I. Kohno, and T. Marumori (IPCR Cyclotron Progr. Rep. Suppl. 4, p. 381 (1975).

4-10. Multi-Step Core-Exchange Analysis of $^{16}O + ^{18}O$ Scattering by Full-Recoil Calculation

B. Imanishi and K. Kubo*

In this report, it is shown that the recoil effect due to the transfer of two neutrons from ^{18}O, which is not taken into account in the LCNO treatment, is important for reproducing the observed variation of the backward cross section of $^{16}O + ^{18}O$ scattering.[1),2)] It is also shown that the effects due to the multi-step process of core-exchange are small.

The coupled integro-differential equation is numerically solved under the following three assumptions: i) Two neutrons in the sd-shell of ^{18}O ground state are transferred as a ^1S di-neutron. ii) The optical parameters of ^{16}O – ^{18}O potential are taken from the work of Siemssen et al.,[3)] which are determined from the analysis of $^{16}O + ^{18}O$ scattering in the forward angular region. They are: V = 100 MeV, r_0 = 1.2 fm, a = 0.49 fm, W (volume type) = 40 MeV, r_W = 1.2 fm, and a_W = 0.32 fm. iii) The potential V_{nc} is chosen as $V_{nc} = -89.094$ MeV/(1 + exp ((R – 3.15)/0.65), from which the di-neutron bound state wave function $\psi_{n\ell}(R)$ with $(n\ell)$ = (2s) is determined for the ground state separation energy of –12.18 MeV.

Using a constant value, 0.8, for the fractional parentage coefficient (cfp), $\langle ^{18}O|\}^{16}O, 2n(^1S)\rangle$, we have carried out two calculations: one is the calculation with full-recoil and the other is with the no-recoil approximation. In Fig. 1, the results are shown together with the experimental data for four different incident energies. The result obtained with no-recoil approximation (shown by the dashed lines) overestimates the backward cross sections at the higher incident energies. That is, as the incident energy increases, the backward cross sections calculated with no-recoil approximation increase faster than those observed. However, the full-recoil calculation (shown by the solid lines) gives good fits to the experimental data for most incident energies and angles.

The value of cfp, 0.8, used in the present calculation is about 1.6 times that obtained from the shell model wave functions.[4)] Such an overestimated value may be required as a consequence of the simplified treatment of the composite particle transfer reaction.

In order to see whether or not the multi-step core exchange process is important, the results obtained above have been compared with those calculated in the first order perturbation treatment. In Fig. 2, such comparisons are made for two different incident energies. It is then found that the effect from multi-step exchange is rather small. The result is not changed in the calculation using a shallow optical potential with "weak" imaginary strength. This fact contrasts with the result given by DWBA treatment with Buttle-Goldfarb approximation, in which the shallow optical potential emphasizes the core-exchange effect too much. It is also found that the contribution from the non-orthogonality term is negligibly small. The cross sections calculated without the non-orthogonality term are very close to those with the full kernel (the solid line in Fig. 2). This result is consistent with the fact the multi-step exchange effect is very small.

* University of Tokyo

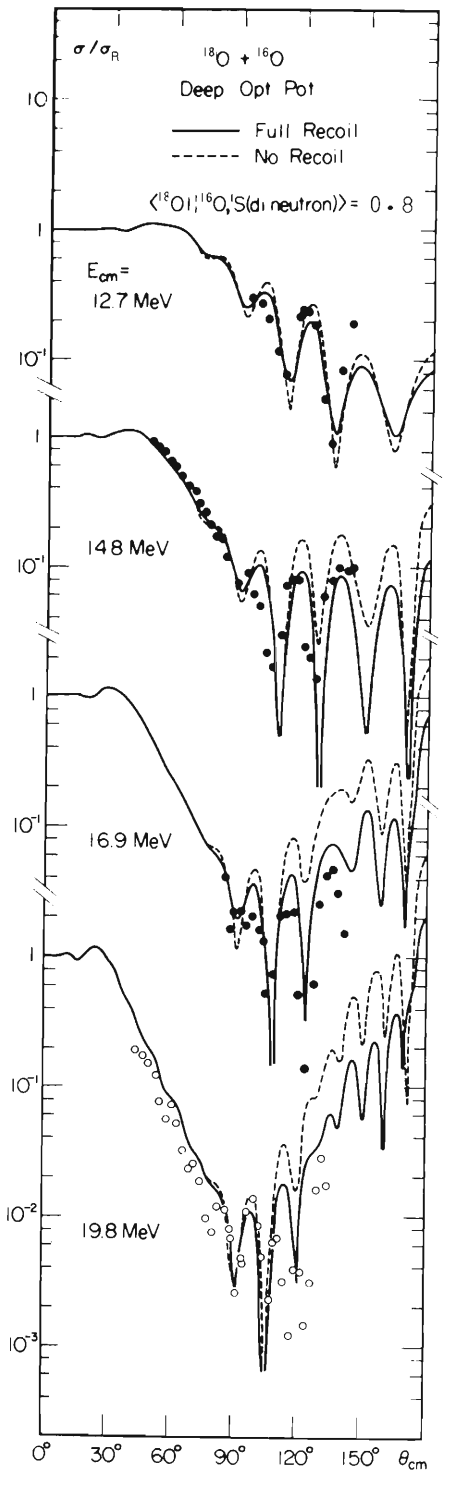

Fig. 1. Angular distributions of $^{16}O + ^{18}O$ elastic scattering for four different incident energies. Two results of calculations with no-recoil approximation (shown by the dotted lines) and with exact recoil treatment (the solid lines) are compared with the observed values. The experimental data are taken from Ref. 1 for the first three energies and from Ref. 2 for the last energy (19.8 MeV).

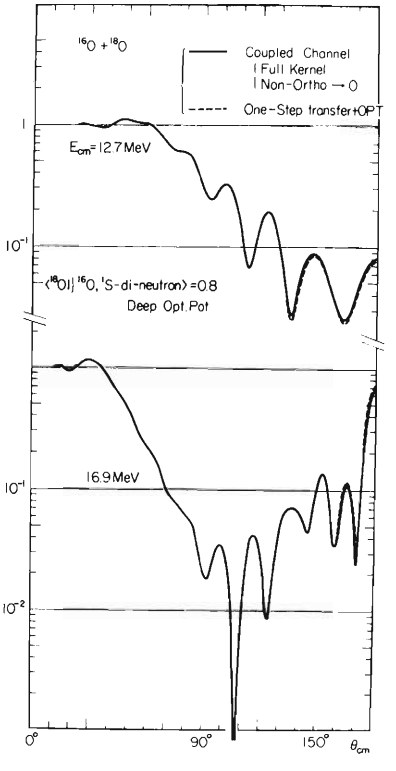

Fig. 2. Calculated angular distributions of $^{16}O + ^{18}O$ elastic scattering for two different incident energies. The solid lines show the results calculated with the full kernel responsible for the core-exchange process. The dotted lines show the results calculated in the first order perturbation treatment.

References

1) C. K. Gelbke, R. Bock, and A. Richter: Phys. Rev., C9, 852 (1974).
2) R. Vandenbosh, W. N. Reisdorf, and P. H. Lau: Nucl. Phys., A230, 59 (1974).
3) R. H. Siemssen, H. T. Fortune, A. Richter, and J. W. Tippie: Phys. Rev., C5, 1839 (1972).
4) S. Kahana: ibid., C5, 2120 (1973).

4-11. The Multi-Step Effects of $^{17}O(^{16}O,^{16}O)^{17}O^{*}(1/2^{+})$ Inelastic Core-Exchange Scattering

B. Imanishi, H. Onishi,* and O. Tanimura**

We analyzed the elastic and inelastic scattering processes, $^{16}O - {}^{17}O$[1] and $^{17}O(^{16}O, ^{16}O)$ $^{17}O^{*}(1/2^{+}, 0.871\ \text{MeV})$,[2),3)] by the method of coupled channels.[4)] The form factor was calculated with no-recoil approximation (but without the Buttle-Goldfarb approximation). We showed that a shallow optical potential is well applicable both to the elastic scattering and the inelastic scattering if the multi-step transfer processes at least up to the fourth order are taken into account. Also, it was shown that the multi-step processes, especially multi-step transfer processes, are important in explaining not only the angular distribution of the inelastic scattering cross section but also the magnitude of the elastic and inelastic differential cross sections.[7)]

It is assumed that the system is composed of $(^{16}O + n) + {}^{16}O$ in which ^{16}O is assumed to be an inert core. The ground state of ^{17}O is a $1s_{1/2}$-single-particle state. The corresponding neutron single-particle wave functions are designated by $\psi_{Od_{5/2}}(\mathbf{R})$ and $\psi_{1s_{1/2}}(\mathbf{R})$, respectively. Then a trial wave function ψ of the total system is expressed[4)] as

$$\psi = (1 + \text{core-exchange operator}) \sum_i \frac{u_i(r)}{r} \phi_i(\hat{\mathbf{r}}, \mathbf{R}), \qquad (1)$$

where $\phi_i(\hat{\mathbf{r}}, \mathbf{R}) = [\psi_{Od_{5/2}}(\mathbf{R}), Y_\ell(r)]_{JM}$ or $[\psi_{1s_{1/2}}(\mathbf{R}), Y_\ell(\mathbf{r})]_{JM}$ and the channel quantum number i denotes $(Od_{5/2}, \ell, JM)$ or $(1s_{1/2}, \ell, JM)$. The symbol $\hat{\mathbf{r}}$ stands for the direction of the displacement vector $\mathbf{r}$ between ^{16}O and ^{17}O. We used the following interaction potential between ^{16}O and n in the effective Hamiltonian of the total system:

$$V(R) = \frac{-53.00}{1+\exp((R-3.15)/0.666)} + (\ell \cdot s)\frac{23.65}{R}\frac{d}{dR}\cdot\frac{1}{1+\exp((R-3.15)/0.666)}\ (\text{MeV}), \qquad (2)$$

which was determined so that the binding energies of the $Od_{5/2}$- and $1s_{1/2}$-orbits are the observed neutron separation energies, 4.412 MeV and 3.272 MeV of the ground state and the $1/2^{+}$ state of ^{17}O, respectively, and at the same time the $d_{3/2}$-resonance in the scattering of n on ^{16}O occurs at the observed energy of $E_{cm} = 0.94$ MeV. The optical potential U(r) between ^{16}O and ^{16}O is assumed to be of the Woods-Saxon form. We tested two sets of the optical parameters which were given by Siemssen et al.[5)] by the analysis of elastic angular distributions. Of the two sets, one is a shallow potential (type A; $r_r = r_w = 1.24$ fm, $a_r = a_w = 0.49$ fm, $r_c = 1.25$ fm, $V = -(12.0 + 0.25E_{cm})$ MeV, $W = -(0.4 + 0.1E_{cm})$MeV) and the other a deep potential (type B; $r_r = r_w = 1.20$ fm, $r_c = 1.25$ fm, $a_r = 0.49$ fm, $a_w = 0.32$ fm, $V = -100$ MeV, $W = -40$ MeV).

We carried out the coupled channel calculation (we denote it by CC) and compared the results with those of the optical model plus DWBA (we denote it simply by DWBA). The curves calculated on the assumption that $\langle {}^{17}O | \} {}^{16}O, n(Od_{5/2})\rangle = \langle {}^{17}O^{*} | \} {}^{16}O, n(1s_{1/2})\rangle = 1$

* Hosei University
** Nihon University

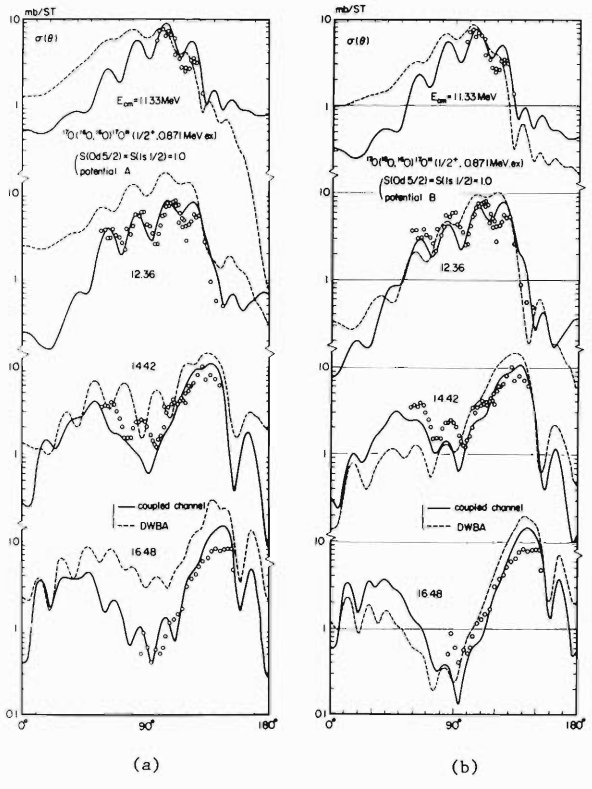

Fig. 1. Comparison of the calculated angular distributions with the experimental results of Ref. 2. The solid lines show the results of coupled channels and the dotted lines those of DWBA. All the cfp-values are taken to be unity in the calculation. In (a) a shallow optical potential (type A) is employed, while in (b) a deep optical potential (type B) is used.

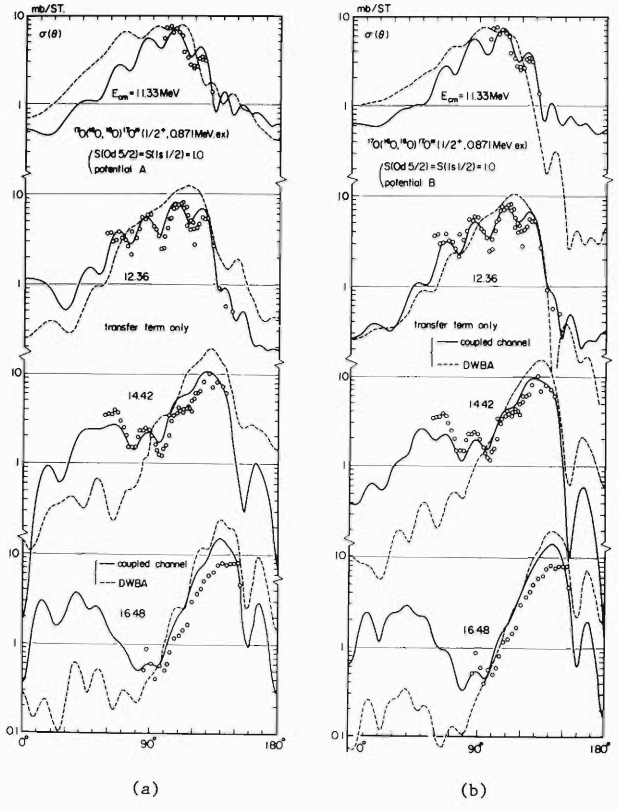

Fig. 2. The inelastic scattering calculated by only the transfer interaction (a) with shallow optical potential and (b) with deep optical potential. The dotted lines show the results (DWBA) with only the one-step transfer, while the solid lines the results (coupled channels) with the one- and multi-step transfers.

show prominent multi-step effects as shown in Fig. 1, especially in (a). It is clear that the inclusion of the multi-step processes is necessary for fitting the data, especially in case of the shallow potential of type A.

Next, we calculated the differential cross sections by CC with transfer processes (TI) only (Fig. 2). Comparing Fig. 2 with Fig. 1, one finds that the result with full processes (direct-plus transfer processes: DI + TI) is not different so much from that with TI only. This may be interpreted as a proof of the TI-dominance in CC. However, this is not true in DWBA as is also clear from comparison of the corresponding curves in Fig. 2 to those in Fig. 1. Therefore, bumps at forward angles in CC results at E_{cm} = 14.42 MeV and 16.48 MeV are due to the contribution of the multi-step transfer processes and presumably not of the direct processes.[6] The oscillatory structure of CC angular distributions at E_{cm} = 11.33 MeV and 12.36 MeV is

a result of the interference of the one- and multi-step transfer amplitudes.

At incident energies well above the Coulomb barrier, the transfers by even number steps affect the cross section in the forward angles and the odd ones that in the backward angles (This is not true if the incident energy is close to the barrier). Therefore, the deviation change of the angular distribution in the backward angles away from the DWBA prediction suggests that the three or more steps of transfer processes are important. The bumps at the forward angles in the CC curves in inelastic scattering cross sections indicate the important contribution of the two or more steps of transfer.

The existence of transfer processes of more-than-three-steps suggests that resonances of the type ^{16}O-n-^{16}O may be formed. The possibility of such quasi-molecular resonances is yet to be investigated.

Finally, it is interesting to note that the results of coupled channels neglecting the DI term (Fig. 2) agree very well with the measured cross sections at all energies and angles irrespective of the choice of U(r). The inclusion of the DI term destroys this agreement. The reason or significance of this fact is not clear at present. A more detailed account of the present calculation will be reported elsewhere.

References

1) C. K. Gelbke, R. Bock, P. Braun-Munzinger, D. Fick, K. D. Hildenbrand, W. Weiss, S. Wenneis, and G. Baur: Phys. Lett., 43B, 284 (1973).
2) C. K. Gelbke, G. Baur, R. Bock, P. Braun-Munzinger, W. Grochulski, H. L. Harney, and R. Bock: Nucl. Phys., A219, 253 (1974).
3) D. Kalinsky, D. Melnik, U. Smilansky, N. Trautner, B. A. Watson, Y. Horowitz, S. Mordechai, G. Baur, and D. Pelte: ibid., A250, 364 (1975).
4) T. Ohmura, B. Imanishi, M. Ichimura, and M. Kawai: Progr. Theor. Phys., 41, 391 (1969); 43, 347 (1970); 44, 1242 (1970).
5) R. H. Siemssen, H. T. Fortune, A. Richter, and J. W. Tippie: Phys. Rev., C5, 1839 (1972).
6) W. Von Oertzen: Private communication. He also argued about the contribution of the two-step process for the bump at forward angles (Intern. Symp. on Cluster Structure of Nuclei and Transfer Reactions Induced by Heavy-Ions, Tokyo, p. 337 (1975).
7) B. Imanishi, H. Onishi, and O. Tanimura: Phys. Lett., 57B, 309 (1975).

4-12. D(α, pα) n Reaction at E_α = 18 MeV

K. Sagara,* T. Motobayashi, N. Takahashi,* M. Hara,
Y. Hashimoto,* T. Fujisawa, and I. Kohno

In order to study three-body correlation at low energies, kinematically complete measurement of the reaction D(α,pα)n was performed at E_α = 18 MeV, the lowest energy hitherto tried. To avoid radiation damage, the target CD_2 of about 250 $\mu g/cm^2$ was brought to a new position in each run (~6 hours). Coincidence measurements were made between protons and α-particles, and their energies and difference of flight times were recorded on a magnetic tape for later analysis. Background subtraction was made by measuring accidentally coincident events which

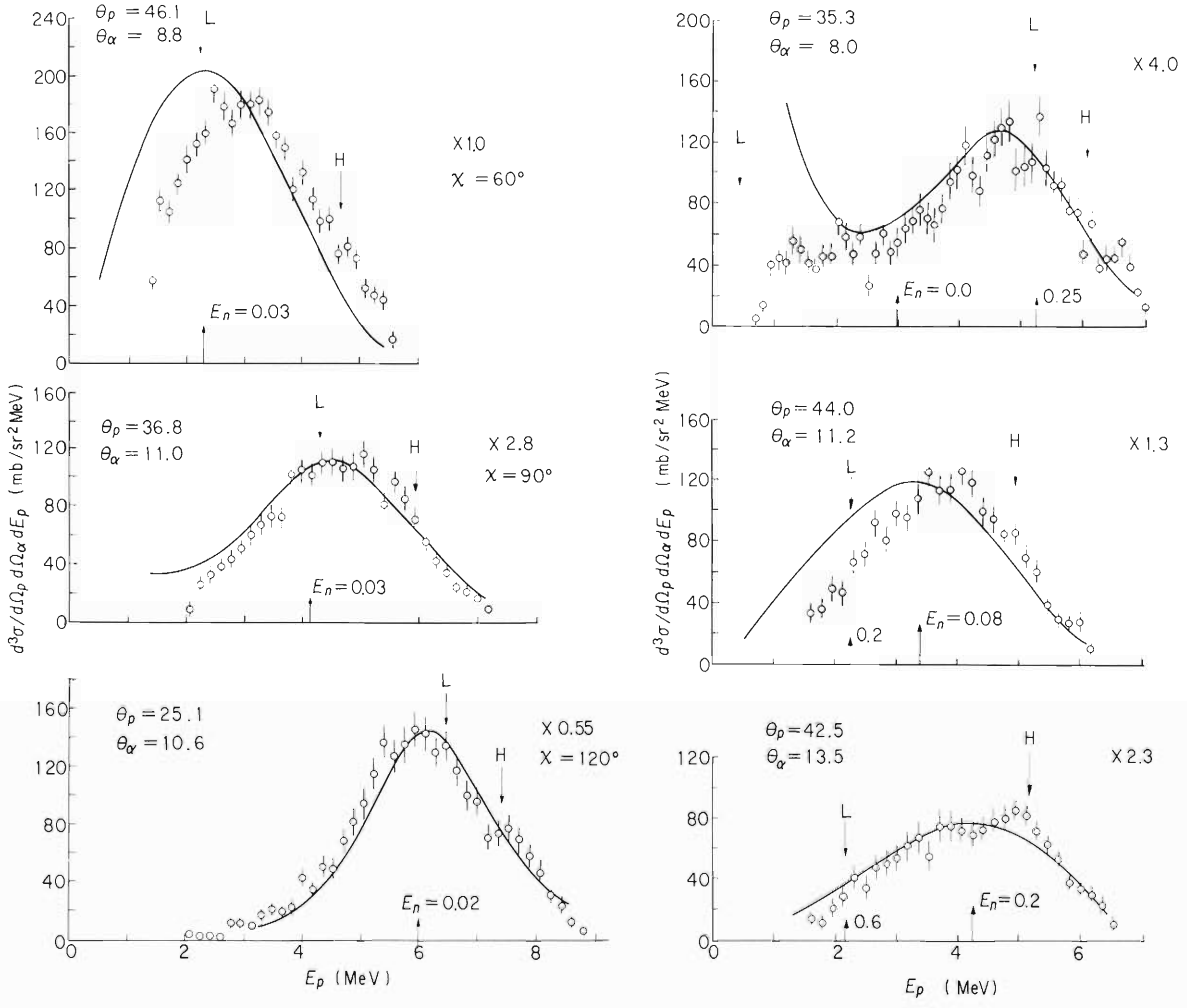

Fig. 1. Differential cross sections of the D(α, pα)n reaction at 18 MeV. The arrows with L and H show the positions of the ground states of ^{5}Li and ^{5}He, respectively, and arrows with triangles show the minimum neutron energies. Solid curves show the results of calculation in $SM_{p\text{-}\alpha}$ multiplied by factors indicated on the right.

happened among different beam bunches.

Data were projected onto the E_p axis. Two kinds of peaks were observed, the p-α quasi-free scattering (qfs) peaks in Fig. 1 and the n-α final state interaction (fsi) peaks corresponding to the ground state of ^{5}He in Fig. 2. The qfs peaks were analyzed in the neutron spectator model ($SM_{p\text{-}\alpha}$) as [1]

$$\frac{d^3\sigma}{\alpha\Omega_p d\Omega_\alpha dE_p} = KF \cdot |\Phi_d(k_n)|^2 \left(\frac{d\sigma}{\alpha\Omega}(\chi_{p\text{-}\alpha})\right)_{p\text{-}\alpha} \cdot PS, \quad (1)$$

where PS and KF stand for the three-body phase space volume and the kinematical factor, respectively, and ϕ_d is the deuteron wave function with a cut-off radius of 5 fm. The p-α differential cross section $(\frac{d\sigma}{d\Omega})_{p\text{-}\alpha}$ was calculated using the empirical p-α phase shifts and the p-α scattering angle $\chi_{p\text{-}\alpha}$. For the n-α fsi peaks, the same formula that is sufficed with p and n in the right-hand side exchanged ($SM_{n\text{-}\alpha}$) was used without the cut-off radius. Results of the calculation are shown in Figs. 1 and 2. Although fits in shape are not so bad, absolute values

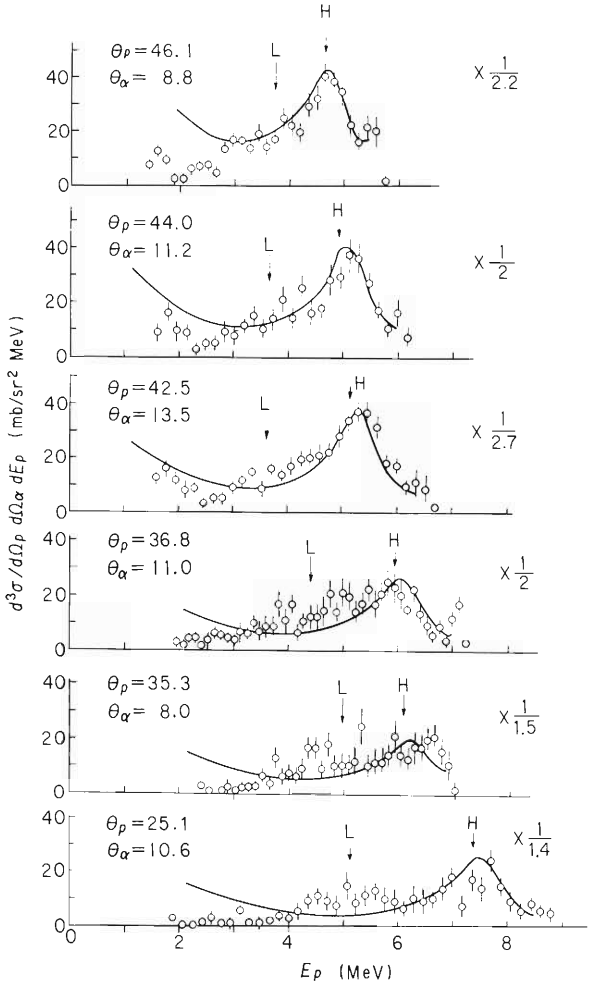

Fig. 2. The same as Fig. 1, except that the curves are those in $SM_{n\text{-}\alpha}$.

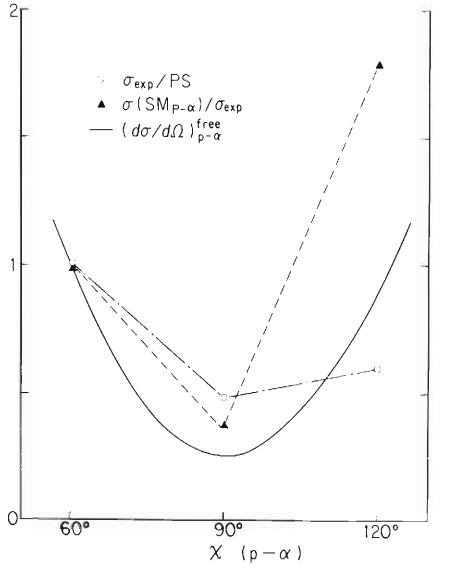

Fig. 3. Ratios (▲) of the p-α qfs peak height to that calculated in $SM_{p\text{-}\alpha}$, and those (○) to the phase space volume normalized at $\chi_{p\text{-}\alpha}$=60°. The triangles had to show the value unity, if the spectator model calculation were correct. The circles show some deviation from the p-α elastic cross section (——) which is normalized at 60°.

of the cross section cannot be reproduced.

In Fig. 3 the p-α cross section derived from the p-α elastic scattering (solid curve) and that extracted from the p-α qfs (circle) are compared. The latter tends to be smooth, especially at backward angle.

The cross sections at the n-α fsi peaks (fsi peak heights) were nearly independent of the n-α scattering angle $\chi_{n\text{-}\alpha}$. The dependence of these peak heights on $\theta_{p\text{-}^5He}$, the scattering angle of the ^{4}He (d, p) ^{5}He reaction, was investigated (Fig. 4). In Fig. 4 three data of ^{4}He (d, pα)n at E_d = 9 MeV[2] are incorporated. As shown in Fig. 4, the data can be divided into two groups, those at forward ($\theta_{p\text{-}^5He} \lesssim 90^\circ$) and backward angles, and peak heights in each group scarecely depend also on $\theta_{p\text{-}^5He}$.

These facts might indicate that multi-step processes play an important role at such a low energy. A more accurate analysis is now in progress.

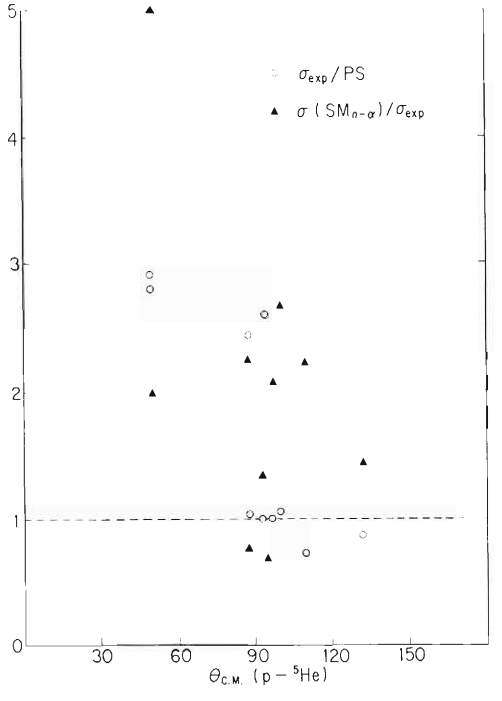

Fig. 4. Ratios (▲) of the n-α fsi peak height to that calculated in $SM_{n\text{-}\alpha}$, and those (○) to the phase space volume multiplied by a common factor. The upper three circles represent the data of the ^{4}He (d, pα)n at 9 MeV.

References

1) A. F. Kukkes, R. Wilson, and P. F. Cooper, Jr.: Ann. Phys., 15, 193 (1961).

2) K. Sagara, M. Hara, T. Motobayashi, N. Takahashi, F. Soga, F. Takeuti, and Y. Nogami: Int. Conf. on Few Body Problem in Nuclear and Particle Physics, Quebéc, August (1974).

* University of Tokyo

4-13. $^{24}Mg(d, p)$ and $^{26}Mg(d, p)$ Reactions at $E_d = 21$ MeV

F. Kakimoto, N. Nakanishi,* and H. Ohnuma

Studies of so-called forbidden transitions provide information on multi-step processes in direct nuclear reactions. The $^{24}Mg(d, p)^{25}Mg$ (1.61 MeV, $7/2^+$) reaction is an example of such forbidden transitions, and many experimental results have been published on this reaction. However, the presence of multi-step processes in this transition has not yet been established. This is because all the existing data were taken below E_d = 15 MeV and the possibility that this level is excited by compound processes could not be ruled out.[1] We have studied the $^{24}Mg(d, p)$ reaction at E_d = 21 MeV. Contributions of compound processes are presumably small at this energy. Higher incident energy has made it possible to obtain reliable angular distributions for the levels above 4 MeV, on which there has been only scarce spectroscopic information so far. The $^{26}Mg(d, p)^{27}Mg$ reaction is also studied to obtain information on the deformation of A = 26 and 27 nuclei from the spectroscopic factors of this reaction.

A momentum-analyzed 21-MeV deuteron beam from the cyclotron was used in the

Table 1. Optical potential parameters used in the analyses.

	Deuteron[2]	Proton[3]	Bound state
V (MeV)	73.98	46.7	
r (fm)	1.145	1.24	1.24
a (fm)	0.753	0.65	0.65
W_d (MeV)	47.8	33.2	
r_d (fm)	1.227	1.28	
a_d (fm)	0.861	0.50	
V_{so} (MeV)	11.92	22.0	25 (= λ)
r_{so} (fm)	1.145	0.92	1.24
a_{so} (fm)	0.753	0.50	0.65
r_c (fm)	1.3	1.25	
NLOC	0.54	0.85	

Potentials are of the form

$$V(r) = Vf(x) + iW_d \frac{df(x_d)}{dr} + V_{so} \frac{1}{r} \frac{df(x_{so})}{dr} \cdot L \cdot S + V_{coulomb},$$

where $f(x_i) = (1 + e^{x_i})^{-1}$ and $x_i = \frac{r - r_i}{a_i}$

NLOC: Nonlocality parameter.

λ : The usual λ factor in describing a Thomas spin orbit term.

* Tokyo Institute of Technology

Table 2. Spectroscopic factors for the $^{24}Mg(d, p)$ and the $^{26}Mg(d, p)$ reactions.

$^{24}Mg(d,p)$					$^{26}Mg(d, p)$					
E_x(MeV)	J^π	a)	b)	c)	E_x(MeV)	J^π	d)	e)	f)	g)
0.0	5/2+	1.88	2.0	2.0	0.0	1/2+	1.6	1.18	1.14	1.4
0.59	1/2+	0.6	0.66	0.56	0.98	3/2+	1.5	3.08	0.64	1.6
0.97	3/2+	1.25	0.934	0.92	1.70	5/2+	0.78	0.78		0.15
1.61	7/2+				1.94	5/2+	0.08		0.18	0.07
1.96	5/2+	0.39	0.4	0.52	3.11					
2.56	1/2+	0.34		0.94	3.43					
2.74	7/2+				3.48	1/2+	(0.52)			0.22
2.80	3/2+	(0.654)		0.98	3.49	(3/2,5/2)+				1.0
3.40	9/2+				3.56	3/2−	1.41			
3.41	3/2−	(1.83)			3.76	7/2−	5.564			
3.90	(3/2,5/2)+				3.79	3/2+				0.52
3.97	7/2−	(2.61)			3.88					
4.06	9/2+				4.15	(3/2,5/2)+	(0.39)			
4.28	(1/2,3/2)−	(0.524)			.....					
4.35	3/2+	0.863			.....					
4.71					4.82	(1/2,3/2)−	(0.92)			
4.72	(3/2,5/2)+	(1.87)								

a), d) Present results

b) Ref. 4. $\beta = 0.3$

c) Ref. 5. $\beta = 0.22$

e) Ref. 6. $\beta = -0.1$

f) Ref. 7. $\beta = 0.1$

g) Ref. 8. Calculations in a truncated $1d_{5/2}\,2s_{1/2}\,1d_{3/2}$ configuration space.

experiment. The beam current was 50 – 150 nA except at very forward angles. Self-supporting targets were prepared by vacuum evaporation of magnesium oxide powder of enriched isotopes with metallic zirconium powder as reductant agent. The thickness of the targets was determined by normalizing measured elastic cross sections to the results of optical model calculation. The reaction products were detected with a ΔE-E counter telescope which consisted of a 300 μm thick silicon surface barrier detector and a 5 mm thick Li-drifted silicon detector. Angular distributions were measured between 10° and 90°.

In Table 1, optical-model parameters used in DWBA calculations are given. Spectroscopic factors deduced from the present experiment are compared with theoretical predictions in Table 2. One can see that the present results for the $^{24}Mg(d, p)$ reaction are in overall agreement with the calculation with deformation parameter $\beta \approx 0.22$. The results for the $^{26}Mg(d, p)$ reaction seem to favor a positive value of β for ^{27}Mg. The shape of the angular distribution for the 1.61-MeV level of ^{25}Mg could not be reproduced by DWBA as expected. In addition, j-dependence in $\ell = 2$ angular distributions was clearly observed, which could not be explained by DWBA either.

In Figs. 1 and 2 some preliminary results of two-step and CCBA calculations are shown.*

* The two-step program TWOSTP by M. Igarashi and M. Toyama and the CCBA program CHUCK by P. D. Kunz are used.

It can be seen that the angular distribution for the 1.61-MeV level of ^{25}Mg can well be reproduced by these calculations. More detailed analyses are under way.

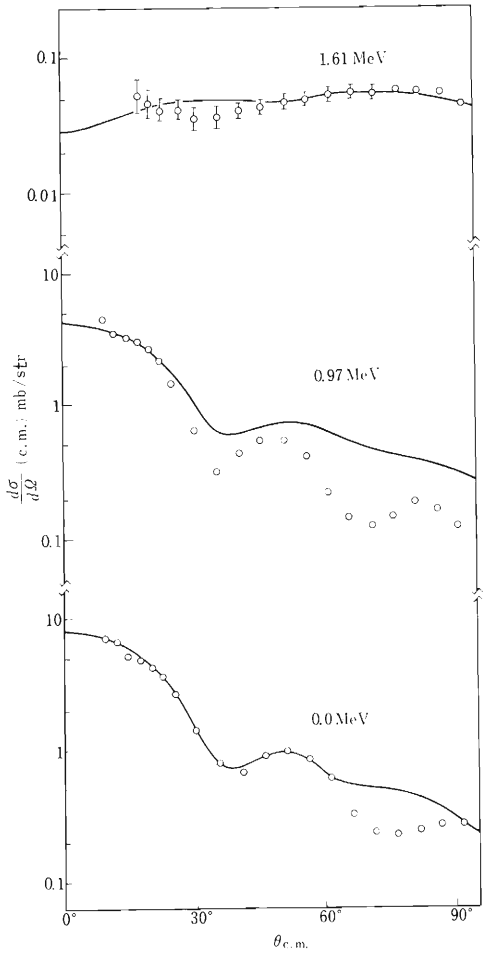

Fig. 1. Angular distributions from the ^{24}Mg(d, p) reaction. Solid lines are the results of two-step calculation.

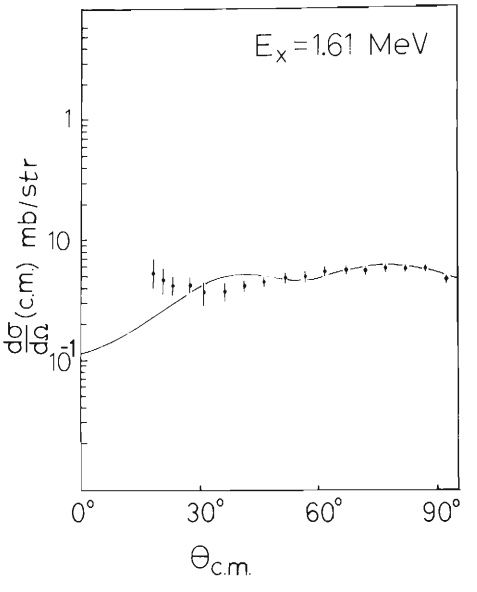

Fig. 2. CCBA calculation compared with the angular distribution for the 1.61-MeV level in ^{25}Mg.

References

1) G. Brown: Nucl. Phys., A232, 125 (1974).
2) C. M. Perey and F. G. Perey: Phys. Rev., 152, 923 (1966).
3) T. A. Schmick, K. W. Kemper, P. K. Bindal, and P. D. Koshel: ibid., C10, 556 (1974).
4) R. S. Mackintosh: Nucl. Phys., A170, 353 (1971).
5) B. Cujec: Phys., 136, B1305 (1964).
6) R. N. Glower: Phys. Lett., 16, 147 (1965).
7) J. M. Lacambra, D. R. Tilley, and N. R. Roberson: Nucl. Phys., A92, 30 (1967).
8) M. J. A. de Voigt and B. H. Wildenthal: ibid., A206, 305 (1973).

4-14. Proton-Unbound States Excited by Cr(^{3}He, d)Mn Reactions

N. Nakanishi

Angular distributions of deuteron were measured on the ^{50,52,54}Cr (^{3}He, d)^{51,53,55}Mn at an energy of 29.29 MeV, and many levels unstable to the proton emission were observed.[1] The angular distribution for the unbound state was found to be reproduced by employing the single particle resonance wave function as a proton form factor.[1]

Another approach using an isobaric analogue doorway state wave function[2] was tried to reproduce the differential cross sections. To describe the behavior of the transferred proton in the residual nucleus, the wave function is divided into three subspaces of the elastic scattering, doorway states and compound states using a projection operator method, that is,

$$|\Psi> = P|\Psi> + D|\Psi> + Q|\Psi>,$$

where P, D, and Q correspond to the three projection operators.

The resultant form factor is

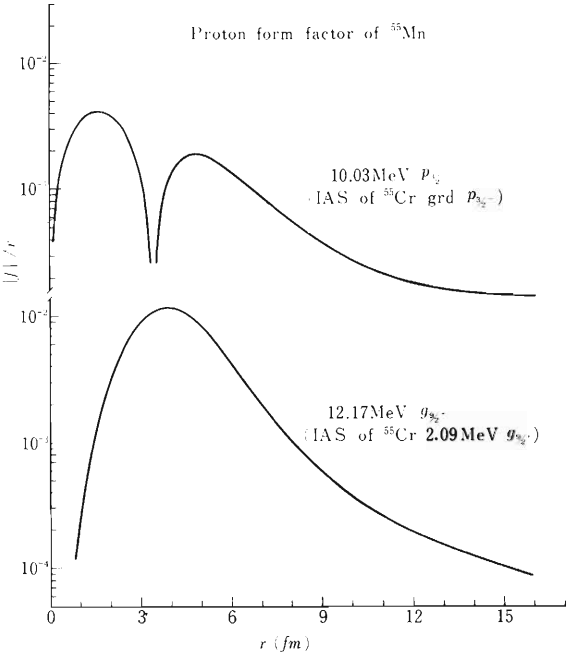

Fig. 1. Form factors corresponding to the 10.03 MeV $p_{3/2}$- and 12.17 MeV $g_{9/2}$+ levels of ^{55}Mn.

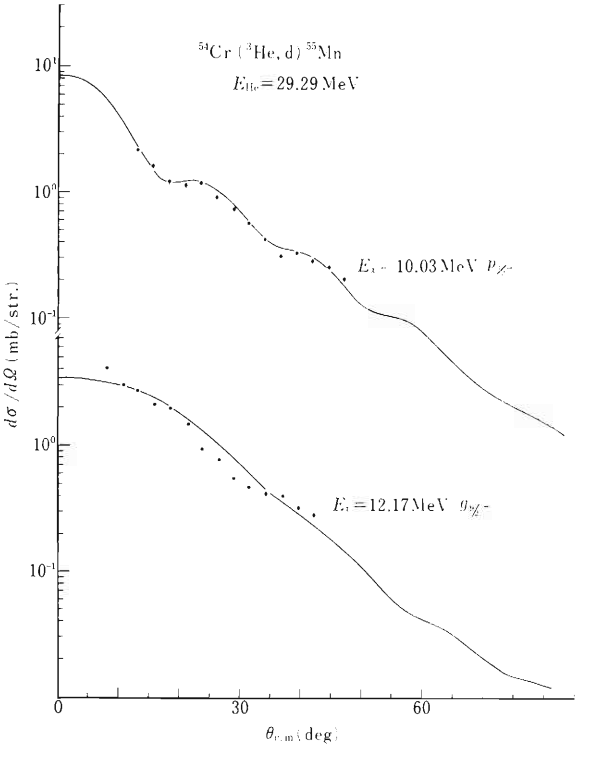

Fig. 2. Angular distributions for the ^{55}Mn 10.03 MeV $p_{3/2}$- and 12.17 MeV $g_{9/2}$+ levels. Calculated curves (solid lines) are adjusted to fit experimental points.

$$<C_r|\bar{P}+\bar{D}|M_n> = p^+ + \frac{1}{\sqrt{2T}}\sum_s \left\{ \frac{1}{E-h_p+i\varepsilon} <C_r|V_c^{(-)}|\pi_s> + <C_r|\pi_s> \right\} \cdot \frac{\gamma_s^{DP}}{E-E_s^R-\frac{1}{2}iP_s},$$

in which the bars of P and D represent energy-average over the fine structures of the compound states. The term h_p is the Hamiltonian which is modified to eliminate the overlap with doorway states from the usual optical model Hamiltonian, and the term p^+ is the eigenfunction to the Hamiltonian which describes the direct breakup of the ^{3}He particle. We can eliminate this term noticing resonance peaks only. The summation is made over dispersing doorway states, where $V_c^{(-)}$, E_s^R, Γ_s, and γ_s^{DP} are charge-changing Coulomb force, resonance energy of the doorway state, total width, and escape reduced width, respectively. Therefore, the second term corresponds to the part which goes to an elastic scattering channel from the doorway states and has an asymptotic form of the scattering state. The third term is for the doorway states and has a form of the bound state wave function of the parent nucleus.

Figure 1 shows the form factors corresponding to the 10.03 MeV $p_{3/2}$- and 12.17 MeV $g_{9/2}$+ levels of ^{55}Mn. These levels are the isobaric analogue states of ^{55}Cr ground $p_{3/2}$- and 2.09 MeV $9/2^+$ states, respectively. Figure 2 shows the angular distributions for these levels calculated using those form factors.

DWBA calculations were carried out using the DWBA 2-2 code.[3)]

References

1) N. Nakanishi, S. Takeda, H. Ohnuma, S. Yamada, H. Sakaguchi, M. Nakamura, S. Takeuchi, and K. Koyama: IPCR Cyclotron Progr. Rep., 7, 42 (1973); 8, 48 (1974).
2) M. Kawai, A. K. Kerman, and K. W. McVoy: Private communication.
3) M. Igarashi: Code I N S -DWBA 2-2.

4-15. Analysis of Elastic Scattering of ^{3}He on ^{13}C

T. Fujisawa, H. Kamitsubo, T. Wada
M. Koike, Y. Tagishi,* and T. Kanai**

The purpose of this analysis is to obtain the best-fit sets of optical potential parameters for elastic scattering of ^{3}He on ^{13}C at incident energies of 29.2, 34.7, and 39.6 MeV. The experimental procedure and results were reported previously.[1),2)] The optical model analysis has been carried out with SEARCH code.[3)] The used potential is of the form:

$$V(r) = -\left\{ V_0 f(x_R) + i4W_D \frac{d}{dx_D} f(x_D) + V_{so} \frac{(\sigma \cdot L)}{r} \left(\frac{\hbar}{m_\pi C} \right)^2 \frac{d}{dr} f(x_{so}) \right\} + V_c(r), \quad (1)$$

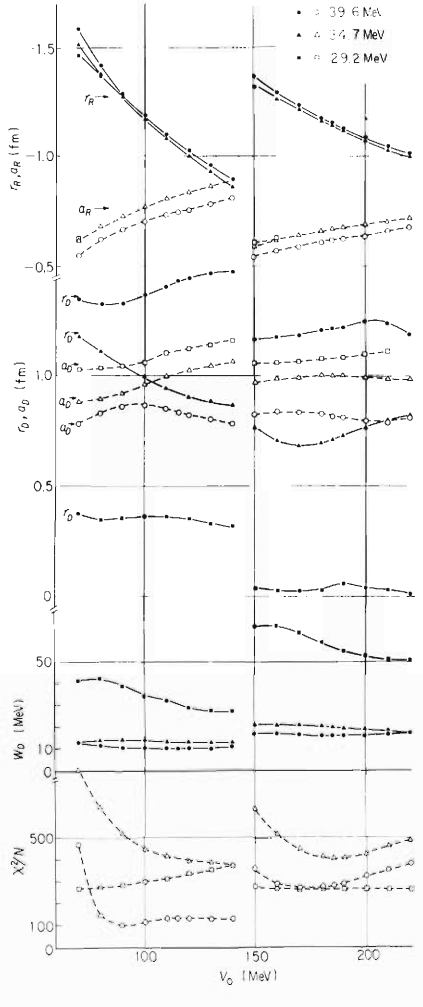

Fig. 1. Potential ambiguities given by five-parameter search at given values of V_0.

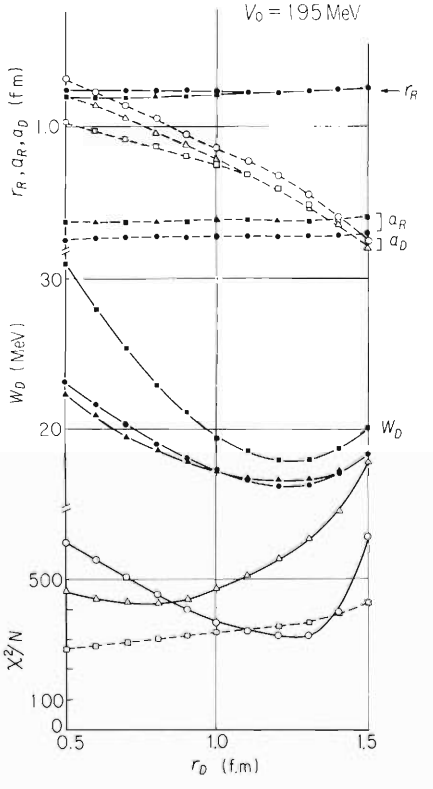

Fig. 2. Variations of W_D; r_R, a_R, a_D, and X^2/N as a function of r_d at V_0 = 195 MeV.

* Tsukuba Univ.
** Natl. Inst. of Radiological Sci.

where $f(x_i)=[1+\exp(x_i)]^{-1}$, $x_i=(r-r_i M^{1/3})/a_i$,

V_c = Coulomb potential due to a uniformly charged sphere of radius $1.4\ M^{1/3}$fm.

The set of parameters was determined by varying the parameters to minimize the quantity:

$$\chi^2=\sum_{i=0}^{N}\left[\frac{\sigma_{th}(\theta_i)-\sigma_{exp}(\theta_i)}{\Delta\sigma_{exp}(\theta_i)}\right]^2,$$

where $\sigma_{th}(\theta_i)$ and $\sigma_{exp}(\theta_i)$ are theoretical and experimental differential cross sections at the scattering angle θ_i, respectively, and $\Delta\sigma_{exp}$ is an error of σ_{exp}.

Figure 1 shows well-known ambiguities of the optical model parameters. The fitting procedure was as follows. The initial sets of parameters were selected according to a preliminary six-parameter search. The value of V_0 was increased or decreased step by step and five-parameter searches were made for a given value of V_0. The starting values of the other parameters for each search for a given V_0 were chosen to be the final values obtained for the adjacent value of V_0.

Since values of r_D are too small at 29.2 MeV in Fig. 1 so the authors examined variations of X^2/N, W_S, r_R, a_R, a_D as a function of r_D at fixed values of V_0. Figure 2 shows the r_D-dependence of the other parameters. We can see that the optimum points of X^2/N vary with incident energies.

The optimum optical model parameters for the fixed value of r_R = 1.1 fm are summarized in Table 1. The differential cross section calculated with these parameter sets are compared in Fig. 3 with the experiment. The following results are obtained from the comparison:

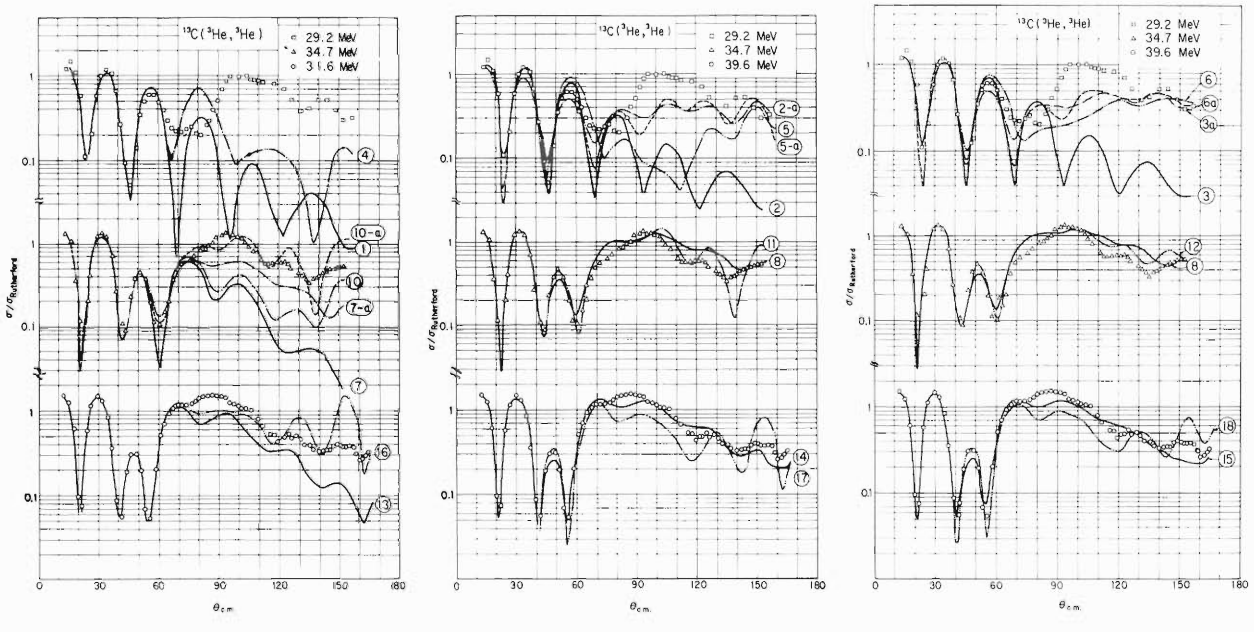

Fig. 3. Ratios of the elastic scattering differential cross section to the corresponding Rutherford cross section. Numbers indicate the potentials in Table 1 used in the optical model calculations.

Table 1. Optical model parameters at the optimum points of X^2/N. Values of r_R are fixed at 1.1 fm and values of r_{so} and a_{so} are equal to those of real parts.

V_o (MeV)	a_o (fm)	W_D (MeV)	r_D (fm)	a_D (fm)	V_{so} (MeV)	X^2/N	Data numbers for X^2 fit	σ_r (mb)	Potential number
$E_{^3He}$= 29.2 MeV									
80.1	0.845	25.7	1.43	0.632	0	158	25	1093	1
66.9	0.896	31.0	1.44	0.595	0	459	52	1081	2
66.9	0.897	31.4	1.44	0.594	1.84	460	52	1082	3
104	0.798	30.3	0.378	1.09	0	310	52	1190	2-a
105	0.798	33.6	0.237	1.13	3.92	289	52	1203	3-a
163	0.715	18.8	1.34	0.701	0	115	25	1096	4
138	0.706	14.6	1.12	0.903	0	425	52	1163	5
126	0.709	11.3	1.25	0.908	7.15	271	52	1183	6
194	0.690	50.7	0.0899	1.09	0	262	52	1185	5-a
193	0.689	52.7	0.0243	1.11	2.92	236	52	1191	6-a
$E_{^3He}$= 34.7 MeV									
103	0.763	14.4	1.42	0.750	0	235	25	1131	7
108	0.804	13.5	0.962	0.991	0	418	64	1159	8
108	0.804	13.4	0.963	0.993	1.24	417	64	1159	9
108	0.803	16.2	1.02	0.917	0	257	25	1143	7-a
182	0.651	16.7	1.19	0.859	0	247	25	1165	10
195	0.694	19.2	0.743	1.01	0	423	64	1159	11
194	0.691	20.6	0.588	1.08	2.27	322	64	1187	12
194	0.677	27.4	0.277	1.18	0	214	25	1230	10-a
$E_{^3He}$= 39.6 MeV									
111	0.739	12.2	1.45	0.772	0	74.2	25	1124	13
110	0.731	10.5	1.42	0.843	0	127	72	1153	14
110	0.732	10.6	1.42	0.835	1.75	110	72	1149	15
195	0.634	13.9	1.23	0.877	0	59.7	25	1150	16
198	0.643	16.1	1.24	0.814	0	311	72	1114	17
198	0.646	16.1	1.22	0.824	1.33	267	72	1116	18

1) The deep potentials are better than the shallow ones at forward angles.
2) The shallow potentials are better than the deep ones when all of the data points are used for fitting.
3) The potentials that have particularly small values of r_D are better than the others when all the data points are used for fitting.

The following problems were pointed out to be carried on:

1) Use of the mixture of surface type and volume type potentials to the imaginary parts.
2) The effect of compound nucleus.
3) The effect of coupling between the elastic channel and others.
4) The effect of two-step process such as $^{13}C(^3He, \alpha)(\alpha, ^3He)^{13}C$.

References

1) T. Fujisawa, H. Kamitsubo, T. Wada, M. Koike, Y. Tagishi, and T. Kanai: IPCR Cyclotron Progr. Rep., 7, 46 (1973).
2) T. Fujisawa, H. Kamitsubo, T. Wada, M. Koike, Y. Tagishi, and T. Kanai: ibid., 8, 34 (1974).
3) T. Wada: Reports I.P.C.R., (in Japanese), 46, 21 (1970).

4-16. Effect of (^{3}He, α) (α, ^{3}He) Two-Step Process in Elastic Scattering of ^{3}He on ^{13}C

T. Matsuura

Optical model analysis of elastic scattering of ^{3}He from nuclei has attracted much interest because of wide ambiguity in the resulted potential parameters.[1), 2)] Recently, elastic scattering of ^{3}He from ^{13}C at E_{Lab} = 29.2, 34.7, and 39.6 MeV has been extensively studied by Fujisawa with a standard optical model.[3)] It has been pointed out that an automatic parameter search including data in a whole range of angle (θ_{CM} = 15° – 160°) ended up with peculiar geometrical parameters in the imaginary potential (e.g., $r_D \to 0$ fm, $a_D \to 1.7$ fm) which are contradictory to the standard values of a conventional optical model (e.g., obtained in case of heavier target nuclei),[1)] while standard parameter sets give a reasonable fit for forward angle data ($\theta_{CM} \lesssim 90°$).

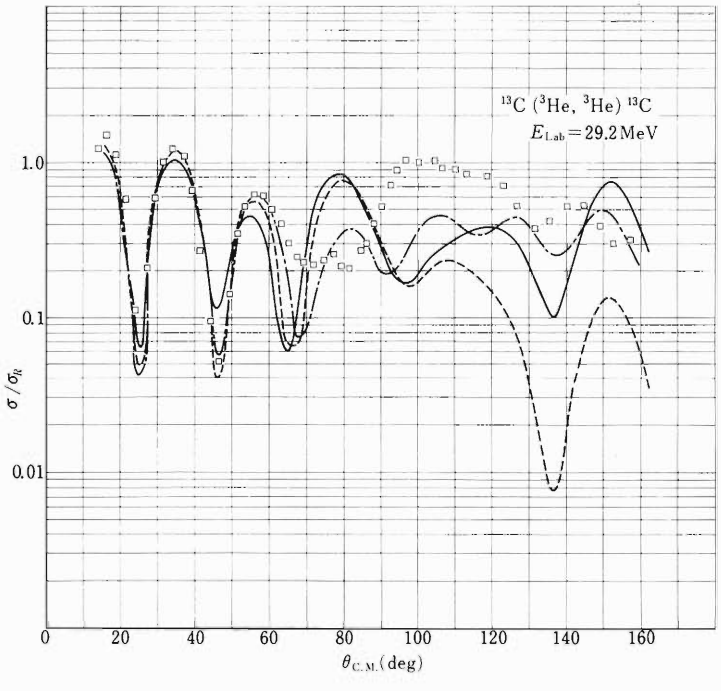

Fig. 1. ^{3}He + ^{13}C elastic scattering cross sections (ratio to Rutherford cross section) at E_{Lab}=29.2 MeV. The blank squares represent the experimental values of σ/σ_R. The solid and the broken lines represent the results of optical potential scattering (Potential No. 4 in Ref. 3-conventional) with and without coherent mixing of the amplitude from (^{3}He, α) (α, ^{3}He) two-step process, respectively. The dot-and-dash line shows the result of optical model analysis using the whole range of data (Potential No. 5-a in Ref. 3 with the peculiar parameter values as mentioned above).

This indicates the possible contribution of coupling of inelastic or reaction channels with ^{3}He elastic channel in backward angles.[4] Here re-examination of optical model analysis was intended with explicit inclusion of the contribution from two-step process of pickup-stripping (^{3}He, α) (α, ^{3}He), in order to see whether or not this reaction process is responsible for the above-mentioned peculiar parameters of conventional optical model. A preliminary result of elastic scattering cross section (Rutherford ratio, $\sigma_{el}(\theta) / \sigma_R(\theta)$) with and without coherent mixing of the two step amplitude is shown in Fig. 1. A considerable effect is seen in backward angles ($\theta_{CM} \gtrsim 90°$) since the optical potential scattering cross section drops very steeply with angle while the contribution from the (^{3}He, α) (α, ^{3}He) process shows rather flat angular distribution which becomes comparable with Coulomb scattering in large angles. Search for optimum values of this optical model is in progress.

References

1) T. Fujisawa, H. Kamitsubo, T. Wada, and M. Igarashi: J. Phys. Soc. Japan, 27, 278 (1969).
2) T. Fujisawa, S. Yamaji, K. Matsuda, S. Motonaga, F. Yoshida, H. Sakaguchi, and K. Masui: ibid., 34, 5 (1973).
3) T. Fujisawa: IPCR Cyclotron Progr. Rep., 9, 46 (1975).
4) J. R. Shepard, P. D. Kunz, and J. J. Kraushaar: Phys. Lett., 56B, 135 (1975).

4-17. Alpha-Gamma Angular Correlation Measurement for the $^{13}C(^{3}He, \alpha\gamma)^{12}C(4.43\ MeV)$ Reaction

T. Fujisawa, T. Matsuura, H. Kamitsubo, T. Wada,
M. Koike, Y. Tagishi,* and T. Kanai**

Angular correlations of α-particles leading to the first excited state in ^{12}C with following gamma rays were measured for the $^{13}C(^{3}He, \alpha)^{12}C^{*}$ reaction at a bombarding energy of 29.2 MeV.

The symmetry property of the reaction matrix[1] or the Bohr theorem[2] gives the relation in a reaction A(a, b)B,

$$M_A - M_B + m_a - m_b = \text{even/odd as } \Delta\pi = \text{even/odd}, \qquad (1)$$

where M_A and M_B are z-components of spins of nuclear states A and B, m_a and m_b are those of particles a and b, respectively, and $\Delta\pi(= \pm 1)$ is the overall parity change in the reaction. From Eqn. (1) there is a simple spin relation in the reaction $^{13}C(^{3}He, \alpha)^{12}C^{*}(4.43\ MeV, 2^{+})$ as shown in Table 1.

Ions of ^{3}He were accelerated with the cyclotron. The beam intensity was kept below 10 nA in order to reduce the chance coincidence. The target was a self-supporting foil of ^{13}C of about 700 $\mu g/cm^2$ in thickness and the purity was 90 %. Emitted particles were detected with a surface barrier detector 2000 μm thick and gamma rays were measured with a 7.6 cm × 7.6 cm NaI(Tl) crystal mounted on a 56 AVP photomultiplier. The gamma detector was placed perpendicular to the reaction plane and shielded with a lead cylinder.

Singles spectra of α-particles were measured at the same time as spectra coincident with the 4.43 MeV gamma rays. Then a ratio of coincidence yields to singles yield was obtained for

Table 1. Relation of spin directions of ^{3}He and ^{13}C, magnetic substate of ^{12}C, and γ-rays.

Spin directions of ^{3}He and ^{13}C	Magnetic substates of the 2^{+} level excited by the reaction	Whether γ-rays are emitted to the z direction (normal to the reaction plane)
Parallel	0, or ± 2	not emitted
Antiparallel	1	Emitted

* Tsukuba Univ.
** Natl. Inst. of Radiological Sci.

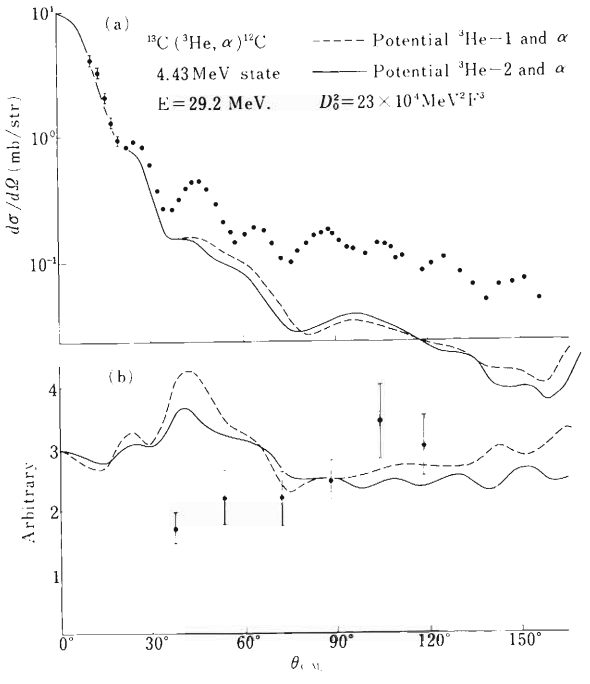

Fig. 1. Differential cross sections of $^{13}C(^3He,\alpha)^{12}C^*(4.43\ MeV)$ (a) and ratios of coincident yield to the singles yield (b).

α-particles leaving ^{12}C in the first 2^+ state. In case of the inelastic scattering, this ratio corresponds to the spin flip probability. Figure 1 shows the angular dependence of this ratio and the angular distribution of α_1 with predicted values by DWBA.[3] The code used was a modified version of DWBA-2.[4] The optical parameters shown in Table 2 give the best fit to the elastic scattering without spin-orbit coupling.[5),6)] The values of V_{so} differ from values given by the optical model calculation.[5)] The experimental values of the cross section and the correlation function are not well reproduced by this analysis. It is, however, noteworthy that the populations of the magnetic substates of the first 2^+ state of ^{12}C predicted by DWBA analysis with any sets of optical parameters are 60%, 30%, and 10% for ±2, ±1, and 0 respectively, if it were not any spin dependent force in the reaction. The deviation of the observed population for ±1 states from the constant value clealy shows the importance of spin dependent force.

Table 2. The optical-model parameters of ^{3}He and α on ^{13}C and ^{12}C.

Potential name	Vo (MeV)	r_R (fm)	a_R (fm)	W_D (MeV)	r_D (fm)	a_D (fm)	V_{so} (MeV)	R_c (fm)
^{3}He-1	105.7	1.1	0.8	24.3	0.57	1.04	8	1.4
^{3}He-2	105.7	1.1	0.8	24.3	0.57	1.04	4	1.4
α	179	1.3	0.7	12	1.3	0.7	0	1.3

References

1) F. Rybicki, T. Tamura, and G. R. Satcher: Nucl. Phys., A146, 659 (1970).
2) A. Bohr: Nucl. Phys., 10, 486 (1959).
3) E. M. Kellogg and R. W. Zurmuhle: Phys. Rev., 152, 890 (1966).
4) M. Igarashi: Code I.N.S.–DWBA 2–2.
5) T. Fujisawa, H. Kamitsubo, T. Wada, M. Koike, Y. Tagishi, and T. Kanai: IPCR Cyclotron Progr. Rep., 8, 34 (1975).
6) S. Yamaji, T. Fujisawa, H. Kamitsubo, K. Matsuda, S. Motonaga, F. Yoshida, H. Sakaguchi, and K. Masui: J. Phys. Soc. Japan, 37, 1191 (1974).

5. NUCLER PHYSICS

Nuclear Spectroscopy

5-1. Gamma-Gamma Coincidence Study of the ^{92}Mo and ^{94}Mo + C Reactions

A. Hashizume, H. Kumagai,
Y. Tendow, and T. Katou

Observation of γ-rays in the decay process after compound nucleus formation gives information about yrast levels and side band levels. However, many channels are opened in the decay of compound nuclei formed by heavy ion reactions and the γ-ray spectra have very complex nature. Though its interpretation becomes rather difficult, the γ-γ coincidence method gives a promising means to analyze such spectra.

Enriched ^{92}Mo and ^{94}Mo targets were bombarded with 80 MeV C-ions to obtain more definite information about the levels in ^{100}Cd and ^{102}Cd produced by the (C, 4n) reaction. The detection of γ-rays was made with 23 and 50 cc Ge(Li) detectors. They were placed at about 55° to each side of the beam direction to avoid strong 511-511 keV coincidence caused

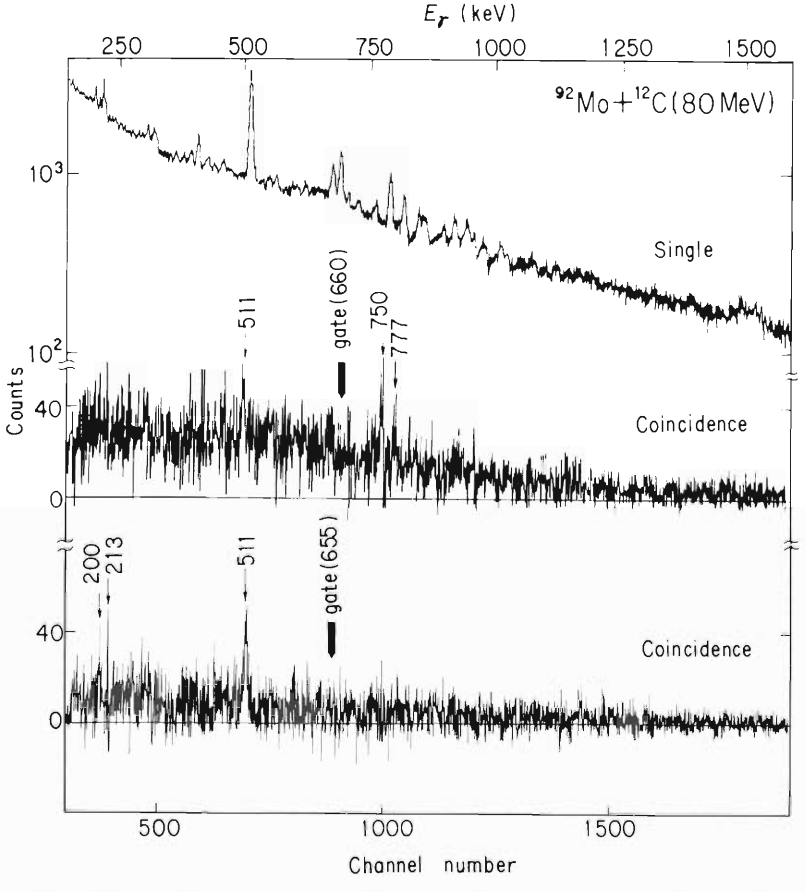

Fig. 1. Singles γ-ray and coincidence spectra observed when ^{92}Mo was bombarded with 80 MeV ^{12}C-ions.

by annihilation radiations of positrons which were emitted from reaction products. Time resolution of the coincidence which was measured using γ-rays from ^{60}Co was 23 ns (FWHM). Accidental coincidence was also monitored by opening the gate after 210 ns from coincidental timing.

In case of ^{92}Mo + C reaction, the coincidence gates were opened at more than 20 places in the spectrum above 511 keV by using digital gates and the coincidence relation of γ-rays was examined. The coincidences between 660, 750, 777, and 804 keV γ-rays were confirmed. The 655 keV γ-ray is emitted from radioactive isotopes and coincidence with the 511 keV γ-ray was observed. Figure 1 shows the spectra obtained at 655 and 660 keV gates. In both coincidence spectra the effect of higher γ-rays was eliminated by opening the gate at 670 keV and by making subtraction from the former spectra.

For the ^{94}Mo + C reaction, the strong γ-rays of 557 and 719 keV energies observed in the singles spectrum were due to decay of radioactive isotopes and found to coincide each other. The 666 keV γ-ray coincides with 143, 189, and 511 keV γ-rays. These situations are illustrated in Fig. 2. We are making further reduction and analyses of data stored event by event in magnetic tapes and the information on the excited levels in ^{100}Cd and ^{102}Cd will be obtained together with the results of excitation functions.

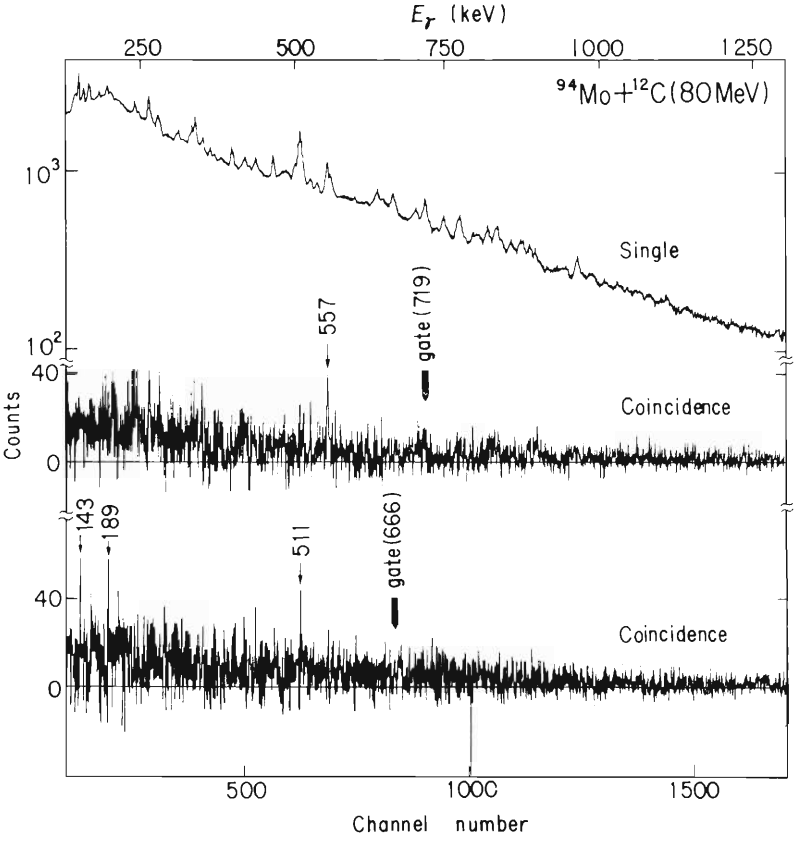

Fig. 2. Singles γ-ray and coincidence spectra observed when ^{94}Mo was bombarded with 80 MeV ^{12}C-ions.

5-2. Cross Sections for ^{88m}Y and ^{90m}Nb via ^{89}Y + α Reaction (2)

A. Hashizume, Y. Tendow,
T. Katou, and H. Kumagai

During the study on nuclear isomers in the ms region of half-lives, a high spin state (8^+, $T_{1/2}$ = 14 ms at 675 keV) in ^{88}Y was found to be excited when ^{89}Y was bombarded with α-particles. The relative excitation functions and the ratios of the yield of this state to the 382 keV (1^+, $T_{1/2}$ = 6.2 ms) state in ^{90}Nb as a function of E_α were reported previously.[1] As such a high spin state is not excited by a direct reaction process,[2] it is believed that the state is excited following the evaporation of α-particles from a compound nucleus.

The levels in ^{88}Y and ^{90}Nb are shown in Fig. 1. The γ-ray energies from 8^+ state to 5^- state and 5^- to ground state were determined to be 442.9 ± 0.4 and 231.8 ± 0.5 keV respectively. The energy of 8^+ state is 674.7 ± 0.7 keV. Cross sections for the 675 keV state

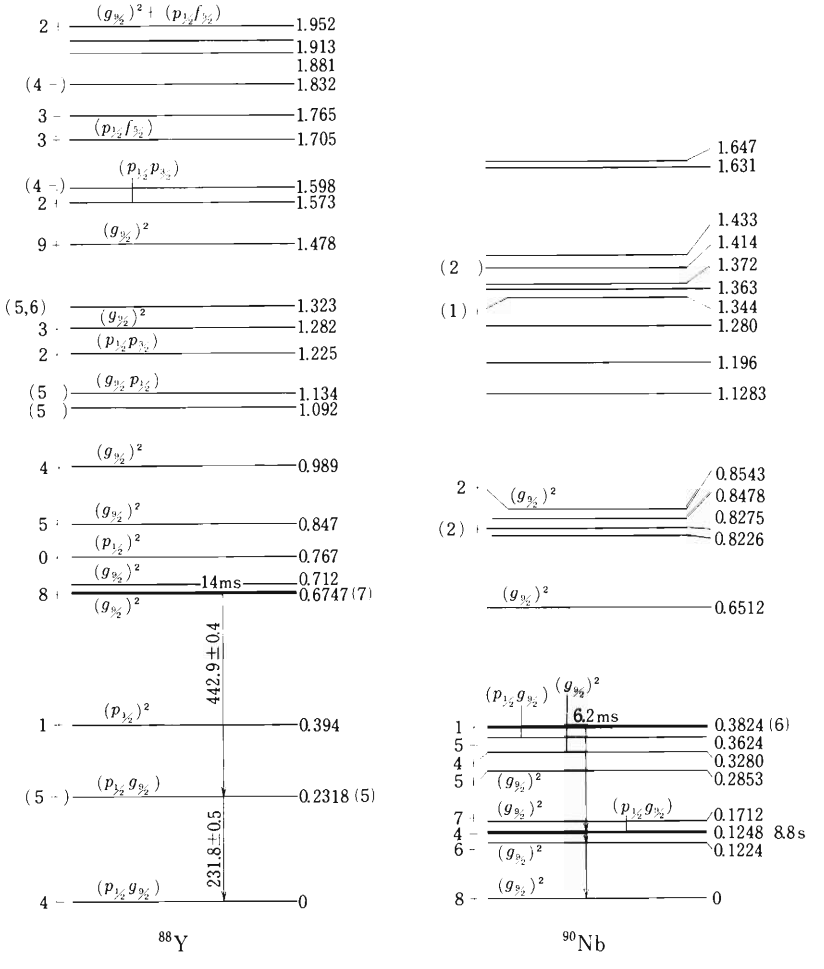

Fig. 1. The excited states in ^{88}Y and ^{90}Nb. The energy of the first 8^+ state in ^{88}Y was measured in the present experiment.

in ^{88}Y and the 382 keV state in ^{90}Nb were measured using Y_2O_3 targets. The mean thicknesses of the targets were 7.40 and 5.34 mg/cm^2. The inhomogeneity of the targets was examined by the x-ray absorption method. The x-rays emitted from ^{241}Am were collimated to 2 mm ϕ and the target was scanned by this x-ray beam, and the thickness of the target was corrected for this inhomogeneity on α-beam position. In a typical experiment, the target was bombarded with α-particles for 5.3 ms and γ-ray measurement was made during 40 ms starting at 5 ms after the end of irradiation and this cycle was repeated. The time and energy spectra were taken by a two-dimensional multichannel analyzer. The decay curve analyses give half-lives of 13.8 ± 0.18 and 6.19 ± 0.08 ms for ^{88m}Y and ^{90m}Nb respectively. The absolute efficiency curve of a pure Ge detector in the experimental set-up was determined as shown in Fig. 2. The preliminary results of the cross sections obtained are shown in Table 1.

Following a statistical model formalism developed by Huizenga and Vandenbosch[3] for the calculation of isomer's ratios in nuclear reactions, programs are being developed to investigate the yield of these isomers. For the estimation of compound nucleus formation cross sections, the transmission coefficients T_ℓ of incident α-particles for yttrium target were calculated by using an approximation of a parabolic potential or an optical potential. The real and imaginary well parameters of the latter potential were taken from the experiment of Park et al.[2] and

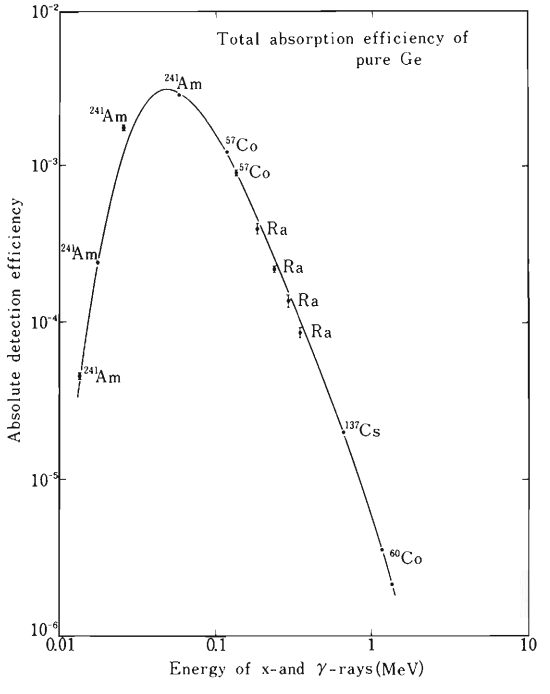

Fig. 2. The absolute efficiency curve of a pure Ge detector.

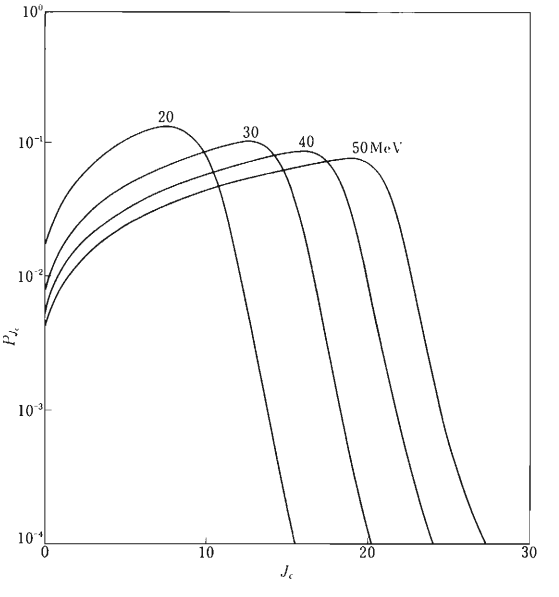

Fig. 3. The normalized spin distribution of compound nucleus when ^{89}Y was bombarded with α-particles. J_C is the spin of compound nucleus, PJ_C is its probability, and the parameter is the energy of incident α-particles in laboratory system.

the program SEARCH was used for the deduction of T_ℓ. Figure 3 shows the normalized initial compound spin distribution when ^{89}Y was bombarded with α-particles. Further analysis is in progress.

Table 1. Cross sections to produce 8^+ state in ^{88}Y and 1^+ state in ^{90}Nb.

Nuclei	Energy of state	Spin and parity	Cross section
^{88}Y	674.7 ± 0.7	8^+	24 ± 2 mb
^{90}Nb	382.4 ± 0.6	1^+	5.8 ± 0.7

References

1) A. Hashizume, Y. Tendow, T. Katou, and H. Kumagai: IPCR Cyclotron Progr. Rep., 8, 76 (1974); A. Hashizume, H. Kumagai, Y. Tendow, and T. Katou: Nucl. Instr. Meth., 119, 209 (1974).

2) Y. S. Park, H. D. Jones, and D. E. Bainum: Phys. Rev., 4, 778 (1971).
J. R. Comfort and J. P. Shiffer: ibid., 4, 803 (1971).

3) W. L. Hafner, Jr, J. R. Huizenga, and R. Vandenbosch: ANL-6662 (1961).

5-3. The Decay of ^{119m}Te

M. Yambe,* M. Hirasawa,* M. Fujioka, M. Ohshima,*
J. Katakura,* S. Hayashibe,* and T. Ishimatsu*

The low lying level scheme of ^{119}Sb has been investigated by means of the decay of ^{119m}Te ($T_{1/2}$ = 4.7 days). Internal conversion electrons and γ-rays were measured with an INS $\sqrt{2\pi}$ iron-free magnetic β-ray spectrometer and 70 and 33 cc Ge(Li) detectors, respectively. Eleven transitions were newly added to the decay scheme previously suggested by Berzins and Kelly[1] and Graeffe et al.[2]

Enriched tin metal was obtained from SnO_2 (^{118}Sn 95.75 %) by the KCN reduction method,[3] and was bombarded with a 44 MeV alpha beam accelerated in the cyclotron. Radioactive tellurium was chemically separated from the target by an ion exchange method, and the carrier-free source was spontaneously deposited onto a copper foil in a 4N-HCl solution.

Singles γ-ray spectra are shown in Figs. 1 and 2. Transition energies, relative intensities of

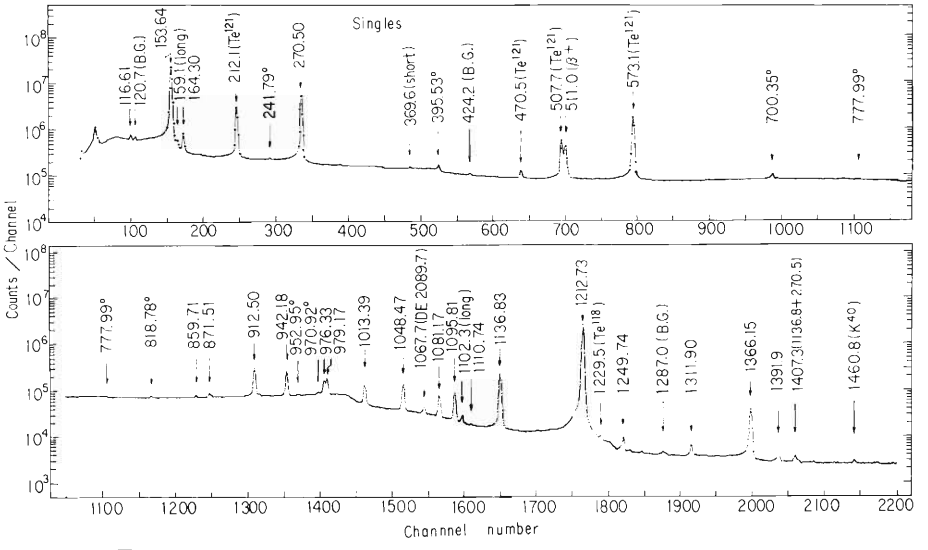

Fig. 1. Singles γ-ray spectrum (lower energy part).

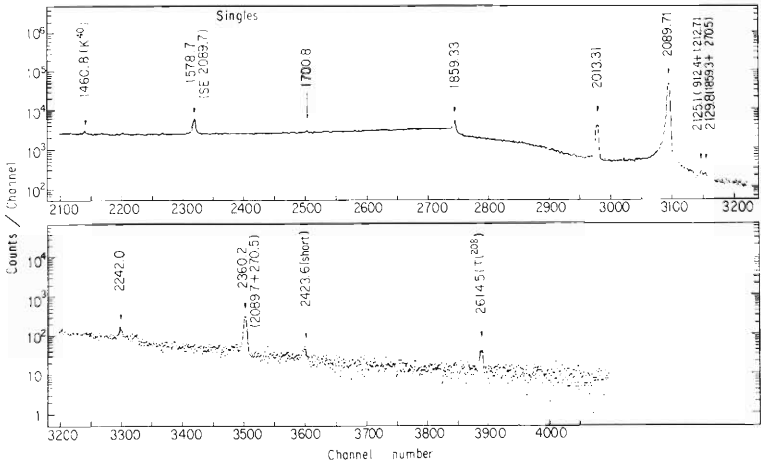

Fig. 2. Singles γ-ray spectrum (higher energy part).

* Department of Physics, Tohoku University

Table 1. Observed γ-rays and electrons in the decay of ^{119m}Te.

γ-ray		Conversion electron			
E_1 (keV)	I_γ	E_2 (keV)		$E_1 - E_2$ (keV)	α_K ($\times 10^{-3}$)
116.61	0.68 (4)[a]	116.591	(91)	0.02	87 (21)
153.64	100.3 (35)	153.601	(86)	0.04	49.4 (9)[b]
164.30	1.94 (8)	164.353	(92)	−0.05	136 (17)
241.79	0.09 (2)				
270.50	42.3 (6)	270.526	(42)	−0.03	35.4 (24)
395.53	0.51 (2)	395.416	(80)	0.11	3.69 (86)
700.35	0.70 (6)	700.33	(11)	0.02	3.00 (65)
777.99	0.10 (2)				
818.78	0.16 (4)				
859.71	0.24 (4)	859.67	(13)	0.04	2.75 (84)
871.51	0.58 (5)				
912.50	9.44 (16)	912.513	(75)	−0.01	1.75 (10)
942.18	7.69 (12)	942.194	(78)	−0.01	1.52 (8)
952.95	0.13 (4)				
970.92	0.35 (9)	[c]			1.20 (35)[d]
976.33	4.10 (11)	976.317	(87)	0.01	0.59 (6)
979.17	4.55 (12)	979.285	(84)	−0.12	1.57 (13)
1013.39	3.78 (9)	1013.205	(90)	0.18	0.76 (10)
1048.47	4.82 (9)	1048.419	(87)	0.05	1.22 (10)
1081.17	2.41 (7)	1081.32	(12)	−0.15	0.48 (5)
1095.81	3.38 (7)	1095.708	(80)	0.10	2.89 (17)
1110.74	0.02 (2)				
1136.83	11.6 (2)	1136.718	(91)	0.11	0.89 (6)
1212.73	100	1212.727	(68)	0.00	0.78 (2)[e]
1249.74	0.26 (2)				
1255.35	0.02 (1)				
1311.90	0.19 (2)				
1366.15	1.61 (4)	1366.339	(95)	−0.19	1.08 (19)
1391.90[f]	0.05 (1)				
1700.79[f]	0.03 (1)				
1859.33	0.21 (3)				
2013.31	0.48 (2)				
2089.71	7.08 (13)	2089.535	(132)	0.18	0.134 (11)
2242.00[f]	0.01 (1)				

a) The number within the parentheses gives the error of the number belonging to the lowest order of most probable value.

b) For the 116.6 and 164.3 keV transitions, the electron intensities were normalized using the theoretical α_K of the 153.6 keV transition, which was uniquely determined to be of E1 from the experimental K/L ratio.

c) Masked by the 942.2 keV M-line.

d) Corrected using the theoretical 942.2 keV M-conversion coefficient (the K/M ratio hardly depends upon the transition multipolarity).

e) For the transitions other than those mentioned in b), the electron intensities were normalized assuming the 1212.7 keV transition to be of pure E2.

f) Line not placed in the decay scheme.

γ-rays, and K-internal conversion coefficients are summarized in Table 1 and the proposed decay scheme in Fig. 3.

Graeffe et al.[2] suggested that the spin-parity of 1407.3 keV level was $9/2^-$, which was an "intruder" state, from the internal conversion electron measurements of the 1136.8 keV transition with a Si(Li) detector. We obtained, however, a conversion coefficient different from their rude data with the iron-free spectrometer. The observed conversion coefficient of the 1136.8 keV transition is apparently not of E1 but of M1-E2. Therefore, the spin-parity of the 1407.3 keV state is concluded to be $9/2^+$ or $11/2^+$.

The 1013.4 keV transition from the 2226.1 keV level ($9/2^-$, $11/2^-$) to the 1212.7 keV level ($9/2^+$) is expected to be of E1, but the experimental conversion coefficient is apparently larger than the theoretical E1 value. If there is no anomalous conversion phenomenon, the 1013.4 keV peak should be a doublet. On the other hand, the 1013.4 keV peak partly appeared in the γ-γ coincidence measurements with the 153.6 keV photopeak gate. These facts suggest that a part of the 1013.4 keV peak is an E1 transition to the 1212.7 keV level and the other part is an M1-E2 or larger-multipolarity transition to the 1366.2 keV level. There may be a new level at 2380 keV, which is also supported by a new 972.7 keV peak coincident with the 1136.8 keV peak gate. This 972.7 keV peak does not appear in singles γ-ray spectrum, because it is masked by the 970.9 keV, 976.3 keV, and 979.2 keV triplet peak.

It is interesting to compare the level scheme of ^{119}Sb with the core-particle coupling model. The analysis is now in progress.

The authors wish to thank Dr. A. Hashizume for his efforts with the cyclotron bombardment, and the cyclotron crew for their operation.

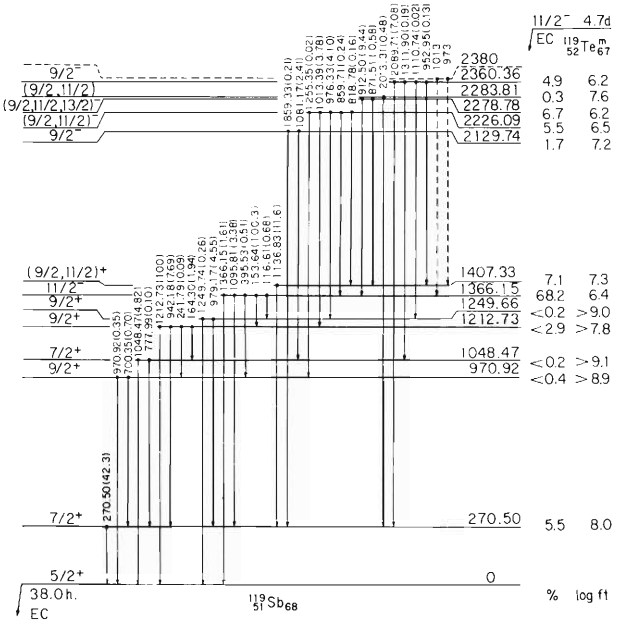

Fig. 3. Proposed decay scheme of ^{119m}Te.

References

1) G. Berzins and W. H. Kelly: Nucl. Phys., A104, 263 (1967).

2) G. Graeffe, E. J. Hoffman, and D. G. Sarantites: Phys. Rev., 158, 1183 (1967).

3) F. Ambe: Private communication (1975).

6. NUCLEAR INSTRUMENTATION

6-1. β-Ray Source Mounting onto a Foil Electrode in a Xenon Gas Chamber

M. Ohshima,* M. Hirasawa,* S. Hayashibe, M. Yambe,*
I. Katakura,* M. Fujioka, T. Ishimatsu,* and A. Hashizume

In this report, we describe a new method for β-ray source preparation. This method is very efficient for alkali metal or alkaline earth isotopes. We employ this method to measure the conversion electrons from the decay of ^{136}Cs.

So far, the ^{136}Cs was produced by (d, α) reaction,[1), 2)] (γ, pn) reaction,[3)] and nuclear fission.[4)] Usual methods for source preparation such as vacuum evaporation, electrodeposition, electrospraying or isotope separation methods need complex devices. Further, these methods often require difficult and time-consuming separation techniques to obtain carrier-free sources. The present approach, on the other hand, has the advantage of great simplicity. When a target chamber filled with noble gas (in our case natural Xe) is bombarded with a proton beam, the reaction products (Cs isotopes) would be ionized through nuclear recoil. Under an electric field the ions can be collected onto an electrode. Namely, the Cs ions can be attached to an electrode foil due to its affinity, but the ionized Xe ions cannot be attached due to its inertness. The

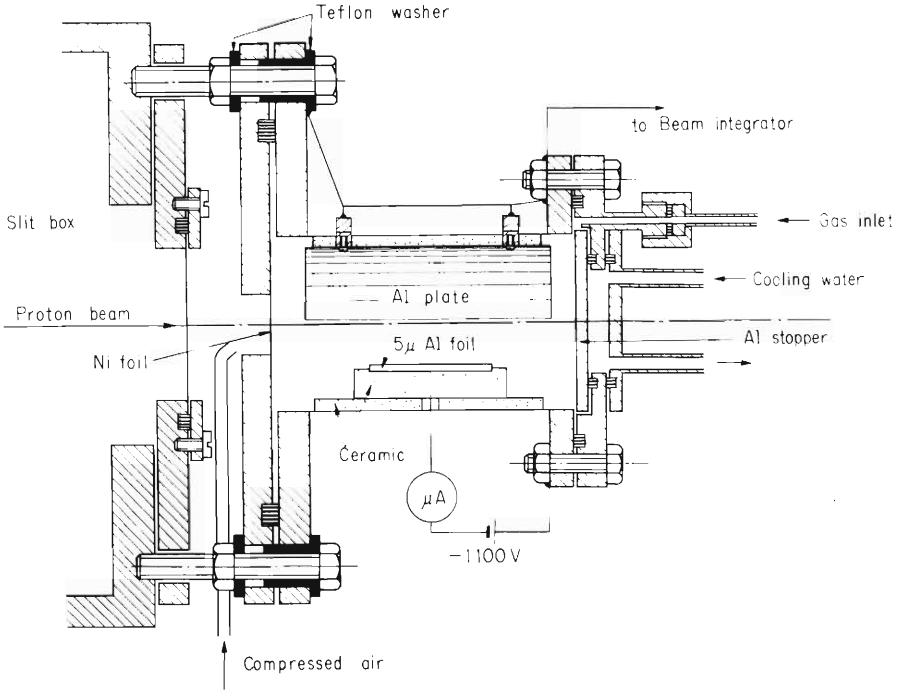

Fig. 1. Cross sectional view of Xe target chamber.

* Tohoku University

electrode foil can be used directly as β-ray source.

The gas chamber is illustrated in Fig. 1. Xe gas was transferred into the chamber from a storage container by freezing the gas with liquid nitrogen. The proton beam was stopped in the chamber which served also as a Faraday cup. To obtain a suitable electric field we made the main part of the chamber of ceramics. The beam stopper and the entrance window foil were cooled with water and compressed air respectively. The electrode was made of 5 μm Al foil to prevent back scattering of electrons during the conversion electron measurement and a potential of -1100 V was applied with respect to the Faraday cup. The positive electrode was made of a semi-cylindrical Al plate.

The energy and current of the proton beam from the cyclotron were 15 MeV and 10 – 20 μA respectively. The target chamber was mounted behind the slit box at the end of the external bombardment channel. The ^{136}Cs activity was made by ^{136}Xe (p, n) reaction (natural abundance of ^{136}Xe : 8.87 %). The gas pressure was about 3 atm, and the effective foil dimension 1.5 mm $\times$ 40 mm. The electrode current was about 10 μA under the beam current of 10 μA. After the bombardment the foil electrode was taken out and mounted onto an Al holder for β-ray spectrometry.

The β-ray was measured with the INS Air-Core β-ray spectrometer. Fig. 2 shows typical K and $L_{I, II, III}$ conversion electron spectra for 163.8 keV transition (2030.3 keV 7^- to 1866.5 keV 4^+ in ^{136}Ba). The instrumental resolution of the spectrometer was 0.05 %.

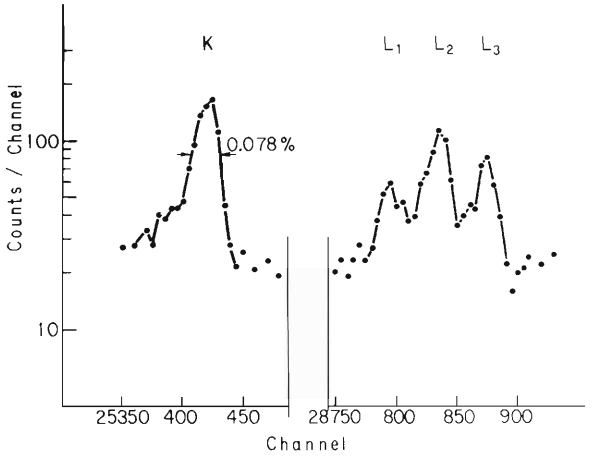

Fig. 2. Typical conversion electron spectrum for 163.8 keV E3 transition in ^{136}Ba.

There remain two problems in this technique: activity collection efficiency and source quality. The collection efficiency obtained now amounts to 20 – 36 %, but this is not sufficient. The electric field distribution in the chamber has a large influence on the efficiency. More suitable chamber with improved field distribution will increase the activity collection. A thick source leads to spectrum distortion due to self-absorption of electrons. In this method a contamination such as an organic substance inside the chamber will seriously affect the source quality. So far, a white substance can be recognized on the foil and it is rather difficult to make the foil free of this substance. These two points are open to further improvement.

References

1) Chr. Bargholtz, L. Eriksson, L. Gidefeldt, L. Holmberg, and V. Stefánsson: Z. Physik, 260, 1 (1973).
2) R. Reising and B. D. Pate: Nucl. Phys., 65, 609 (1965).
3) S. Hayashibe, M. Ohshima, M. Yambe, J. Katakura, and T. Ishimatsu: Research Report of Laboratory of Nuclear Science, Tohoku University, 7, 312 (1974).
4) M. Fujioka, T. Miyachi, and H. Adachi: Nucl. Phys., A95, 577 (1967).

6-2. Elimination of Unnecessary Peaks by Recoil Coincidence Technique

T. Motobayashi, I. Kohno, T. Ooi, and S. Nakajima

When we studied the reaction $^{16}O(^{14}N, ^{13}N)^{17}O$[1] using a Li_2CO_3 target, the peak of the ground state transition of the reaction $^{12}C(^{14}N, ^{13}N)^{13}C$ overlaps the peaks of the reactions on ^{16}O populating the $1/2^+$ and $5/2^+$ states of ^{17}O. In order to eliminate the peak of $^{12}C(^{14}N, ^{13}N)^{13}C$, a recoil coincidence technique was employed. This technique has been used[2] in low energy reactions studied at intermediate angles (50° – 130°), where the energies of two particles in coincidence are relatively high. Since in our case the incident energy of ^{14}N was high (79 MeV), emitted particles (^{13}N) have large yield only at the forward angles where the energy of associated recoil particles (^{17}O) is small (2-10 MeV). Therefore a main problem is how to detect such low energy particles in sufficient efficiency.

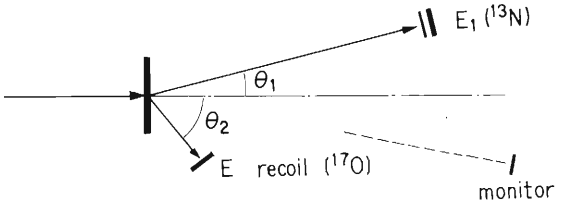

Fig. 1. Detection system used.

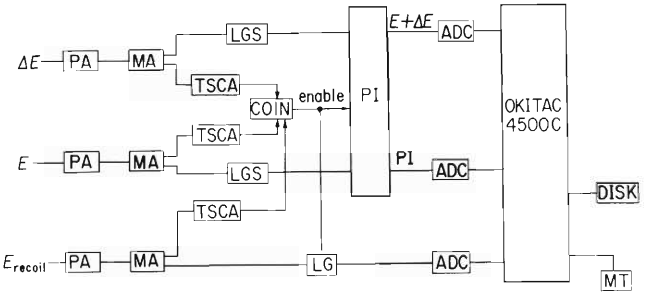

Fig. 2. Block diagram of the circuit.

Figure 1 shows the arrangement of the detectors. The recoil counter system has a large solid angle (28 msr) to obtain large coincidence efficiency and consists of 60 μm – 400 mm^2 SSD and an electron suppressing magnet. As shown in Fig. 2, ΔE and E signals were converted to E + ΔE and PI signals by a particle identifier, and these signals together with the signals of the energy of recoil particle (E_{recoil}) were recorded on a magnetic tape. Typical spectra of PI and E_{recoil} are shown in Fig. 3, together with an energy spectrum of the reaction $^{16}O(^{14}N, ^{13}N)^{17}O$ which was obtained by putting gates on the appropriate positions shown by arrows in Fig. 3. of PI and E_{recoil} spectra. It should be noticed that taking the coincidence (between E + ΔE and E_{recoil} signals) only is not good enough to distinguish the reactions on ^{12}C and ^{16}O. Information on the energy of the recoil particles is absolutely needed in addition.

The detection efficiency was calibrated using the elastic scattering and plotted as a function of E_{recoil} in Fig. 4. The efficiency was obtained by the relation,

$$\text{efficiency} = \frac{Y\ (\text{coincidence})}{Y\ (\text{single})},$$

where Y (coincidence) and Y (single) are elastic scattering yields with and without coincidence

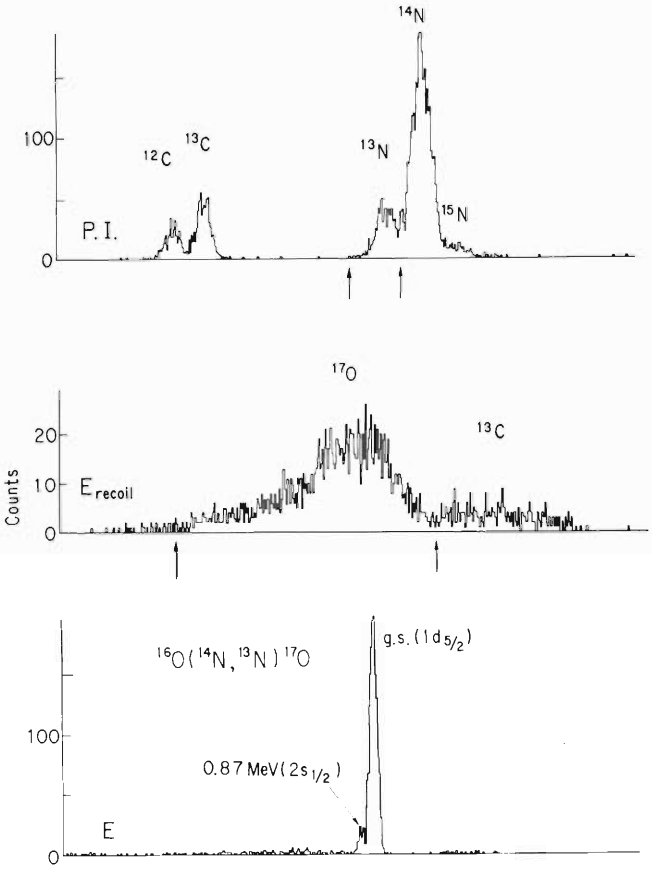

Fig. 3. Coincidence spectra of particle identification (PI), energy of recoil particle (E_{recoil}), and energy of ^{13}N particle of the reaction ^{16}O(^{14}N, ^{13}N)^{17}O.

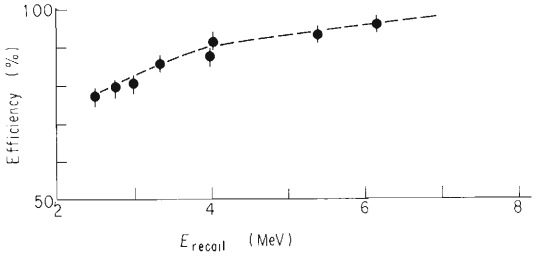

Fig. 4. Detection efficiency of the reaction ^{16}O(^{14}N, ^{13}N)^{17}O obtained from elastic scattering of ^{14}N on ^{16}O.

respectively. The efficiency is reduced mainly by multiple scattering in the target. It is seen that the detection in coincidence with recoil particles was achieved with more than 70 % efficiency in the energy range higher than 2.5 MeV.

References

1) T. Motobayashi, I. Kohno, K. Katori, M. Yoshie, T. Ooi, and H. Kamitsubo: IPCR Cyclotron Progr. Rep., 9, 19 (1975).

2) For example, D. Kalinsky, D. Melnik, U. Smilansky, N. Trautner, B. A. Watson, Y. Horowitz, S. Mordechai, G. Baur, and D. Plete: Proc. of Conf. on Reactions between Complex Nuclei, Nashville, 10, (1974); K. Takimoto, K. Fujii, J. Schimizu, and J. Muto: Bull. Inst. Chem. Res., Kyoto Univ., 52-2, 240 (1974).

6-3. Position Sensitive Multiwire Proportional Counter with Rear Helical Cathode Wire

J. Fujita

In order to develop a multiwire proportional counter for the position sensitive detector of the particle analyzer, a model with a cathode helical wire at the rear of anode was made and tested.

The structure of the model is shown in Fig. 1. Fifteen goldplated anode tungsten wires of 22 μm in diameter and of 26 cm in length are strained horizontally with a tension of 15 g at intervals of 2 mm and soldered on the terminal end of an epoxy circuit board. Furthermore, eight copper wires of 0.1 mm in diameter are stretched on the upper and lower sides of the anode wire plane in the same manner to hold the electric field constant and minimize the edge effect of the anode.

The cathode wire is wound keeping 3 mm spacing with acryl plates around an aluminum rectangular pipe of 6 cm in height, 26 cm in length, and 12 cm in depth. The diameter, length per turn and separation of the wire are 0.1, 384, and 1 mm respectively. Gap spacing between the anode and cathode is 3 mm. Read-out taps are soldered at 5 cm intervals on the helical cathode line and bring the position signal to amplifiers composed of one stage of SN 72733 which has a voltage gain of about four at 200 MHz.

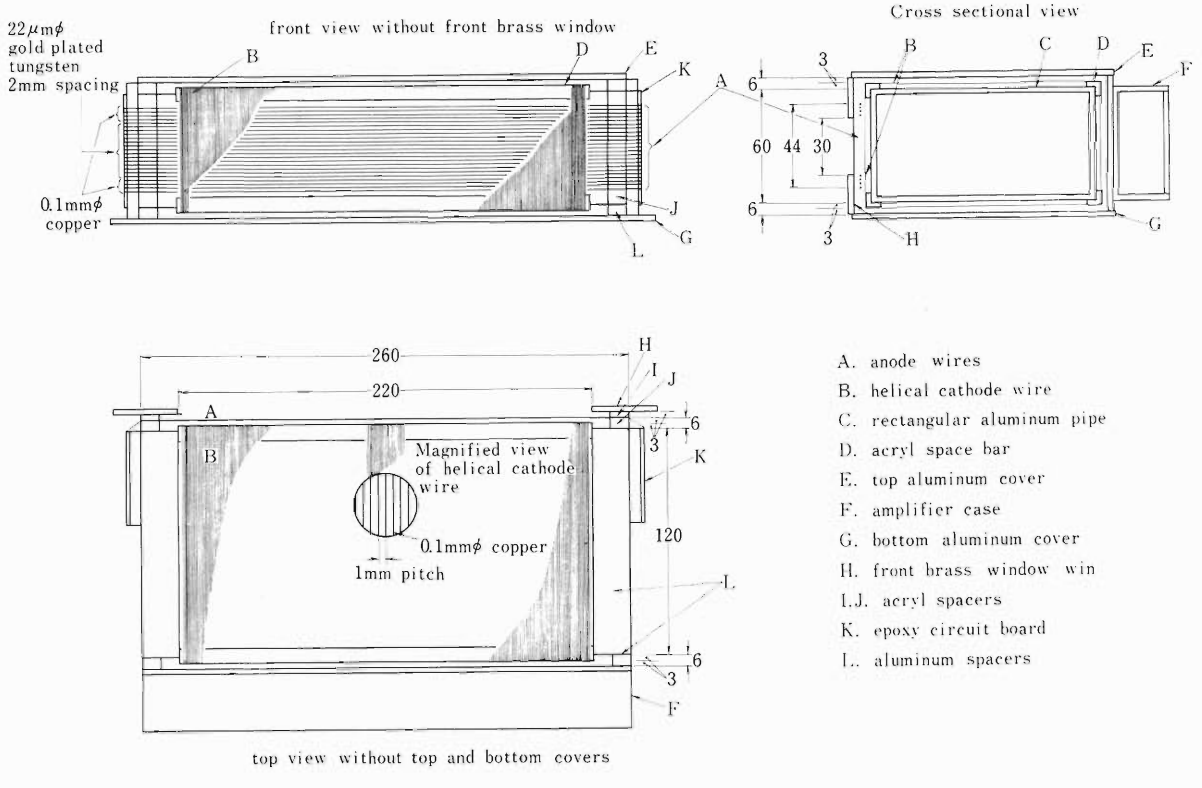

Fig. 1. Structure of MWPC model with rear helical cathode wire.

The filled gas is a mixture of Ar and CO_2 at one atmosphere; CO_2 gas prevents thin anode wires from corona sparks and allows the chamber to operate at higher voltages. The electron avalanche caused by incident charged particles is localized at a narrow region on the anode wire. Negative signal is induced by drifted electrons on the anode and that of opposite polarity by gas ions on the cathode. The positive pulse propagates on the helical cathode wire with the velocity of light and arrives at a tap in a time proportional to wire length or its turn number between the location of avalanche and the tap. The time interval is measured using a time to amplitude converter (TAC).

Test Results

Tests were carried out with collimated α-particles of ^{241}Am in a closed chamber.

(1) Flatness of anode wire plane.

Fifteen anode wires lined at a spacing of 2 mm to cover the focal plane of 2 cm in height are connected altogether at their ends and fed out to a charge sensitive amplifier. Figure 2 shows the dependence of anode signal amplitude on the vertical position of the source position. The waving of flatness is due to irregular alignment of hand-stretched wires.

(2) Relations of high voltage and CO_2 partial pressure to gas multiplication.

Figure 3 shows the dependence of anode signal amplitude on the gap voltage between anode and cathode in pure Ar gas at one atmosphere. Metal guard plates are inserted into the gap ends in order to reduce leakage current from the edges as shown in Fig. 3. Gas multiplication increases rapidly with applied voltage but at the same time noise levels go up. High voltage above 1600 V induces destructive breakdown. On the other hand, gas multiplication decreases with increase of the content of CO_2 gas in the mixture as shown in Fig. 4 and CO_2 gas suppresses corona sparks. With a mixture of 70 % Ar and 30 % CO_2 the chamber can work at 2700 V without destructive breakdown.

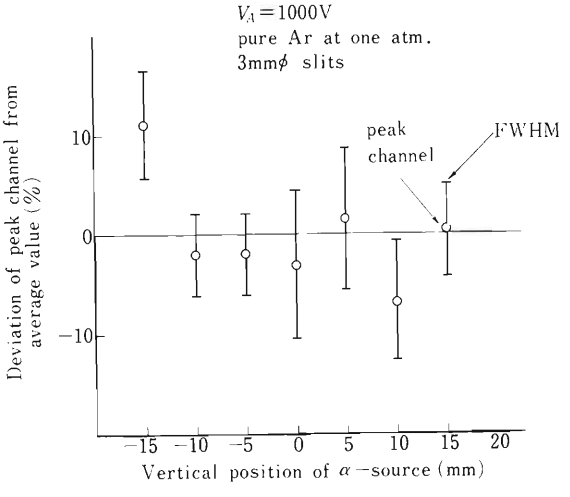

Fig. 2. Dependence of MWPC anode wire signal on vertical position of α-source.

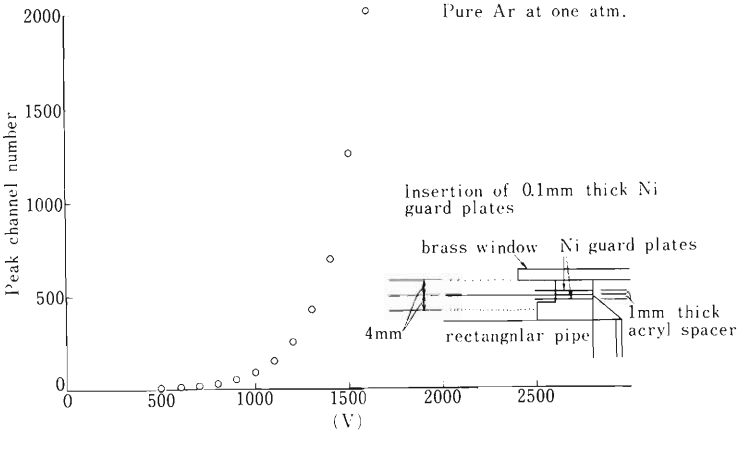

Fig. 3. Dependence of MWPC anode signal amplitude on gap voltage.

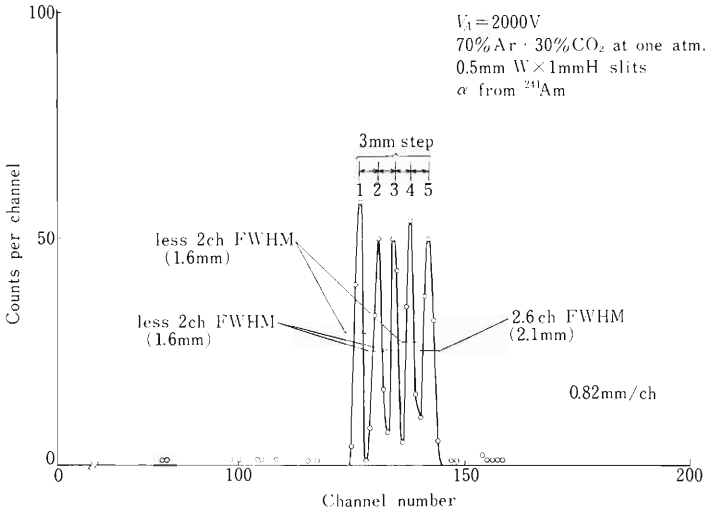

Fig. 4. Influence of CO_2 gas added to Ar on gas multiplication.

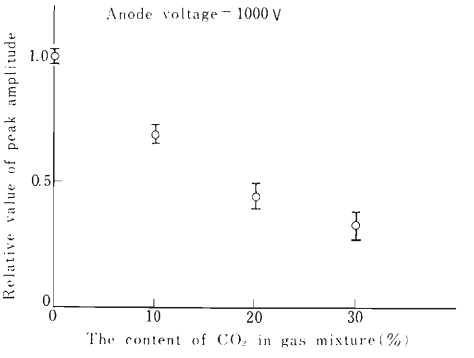

Fig. 5. Spatial resolution of MWPC with rear helical cathode line.

(3) Spatial resolution

Figure 5 shows a result of spatial resolution. Starting pulse for TAC is picked up from the anode wire and stopping pulse from the tap on the helical line.

Since the position signal on the cathode was found very small, the content of CO_2 in the gas mixture was increased up to 30 % to apply anode voltage of 2000 V. The FWHM of spatial resolution obtained is about 1.6 mm. Wire spacing less than 1 mm is necessary to obtain better spatial resolution. The helical cathode line is directly coupled with amplifier input resistance of 2.2 kΩ at each tap. Since the characteristic impedance of the helical cathode is not such a pure resistance as a coaxial cable but is a function of frequency, the condition of no-reflection cannot be fulfilled. The reflected signals retrigger the discriminator and give rise to false stopping pulses. Expansion of pulse duration in the discriminator and the stretched time of TAC enable to select only the first one of the successive pulses as a true stopping pulse. The energy spectrum obtained from the anode at 2000 V has a broad range of distribution because of corona sparks on the anode wires and leakage currents at their ends. Efficiency of the counter is not yet measured. Test is continued with another model whose cathode wire has thicker diameter, 0.2 mm, less separation, 0.5 mm, and shorter length per turn, 204 mm, in order to obtain better spatial resolution and less signal attenuation which makes coverage of the wider area of the focal plane possible.

6-4. On a Simple Raw Data Acquisition System with a Magnetic Tape Recorder

H. Kumagai and A. Hashizume

For γ-γ coincidence experiments, the address of a multichannel analyzer requires a large capacity such as 2000 × 2000 channels to store a two-dimensional spectrum. Because it is impossible to occupy a computer for a long time, a system has been made to store digitalized raw data of coincidences event by event in a magnetic tape using tape recorders for audio frequency. The waveforms of write-in and read-out signals are shown in Fig. 1. By using this system different from NRZI, FM or PM method, good performance is obtained such that the error rate is smaller than 10^{-7} with 2000 bits per inch of recording density. Between ADC and write-in circuit a 24 bit 64 word buffer of IC memory is placed. The write-in circuit consisting of a shift register, a clock pulse generator and an encorder, is shown in Fig. 2. The frequency of the clock pulses can be switched to 3.75 kHz in case of a cassette tape recorder and 7.5 and 15 kHz were employed for the open reel recorder with 9.52 and 19 cm/s tape speeds. The data reduction was made with a block diagram shown in Fig. 3. Further details of the circuits and their function were described in Ref. 1.

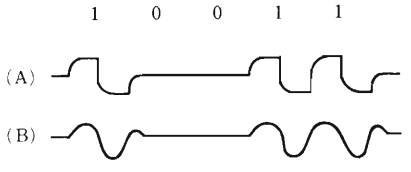

Fig. 1. Waveforms of write-in and read-out signals.

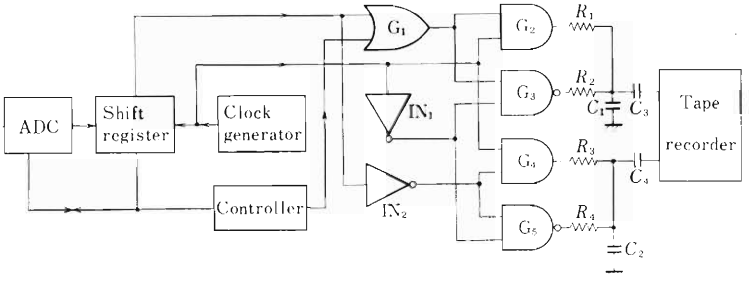

Fig. 2. Write-in system.

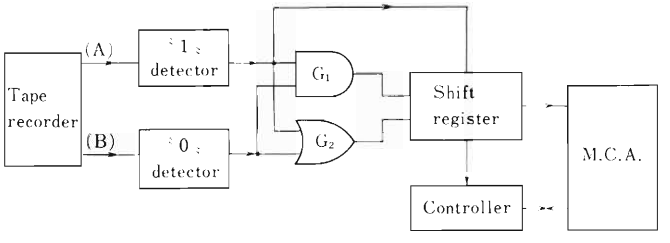

Fig. 3. Read-out system.

Reference

1) H. Kumagai, M. Okano, and A. Hashizume: Reports I.P.C.R., (in Japanese), 51, 120 (1975).

6-5. Upgrading of OKITAC-4500C

T. Inamura, T. Wada, M. Ishihara,
T. Nomura, and H. Kamitsubo

It was two years ago that an OKITAC-4500C computer was installed as an on-line computer to analyze experimental data on nuclear reactions and structure.[1] The initial core memory size was of 16 kW and monitor and PHA system programs took up 6 kW. Only 10 kW were available for the data area. This limited the utility of the computer. The core memory has now been extended up to 32 kW, and a temporary 32 kW system is operating. The final version of the 32 kW system will be completed by the beginning of next year.

Programs for the monitor and PHA systems occupy 8 kW of the 32 kW core memory and another 4 kW will be available for additional data processing programs. The remaining 20 kW will be used for the data area only. The utility area will become twice as large as that of the previous 16 kW system.[1] Functions of the new system are essentially the same as those of the 16 kW system, but the display on CRT is not interrupted by execution of any program for data manipulation.

It should be mentioned that DOS 45 (Disk Operating System for OKITAC-4500) will operate on our upgraded OKITAC-4500C. Since this computer can be used as an off-line computer, this additional system will provide another utility in programming.

Reference

1) T. Wada, T. Nomura, H. Kamitsubo, Y. Chiba, and F. Yoshida: IPCR Cyclotron Progr. Rep., 7, 83 (1973).

6-6. Computation of Multiple Coulomb Excitation

T. Inamura

An extended computer program COULEX for multiple Coulomb excitation* has been modified for the RIKEN FACOM 230-75 computer and tested by computing multiple Coulomb excitation of ^{164}Dy and ^{181}Ta with a ^{84}Kr beam. This computer program is based on the one developed by Winther and de Boer,[1] so that the way of computation is essentially the same with theirs. It gives total and differential cross sections, amplitudes of sub-magnetic state wave functions, and statistical tensors for excited states as many as ten. An introduction of de-orientation effects caused by hyperfine fields acting on the recoils will be made in the near future.

To analyze gamma-ray angular distributions in multiple Coulomb excitation, a separate program CEGAMM has been written following Winther-de Boer formula[1] and operates on the FACOM 230-75. Statistical tensors for excited states which are needed in the CEGAMM are calculated using the program COULEX and stored on a disk in direct access mode. We can save the computation time considerably by creating such a disk file.

The author would like to acknowledge the courtesy of Prof. W. R. Phillips of the University of Manchester who kindly left the computer program COULEX at his disposal.

Reference

1) A. Winther and J. de Boer: "Coulomb excitation", (Ed. K. Alder and A. Winther), Academic Press, p.303 (1966).

* A computer program for multiple Coulomb excitation which operates on a CDC-7600 computer at the University of Manchester.

6-7. Performance of SEM (Space Environment Monitor) for Protons and Alpha-Particles

R. Nagura,* Y. Narimatsu,* and N. Nakanishi

A subsystem of GMS (Geostationary Meteorological Satellite), SEM, which is composed to measure solar protons on the synchronous orbit, is tested by proton and alpha beams from the cyclotron. The function of this equipment is to identify protons, alpha-particles and electrons from other charged particles to count the numbers of them by discriminating theis energies. The energy is ranged between 1 and 500 MeV for protons, 8 and 390 MeV for alpha-particles, and less than 2 MeV for electrons and divided into 7, 5 and 1 channels, respectively.

Elastically scattered protons and alpha-particles by a Au target were employed to check the performance of the system. In the lower energy region below the capability of the cyclotron, an Al foil was used as an energy degrader. The detectors of SEM are composed of 300 μm, 400 μm, and three 3000 μm Si detectors which are labeled as D_1, D_2, · · , and D_5, respectively, and each of them is followed by a pre-amplifier, discriminator, and compression counter. The

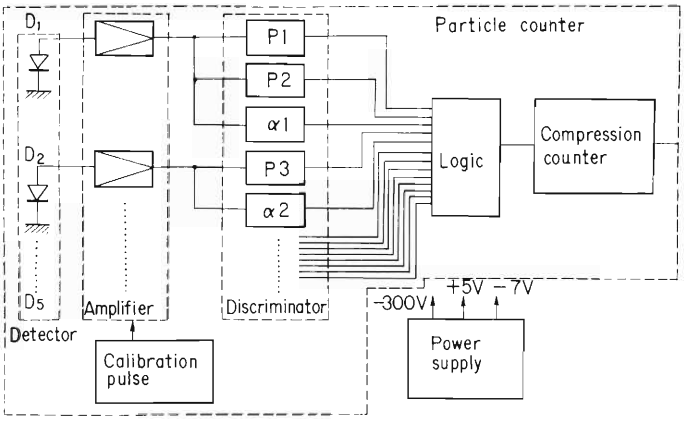

Fig. 1.
Functional block diagram of SEM.

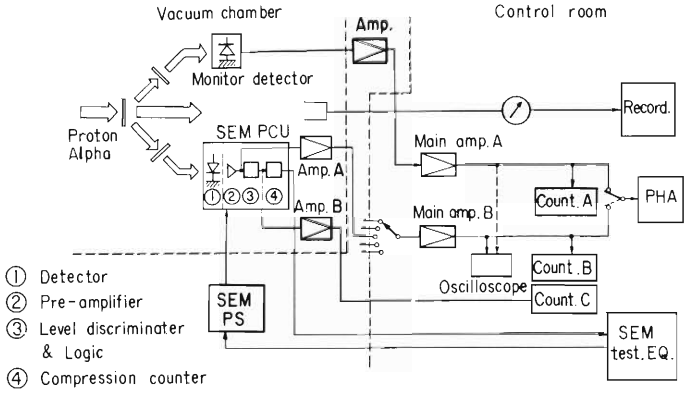

Fig. 2.
Block diagram of the present test.

* Nippon Electric Co., Space Development Division

functional block diagram of SEM is shown in Fig. 1. The detector panel, on which the five detectors were set, was mounted in a vacuum chamber to count scattered particles. The energy of the beam was calibrated using elastic scattering of the analyzed beam by a very thin organic material foil. A counter was set opposite to the center of the detector panel with respect to the beam axis, and was used as a monitor of the particle energy and the number. The output of SEM was measured by an oscilloscope and a multi-channel pulse height analyzer. A block diagram of the present test is shown in Fig. 2.

Figure 3 shows the experimental values of pulse height observed at various incident particle energies and calculated curves. The measured values agree with the predicted ones very well. As for the pulse number, the experimental values are in agreement with those of the monitoring counter and calculated ones.

As a result of the present test we concluded that the detectors and analyzing circuits of SEM perform the functions adequately.

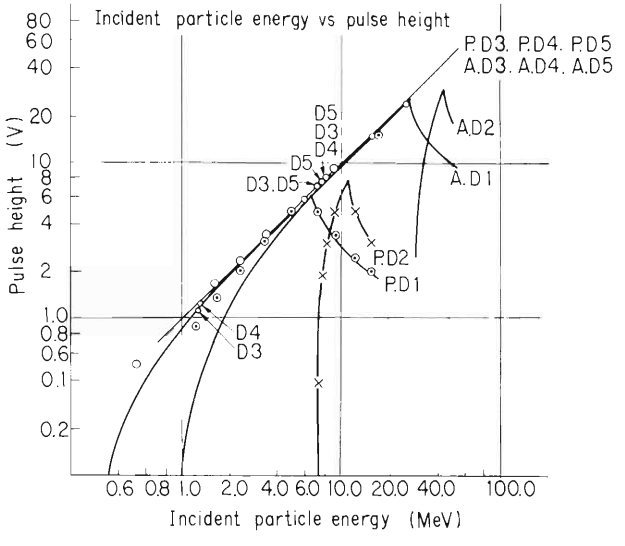

Fig. 3. Pulse height corresponding to the incident proton at various energies. Symbols ⊙ , ×, and ○ represent the measured values of detectors D_1, D_2 ・・ , and D_5, respectively, and the curve correspond to the calculated values.

6-8. Model Magnet of a Separate Sector Cyclotron

S. Motonaga

A linac-injected separate sector cyclotron with four sector magnets was proposed as a best candidate for a future HI accelerator at this institute.[1] A model magnet of about 1/5 scale was designed to study the magnetic field configuration which fulfills a condition of isochronism and focusing to obtain orbital stability.

A focusing properties of an accelerator of this type were discussed for an idealized magnet (hard-edged) which gives zero field outside the sector.[2] Practically, the magnets have a soft-edged field contour which results from the fringing field of the magnets. Such a magnetic field contour reduces the focusing strength slightly compared with a hard-edged sector. This effect depend on the ratio of the gap to the path length in the magnet.

The shape of the model magnet is shown in Fig. 1. Materials of poles and yokes are 0.01 % carbon forged steel and 0.06 % carbon cast steel, respectively. The poles shaped into Rogowski curve.[3]

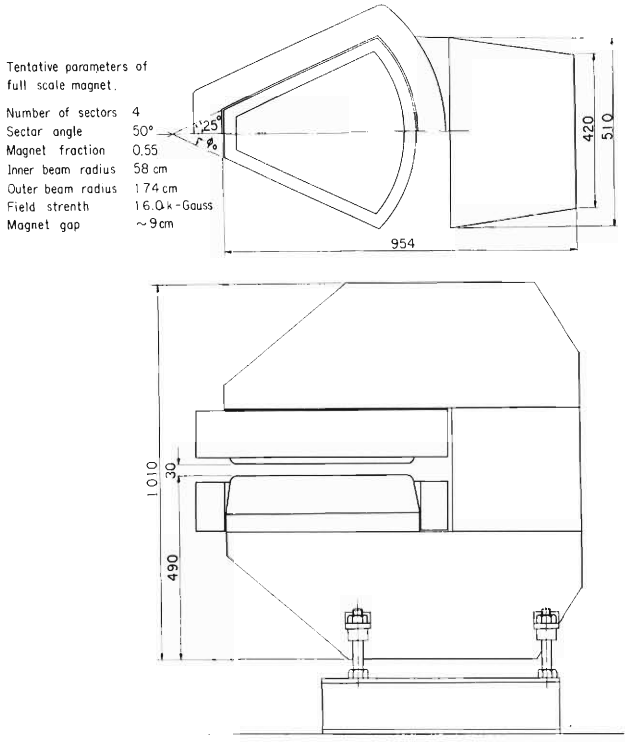

Fig. 1. Shape of model magnet.

References

1) M. Odera and H. Kamitsubo: IPCR Cyclotron Progr. Rep., 7, 151 (1973).

2) M. M. Gordon: Ann. Phys., 50, 571 (1968);
Nucl. Instr. Methods, 58, 245 (1968).

3) H. A. Enge: Proc. 1st Conf. Mag. Tech., Stanford, p. 84 (1965).

7. ATOMIC AND SOLID-STATE PHYSICS

7-1. Ar-K X-Rays Induced by 66 MeV C-Ion Impact

H. Tawara, Y. Awaya, Y. Tendow,
T. Katou, and M. Akiba

The strong dependence of K-shell X-ray production cross sections on the charge state of the projectile was first reported by McDonald et al.,[1] who showed Ar-, Kr-, and Xe-K X-ray yields by 35 MeV F-ion impact increased drastically by changing the charge state of the ions from 5+ to 9+. Mowat et al.[2] also observed that, in 80 MeV Ar-ion impact, Ne-K X-ray yields increased

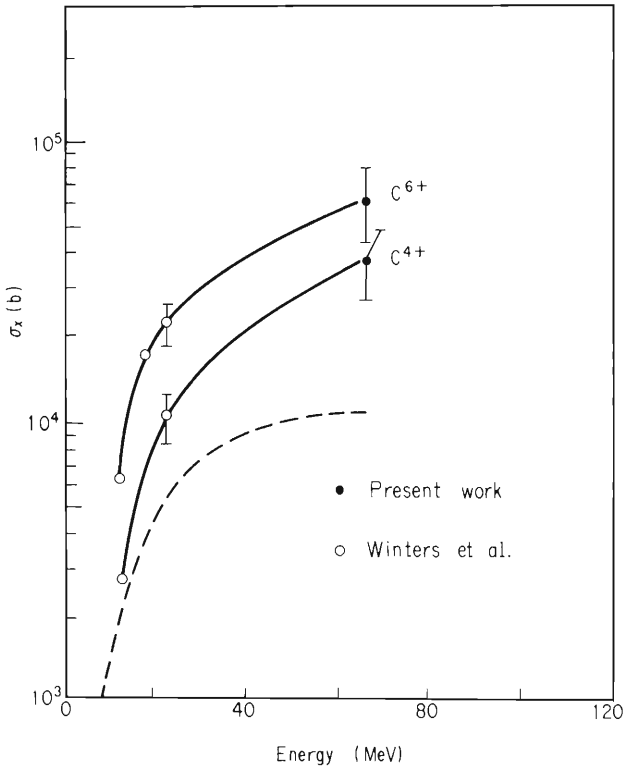

Fig. 1. The Ar-K X-ray production cross section in C^{6+}- and C^{4+}-ion impacts as a function of ion energy. Data at lower energies (open circles) are taken from Ref. 3. The dotted curve shows the relative ionization cross section predicted by BEA calculation. The solid curve is a guide to the eye.

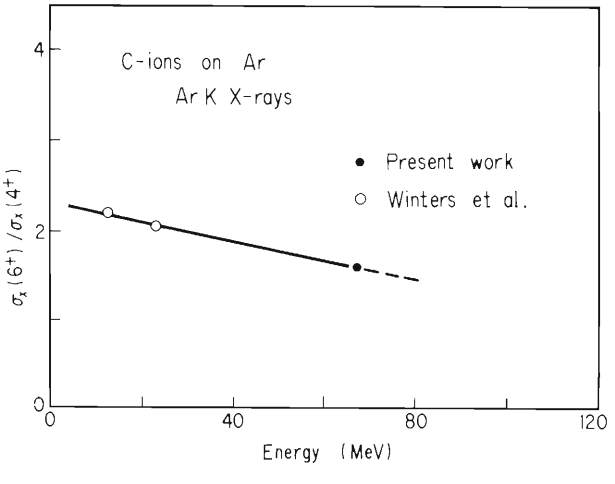

Fig. 2. The ratios of Ar-K X-ray production cross sections in C^{6+}-impact to those in C^{4+}-impact.

by a factor of 60 and Ar-K X-ray yields from the projectile by a factor 1000, when the charge state of Ar-ions was varied from 6+ to 17+.

In the present work, we have measured Ar-K X-rays by 66 MeV (5.5 MeV/amu) C-ion impact. The C^{4+}-ions accelerated with the cyclotron were guided to a gas collision chamber using a differential pumping. By passing the C^{4+}-ion beam through a 100 $\mu g/cm^2$ Ag foil, the projectiles are thought to be in a completely stripped state (C^{6+}), because the average charge of C-ions at this energy is 5.91. Typical ion beam current was 10 – 30 pA and the gas pressure in the chamber was about 1.8×10^{-2} Torr. Under this pressure, 3–4 % of C-ions were estimated to undergo charge transfer.

In Fig. 1 are shown the Ar-K X-ray production cross sections (σ_X) in C^{6+}- and C^{4+}-ion impacts as a function of ion energy. Data at lower energies are taken from a study of Winters et al.[3] The dotted curve shows the relative ionization cross sections predicted by the binary encounter approximation (BEA). The fact that the observed energy dependence are clearly different from the BEA means that some mechanisms other than the direct Coulomb ionization work at these highly ionized heavy ion impacts with high energy.

In Fig. 2 are shown the ratios of Ar-K X-ray production cross sections in C^{6+}-impact to those in C^{4+}-impact. With increasing impact energy, the ratios decrease and approach unity. This shows that the ionization cross section at higher energies tend to be independent of the charge state of the projectile. Similar reduction has been observed in the ratios of Ar-K X-ray yields in O^{8+}- to O^{6+}- and also in F^{9+}- to F^{7+}-ion impacts with increasing ion energy.[3]

One of the reasons for the ionic charge dependence is the variation of fluorescence yields due to multiple ionization. However, Winters et al.[3] have shown that the fluorescence yields may be different by at most 5 % in C^{6+}- and C^{4+}-ion impacts. The screening effect of the projectile nuclear charge by its electrons is also one of the probable causes. The screening effect, however, becomes larger with increasing projectile energy[4] and this is in opposite to the present measurement.

The most important reason of the charge state dependence of the ionization might be electron transfer processes where highly ionized ions capture the target electrons with a considerably high probability. Halpern and Law[5] argued that the agreement between the observed data and theories can be obtained by taking the ionization cross section by naked heavy ion impact with the nuclear charge Z, σ_{iz}, as follows:

$$\sigma_{iz} = Z^2 \sigma_{ip} + X\sigma_{BK} ,$$

where σ_{ip} is the direct Coulomb ionization cross section by proton impact with the same velocity as the heavy ion, σ_{BK} is the K-electron transfer cross section of Brinkman-Kramers, and X is the strength of the electron transfer process to the total inonization. In Fig. 3 is shown the dependence of X on the velocity of the naked projectile (C^{6+}-ions) expressed in V_1/V_0, where V_1 and V_0 are the velocities of the projectile and target electron, respectively. The quantity X increases very rapidly with the projectile velocity, showing that at higher energies the K-shell ionization due to the electron transfer becomes more important.

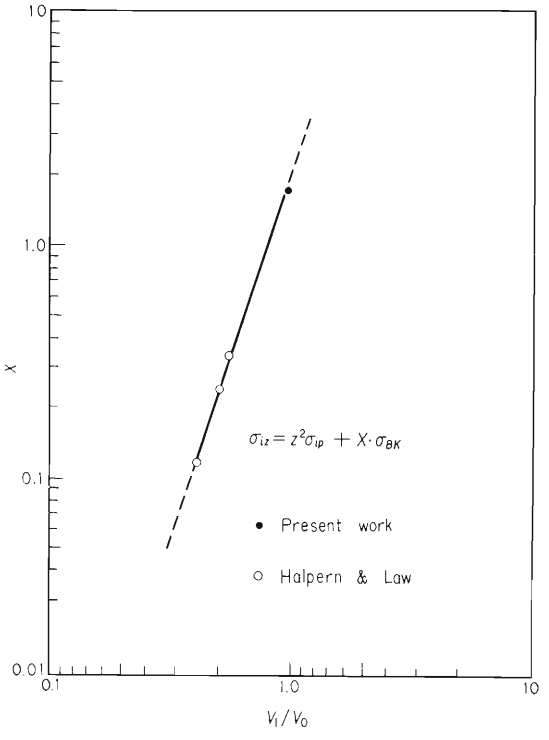

Fig. 3. The dependence of X on V_1/V_0 for C^{6+}-ions.

The observed disappearance of the projectile charge dependence of the ionization cross section at higher impact energies (Fig. 2) can be understood, at least qualitatively, as follows. It is unlikely that probabilities of the K-shell electron transfer to C^{4+}-ions increase more rapidly at higher energies than those to C^{6+}-ions. Alternatively the electron stripping cross sections of C^{4+}-ions at high energy are considerably larger than K-shell ionization cross sections (by two orders of magnitude). Therefore, C^{4+}-ions easily lose their electrons in the interaction with outer shell electrons of the target atom, for example, in the incoming way of the collision, resulting in C^{5+}- or C^{6+}-ions which interact with the K-shell electrons of the target in the outgoing way. Then, the difference in the ionizations between C^{4+}- and C^{6+}-ion impacts tends to disappear at higher energies.

Coincidence experiments between the charge-changed projectiles and X-rays would be interesting and useful to understand the inner-shell ionization phenomena.

References:

1) J. R. McDonald, L. Winters, M. D. Brown, T. Chiao, and L. D. Ellsworth: Phys. Rev. Lett., 29, 1291 (1972).
2) J. R. Mowat, D. J. Pegg, R. S. Peterson, P. M. Griffin, and I. A. Sellin: ibid, 29, 1577 (1972).
3) L. Winters, J. R. McDonald, M. D. Brown, T. Chiao, L. D. Ellsworth, and E. W. Pettus: Phys. Rev. A, 8, 1835 (1973).
4) G. Basbas: Abstract of IX ICPEAC (1975).
5) A. M. Halpern and J. Law: Phys. Rev. Lett., 31, 4 (1973).

7-2. A Bragg Crystal Spectrometer

Y. Awaya, Y. Tendow, H. Kumagai,
M. Akiba, T. Katou, and T. Hamada

An on-line Bragg crystal spectrometer has been installed for the study of X-rays induced by charged particles, especially by heavy ions. An outline of the spectrometer is described in this report.

A commercially available X-ray goniometer was obtained, to which a step-scanning mechanism was added to order.* The vacuum chamber of the goniometer contains an entrance Soller slit, a plane crystal, a proportional counter with a Soller slit, and a Soller slit for a scintillation counter which is held by an arm outside the vacuum separated by a Mylar window. The geometrical arrangement is shown in Fig. 1. Measurable Bragg angles (2θ) are from 0° to 120° for the scintillation counter and from 25° to 150° for the proportional counter. Intervals of step-scanning are variable at 0.01°, 0.02°, 0.05°, and 0.1°. The standard size of Soller slits (length × blade-spacing) is 10 cm × 0.45 mm for the entrance collimator, 10 cm × 0.15 mm for the scintillation counter, and 3 cm × 0.45 mm for the proportional counter. The gas flow, side window proportional counter was commercially obtained, whereas the scintillation counter with a noise rejector was devised and prepared by one of the authors.

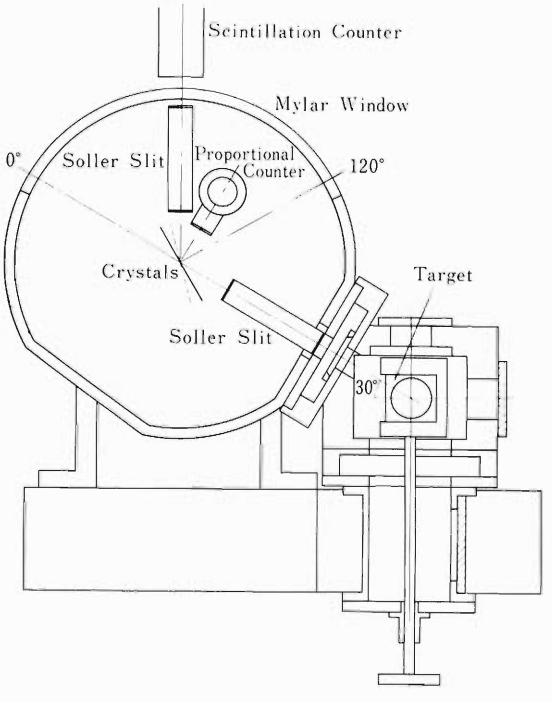

Fig. 1. Schematic view of the goniometer assembly.

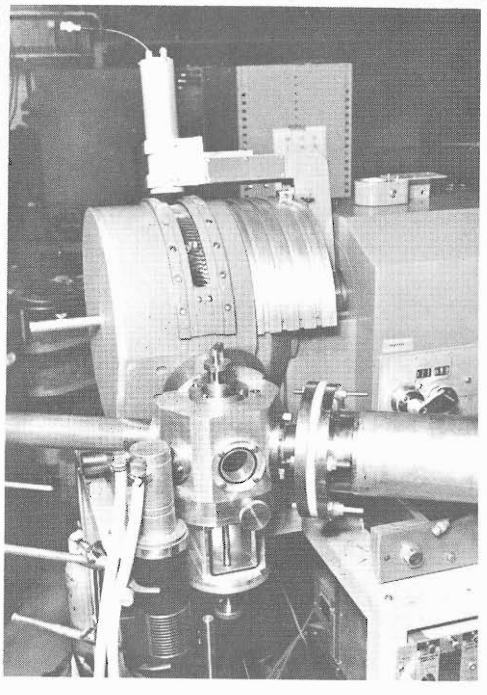

Fig. 2. Picture of the target chamber and the goniometer.

* Rigaku Corp., Cat No. 3122B1 from which a chamber for specimen was taken off.

A target chamber, a step-scan-control system, and a system of data accumulation were designed and made in this laboratory. The target chamber has two windows besides a port to the goniometer. One is usually used for viewing the target, while the other is covered with a Be foil and an X-ray tube is set outside this window. The characteristic X-rays of target element induced by photons from the X-ray tube are used for the alignment of the goniometer. A picture of the target chamber and the goniometer is shown in Fig. 2.

A block diagram of the spectrometer assembly is shown in Fig. 3. Measurements by step scanning from $2\theta = \theta_i$ to θ_f with interval $\Delta\theta$ can be repeated automatically. A four-parameter multiscaler is designed to record four kinds of information at the same time. The data are recorded by a multichannel-pulse-height-analyzer (ND2200) used in a dual parameter mode. The n-th channel number corresponds to the n-th angle from θ_i. When the count of pulses from the current integrator reaches a preset value, the step-scan-controller orders the goniometer to step up the angle and, at the same time, the multiscaler to stop counting and to advance the channel. After the detector reaches the next position, a pulse is sent from the goniometer to the controller to start counting.

A tentative energy resolution of this spectrometer is 22 eV FWHM for the photon-induced Ti K_α X-ray (4.51 keV) using a Ge (111) crystal and the scintillation counter, and 3.9 eV FWHM for the photon-induced Al K_α X-ray (1.49 keV) using a EDDT (020) crystal and the proportional counter. An example of Al K_α X-ray spectrum induced by 6-MeV/amu N-ion bombardment

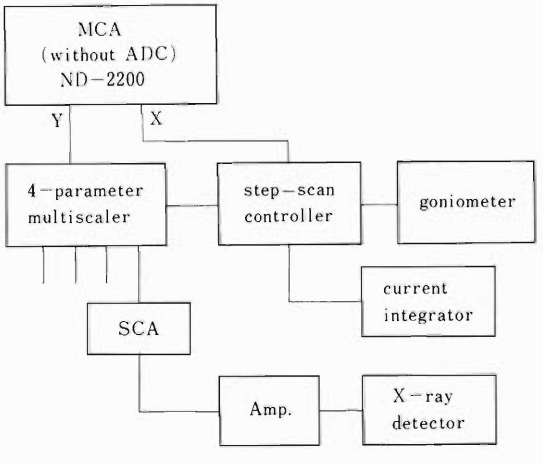

Fig. 3. Block diagram of the spectrometer assembly.

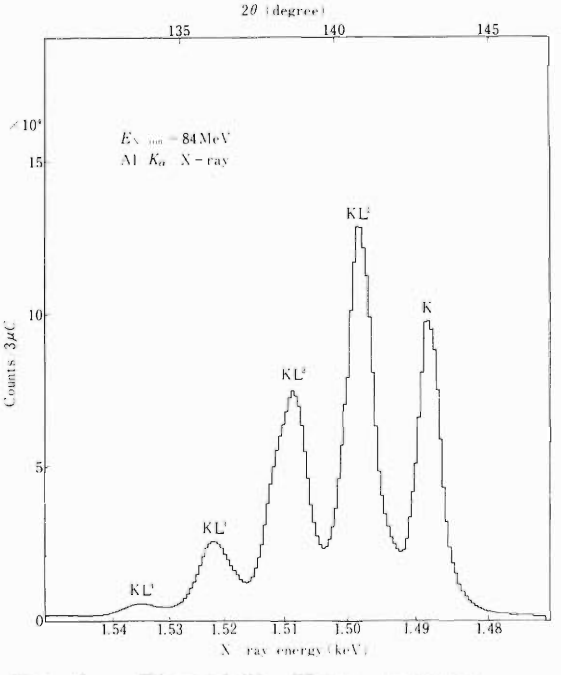

Fig. 4. The Al K_α X-ray spectrum induced by 6-MeV/amu N-ions. Each line is labeled by the electron vacancies in the initial state.

measured using the EDDT crystal and the proportional counter is shown in Fig. 4. Peaks are due to single K-plus multiple L-shell ionization. The initial vacancy configurations[1] are indicated above peaks.

Improvement of the energy resolution is in progress.

Reference

1) A. R. Knudson, D. J. Nagel, P. G. Burkhalter, and K. L. Dunning: Phys. Rev. Lett., 26, 1149 (1971).

7-3. Channeling Experiments with High Energy α-Particles

E. Yagi, A. Koyama, H. Sakairi, and R. R. Hasiguti

Channeling effects have hitherto been studied extensively using electrons, positrons, and heavy ions at energies ranging from a few keV to about one hundred MeV. In case of proton and He ions, such experiments have been performed mostly in the energy region below 10 MeV. There are various difficulties in the experiments with higher energy particles such as that the critical angle for channeling effects decreases with increasing energy. However, if such experiments are applied to the studies of solid state physics, energy loss, lifetime in nuclear reactions and so on, they will give useful information. Therefore, as the first step, in the present work the channeling effects were investigated on a Ge single crystal by means of backscattering with 23 MeV α-particles from the cyclotron.

The assembly consisting of a goniometer for the target, a detector, and a collimator is illustrated in Fig. 1. The crystal orientation of the target could be changed with respect to the collimated incident beam by varying the angle θ and ϕ which could be reset within the accuracy of $\pm 0.01^\circ$ and $\pm 0.02^\circ$, respectively. The beam divergence was less than 0.05°. The bombardment

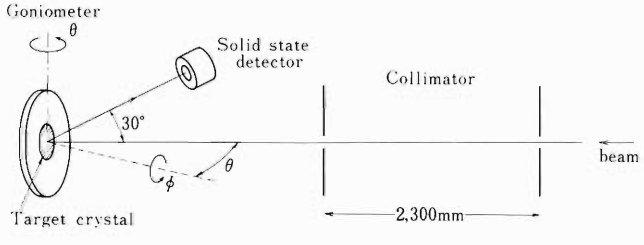

Fig. 1. The goniometer, detector, and collimator assembly for back-scattering experiments.

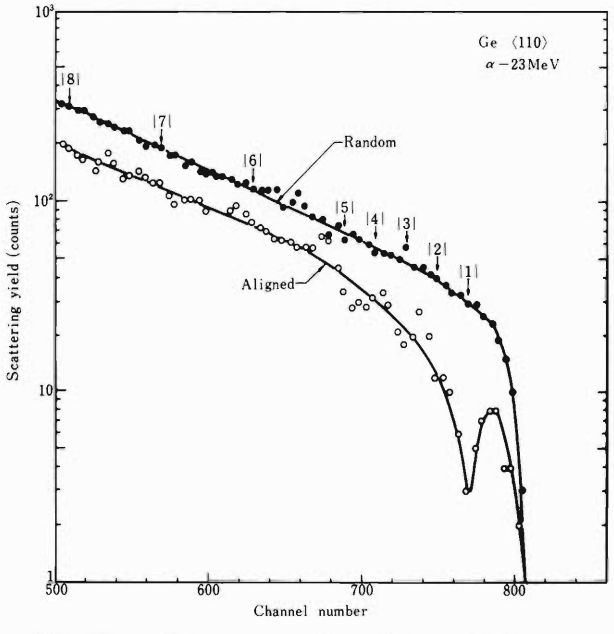

Fig. 2. Energy spectra of α-particles backscattered from a Ge crystal for the incident beam in random orientation (random spectrum) and in the $<110>$ direction (aligned spectrum). Incident beam: 23 MeV.

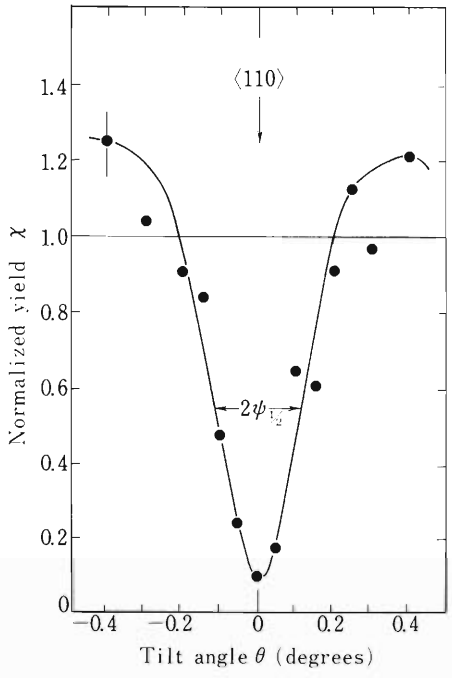

Fig. 3. Orientation dependence of backscattering yield around the < 110 > direction of Ge crystal measured in the energy region indicated by the symbol | 1 | in Fig. 2.

zone was 0.8 mm^2 and the beam current was 2 – 3 nA. The backscattered α-particles were measured by a solid state detector placed at a scattering angle of about 150° and energy-analyzed with a 1024-channel pulse-height-analyzer. Figure 2 shows the energy spectrum of α-particles backscattered from the Ge crystal when the crystal was oriented in random orientation and that obtained when it was aligned in the <110> direction to the incident beam. Figure 3 illustrates the orientation dependence of scattering yield χ around the <110> direction, which was measured in the energy region indicated by the symbol |1| in Fig. 2 and normalized to the value for random orientation. Strong attenuation was observed when the beam enters the crystal within a small angle to the <110> direction, i. e., axial channeling. Similar orientation dependence was measured around {110} planar direction. The critical angle $\psi_{1/2}$ and the normalized minimum yield χ_{min} for <110> axial and {110} planar channeling were obtained from the extrapolation of the observed values to the crystal surface. They are listed in Table 1.

Barrett made detailed Monte Carlo calculations and derived empirical formulas for $\psi_{1/2}$ and χ_{min} except χ_{min} for planar channeling.[1] These formulas fitted well a great variety of experimental values obtained in the energy region below 10 MeV. The values calculated from these formulas were also listed in Table 1. Since the energy dependence of χ_{min} for {110} planar channeling can be considered to be weak, it might be compared with 0.23 obtained from

Table 1. The critical angle $\psi_{1/2}$ and the normalized minimum yield χ_{min} for <110> axial and {110} planar channeling.

	$\psi_{1/2}$ (obs.)	$\psi_{1/2}$ (calc.)	χ_{min} (obs.)	χ_{min} (calc.)
<110>	0.18 ± 0.05°	0.194°	0.020 ± 0.004	0.025
{110}	0.071 ± 0.004°	0.065°	0.20 ± 0.02	–

the experiment with 1.5 MeV proton.[2] We can see from Table 1 that there exists good agreement between the experimental results obtained from the present work and the calculated values from Barrett formulas.

References

1) J. H. Barrett: Phys. Rev., B3, 1527 (1971).
2) K. Morita and N. Itoh: J. Phys. Soc. Japan, 30, 1430 (1971)

7-4. Positron Annihilation in Aluminum

T. Okada, H. Sekizawa, and N. Shiotani

The angular distribution of two photons resulted from annihilation of positrons in aluminum single crystals has been studied with a parallel-slit system. The experimental results shown in Figs. 1 and 2 reveal small but definite crystalline anisotropies of the electron momentum distribution in aluminum. It has been believed for a long time that the valence electrons in aluminum are nearly-free and therefore the angular distribution curves are almost isotropic and have a parabolic shape. Indeed, the early experiments by Berko and Plaskett[1] and theoretical calculations by Stroud and Ehrenreich[2] have failed to find these crystalline anisotropies. Recently, Kubo et al.[3] have made very elaborate theoretical calculations of the angular distribution curves for aluminum. Their results are also shown in Figs. 1 and 2. The agreement between the experiment and theory is remarkable.

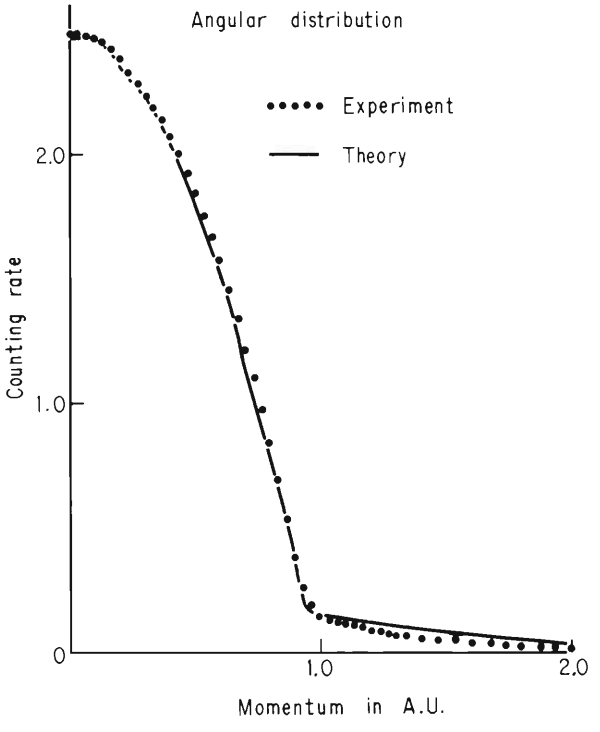

Fig. 1. Measured angular distribution of two photons from positron annihilation in aluminum along [111] direction; errors are smaller than the size of the points. The theoretical curve is taken from Ref. 3.

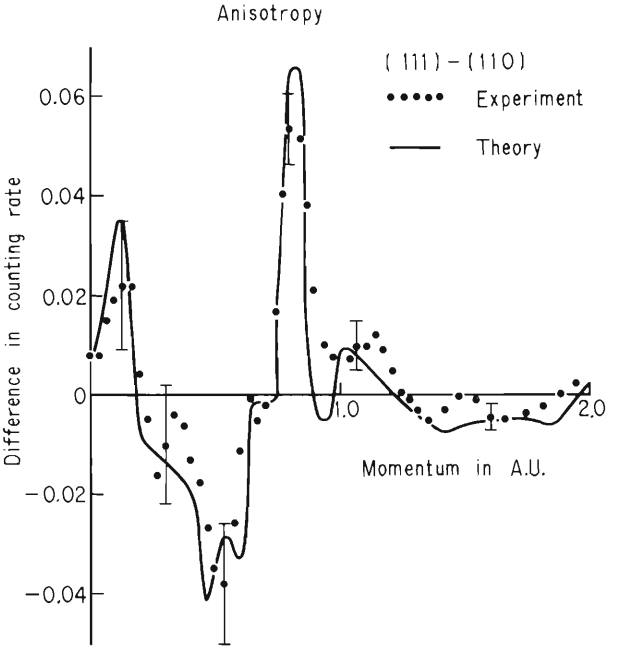

Fig. 2. Anisotropy, i.e., the difference in counting rate between the angular distributions along the [111] and [110] direction. Typical error bars are indicated. The theoretical curve is taken from Ref. 3.

References

1) S. Berko and J. S. Plaskett: Phys. Rev., 112, 1877 (1958).
2) D. Stroud and H. Ehrenreich: ibid., 171, 399 (1968).
3) Y. Kubo, S. Wakoh, and J. Yamashita: Private communication.

7-5. Mössbauer Effect of ^{61}Ni in Various Magnetic Oxides and Sulfides

H. Sekizawa, T. Okada, and F. Ambe

Mössbauer effect of the 67.4 keV γ line of ^{61}Ni was utilized in investigating magnetic compounds containing nickel through the measurement of magnetic hyperfine fields, and a part of the results has already been published.[1)]

The γ-ray source is prepared as follows: A Ni-V alloy disk of about 20 mm in diameter is irradiated with 21 MeV α-particles from the cyclotron and ^{61}Cu is produced by the following reactions, ^{58}Ni(α, p)^{61}Cu and ^{58}Ni(α, n)^{61}Zn $\xrightarrow{\beta^+,\ EC}$ ^{61}Cu. Disintegration of ^{61}Cu with a half-life of 3.3 h yields the 67.4 keV isomer in ^{61}Ni. The disk is utilized as a Mössbauer source without chemical separation. The Mössbauer spectrometer is a conventional one driven in constant acceleration mode. The source is kept at liquid nitrogen temperature to increase the recoilless emission fraction. The spectra obtained were analyzed by least squares fitting. As the analysis is still going on, only a preliminary description of the results obtained at the liquid helium temperature will be given below.

As has been reported previously, the oxides with octahedral nickel ions such as $NiFe_2O_4$, $NiCo_2O_4$, and $NiMn_2O_4$ all showed spectra indicating the presence of a hyperfine field of several tens of kOe, while an oxide with tetrahedral nickel ions $NiCr_2O_4$ gave a spectrum with an extraordinarily large field of 450 kOe, so that an investigation of its origin seems very interesting.[1)] By replacing half of the nickel ions in $NiCr_2O_4$ by manganese ions, that is, in $Ni_{0.5}Mn_{0.5}Cr_2O_4$, it was found that the hyperfine field decreased rapidly to a value comparable to the values in other magnetic oxides. The hyperfine field in an isomorphous antiferromagnetic oxide $NiRh_2O_4$ was found to be very small, and the effect of the electric field gradient was rather dominating, reflecting the Jahn-Teller distortion of the crystal. Numbers of magnetic

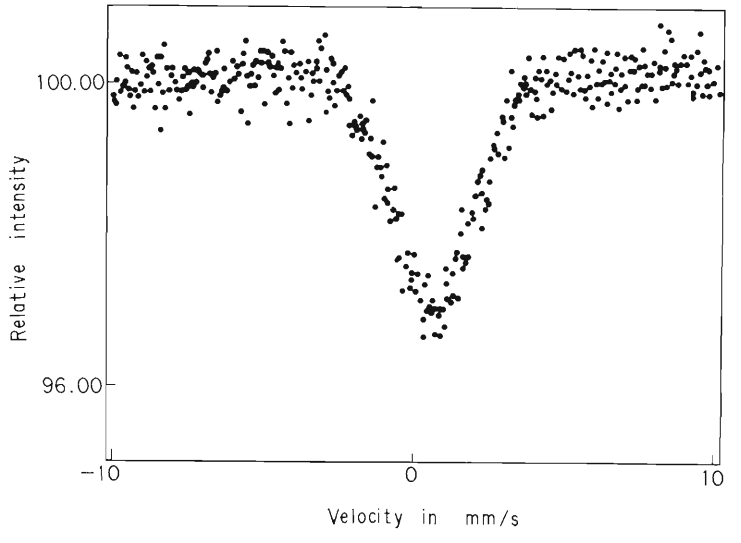

Fig. 1. The Mössbauer spectrum of ^{61}Ni in $Ni_{0.4}Cu_{0.6}Cr_2S_4$ taken at liquid helium temperature.

oxides containing nickel ions in the octahedral site such as Ni_2GeO_4 with spinel structure, $Ni_{0.55}Li_{0.45}O$ with rock-salt structure, and $Y_3Fe_3NiGeO_{12}$ with garnet structure all showed similar ordinary values of hyperfine magnetic field of several tens of kOe. $CuCr_2S_4$ is a ferromagnetic chalcogenide spinel in which the copper ions occupy the tetrahedral site. A specimen $Ni_{0.4}Cu_{0.6}Cr_2S_4$ was prepared in replacing Cu by Ni in $CuCr_2O_4$ and the Mössbauer spectra were taken on it. An example is shown in Fig. 1. As can be seen, the hyperfine field is not high, amounting to only 76 kOe.

These results established the peculiarity of the electronic state of Ni ions in $NiCr_2O_4$.

Reference

1) H. Sekizawa, T. Okada, and F. Ambe: J. phys. (Paris), 32, C1-326 (1971).

8. RADIOCHEMISTRY AND NUCLER CHEMISTRY

8-1. Mössbauer Emission Studies of Defect Atoms in Solid after Nuclear Decay and Reaction

F. Ambe and S. Ambe

The ^{119}Sn-Mössbauer emission studies of defect atoms in solid[1)-8)] have been continued on ^{119}Sb and ^{119m}Te produced by proton and α-reactions in SnSb and SnTe. Comparative studies have also been begun on ^{121}Sb after the β^--decay of ^{121m}Sn,[9)] which may be regarded as a mirror image system of the hitherto-studied one, ^{119}Sb $\xrightarrow{EC}$ ^{119}Sn.

In a preceding report,[10)] we showed that the final lattice position of the recoil ^{119}Sb atoms produced by proton reactions in SnSb and SnTe can be determined from the isomer shift of their daughter, ^{119}Sn, since the recoil energy accompanying the EC decay of ^{119}Sb is much smaller than the minimum displacement energy of atoms in solid. In this way, the recoil ^{119}Sb atoms were found to be distributed between the Sn- and Te-sites after proton reactions in SnTe.

The effect of thermal annealing on the recoil ^{119}Sb atoms in SnTe has been studied. The

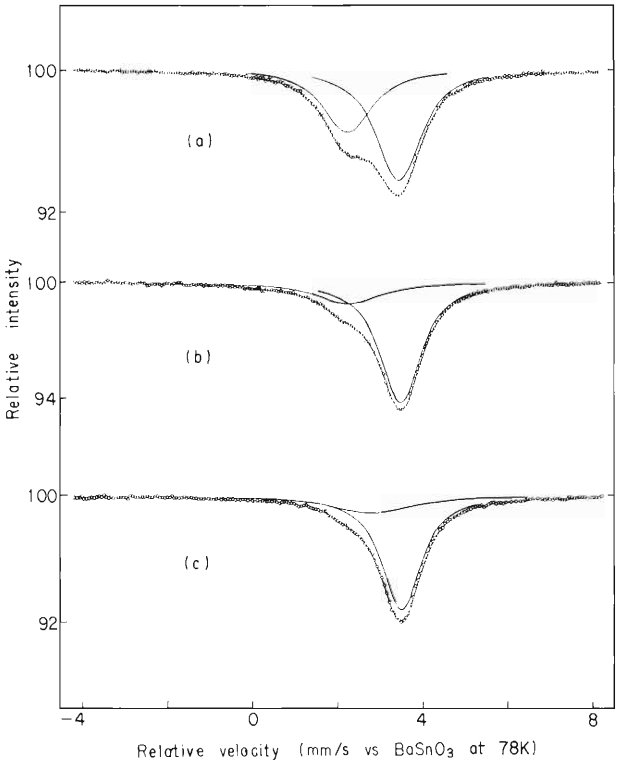

Fig. 1. ^{119}Sn-Mössbauer emission spectra of proton-irradiated ^{120}SnTe. (a) No annealing, (b) annealed at 500°C for 1 h, and (c) annealed at 600°C for 1 h.

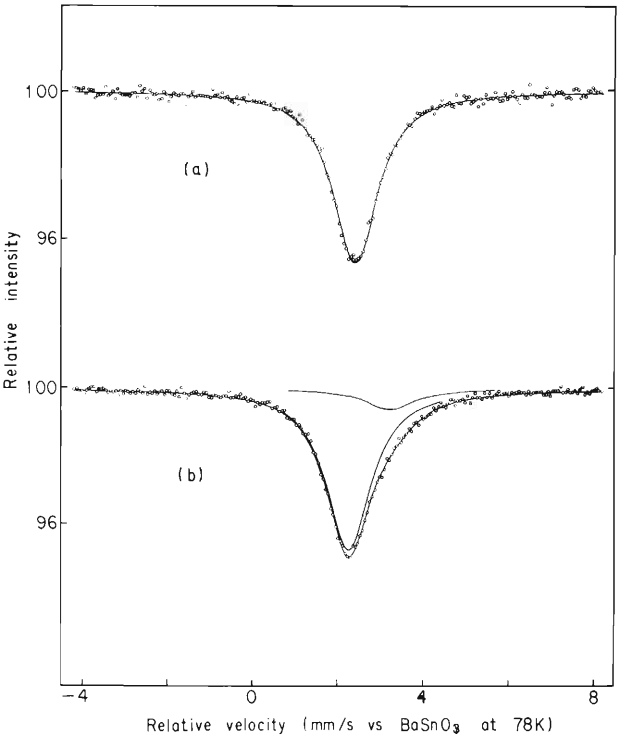

Fig. 2. ^{119}Sn-Mössbauer emission spectra of α-irradiated (a) ^{117}SnSb and (b) ^{117}SnTe.

proton-irradiated ^{120}SnTe samples were heated at constant temperatures in argon atmosphere, and the variation of the ^{119}Sn-Mössbauer emission spectra was followed. Typical examples are shown in Fig. 1. The spectra show that the ^{119}Sb atoms in the Te-site are transferred to the Sn-site in the thermal annealing process. This may be interpreted on the basis of the fact that the electronegativity of antimony is much closer to tin than to tellurium.

The fate of recoil ^{119m}Te after α-reactions was also studied in the SnSb and SnTe matrices. The ^{117}SnSb and ^{117}SnTe samples (^{117}Sn: ^{117}Sn 84.23 %, ^{119}Sn 1.24 %) were irradiated with 32 MeV α-particles in a target box filled with helium gas. The results are shown in Fig. 2. From the energy of α-particles and the isotopic composition of the samples, it is evident that the dominant nuclear reaction leading to ^{119m}Te is the ^{117}Sn (α, 2n) ^{119m}Te reaction. Thus, we observe here the Mössbauer emission spectra of ^{119}Sn following the sequence of nuclear processes: ^{117}Sn (α, 2n) ^{119m}Te $\xrightarrow{EC}$ ^{119}Sb $\xrightarrow{EC}$ ^{119}Sn. As the recoil energy associated with the EC decay of ^{119m}Te to ^{119}Sb is of the same order of magnitude as the displacement energy, it cannot be assured a priori whether or not the observed lattice site of ^{119}Sn is the same as the final position of ^{119m}Te after the recoil due to the α-reactions. However, the measurements on SnTe and Sb_2Te_3 samples labeled with ^{119m}Te show that the dominant emission lines correspond to ^{119}Sn in the Te-site of the compounds, the subsidiary ones being attributable to the other site.[10] Therefore, we assume that the emission line of the α-irradiated ^{117}SnSb (Fig. 2 (a)) with an isomer shift of 2.42 mm/s (vs $BaSnO_3$ at 78 K) corresponds to ^{119}Sn arising from the recoil ^{119m}Te atoms which have come to rest at the Sb-site of ^{117}SnSb. The emission spectra of α-irradiated ^{117}SnTe were composed of two lines with isomer shifts of 2.27 and 3.2 mm/sec, which are assignable to the ^{119}Sn atoms in the Te- and Sn-sites respectively (Fig. 2 (b)). The whole shape of the spectra is quite similar to that of the labeled compound source, Sn^{119m}Te.[10] Therefore, we conclude that all the recoil ^{119m}Te atoms were stabilized at the Te-site after the α-reactions, the ^{119}Sn in the Sn-site being considered to have resulted from the recoil accompanying the EC decay of ^{119m}Te to ^{119}Sb.

Studies of SnTe samples deviating slightly from the stoichiometry are in progress.

References

1) F. Ambe, H. Shoji, S. Ambe, M. Takeda, and N. Saito: Chem. Phys. Lett., 14, 522 (1972).
2) S. Ambe, F. Ambe, and N. Saito: Radiochim. Acta, 19, 121 (1973).
3) F. Ambe and S. Ambe: Phys. Lett., 43A, 399 (1973).
4) F. Ambe, S. Ambe, and H. Shoji: Radiochem. Radioanal. Lett., 15, 349 (1973).
5) S. Ambe and F. Ambe: Radiochim. Acta, 20, 141 (1973).
6) F. Ambe, S. Ambe, H. Shoji, and N. Saito: J. Chem. Phys., 60, 3773 (1974).
7) F. Ambe and S. Ambe: Bull. Chem. Soc. Japan, 47, 2875 (1974).
8) S. Ambe and F. Ambe: Inorg. Nucl. Chem. Lett., 11, 139 (1975).
9) S. Ambe and F. Ambe: J. Chem. Phys., 63, 4077 (1975).
10) F. Ambe and S. Ambe: IPCR Cyclotron Progr. Rep., 8, 108 (1974).

9. RADIATION CHEMISTRY AND RADIATION BIOLOGY

9-1. Heavy-Ion Radiolysis of Liquid Isobutyraldehyde

M. Matsui and M. Imamura

In a previous study[1] of the heavy-ion radiolysis of liquid aliphatic ketones, the thermal decomposition of free radicals (thermal-spike effect) was assumed to take place in the high-LET track cores; this effect gives rise to a marked increase in the yields of H_2 and CO as well as in $G(H_2)/G(CO)$ in the high-LET region.

A similar thermal-spike effect has also been observed for the heavy-ion (C and N ions; LET = 34 – 76 eV $Å^{-1}$) radiolysis of liquid isobutyraldehyde.

Major gaseous products are H_2, CO, C_3H_8, and C_3H_6, the yields of which were determined by gas-chromatography. The yields of H_2 and CO were observed to increase steadily with an increase in LET as in the case of other liquid organic compounds examined. The ratio of the yields of these two products also shows an increase with LET. These results are qualitatively similar to those for liquid ketones and may be explained by decomposition of free radicals in the high-LET track cores.

Another noteworthy result is an unusual increase in the yield of C_3H_8. Propane was not detected from isobutyraldehyde irradiated with low doses and at low dose-rate. However, C_3H_8 is produced by prolonged irradiation; the dose dependence is shown in Fig. 1. In addition, the induction period for C_3H_8 formation diminishes with an increase in dose rate and its yield shows

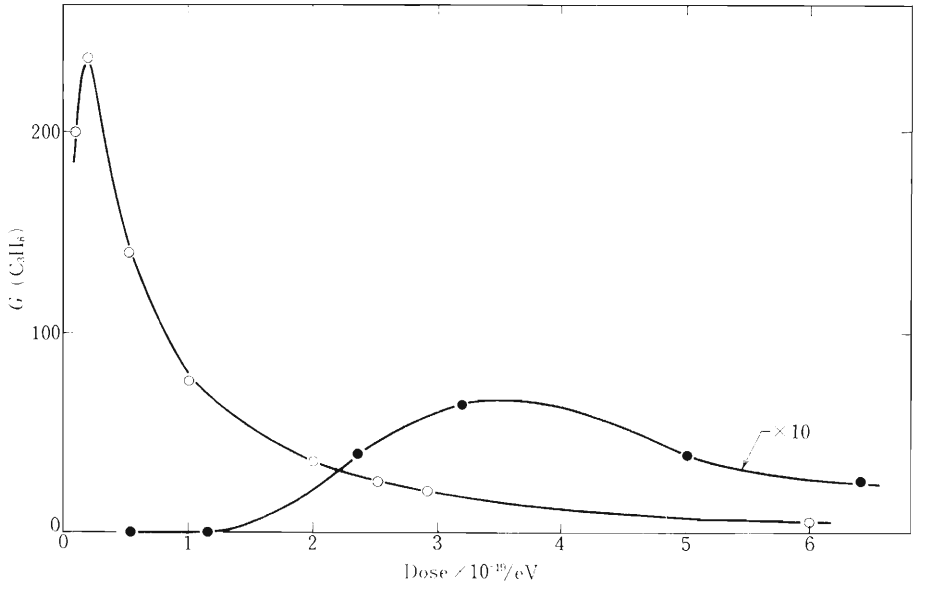

Fig. 1. N-ion radiolysis of isobutyraldehyde. Dose and dose-rate dependence of $G(C_3H_8)$. ●, 0.4 – 1.2 nA; ○, 2.7 – 6.7 nA.

a steep increase. The yield reaches 230, about 20 times as large as that of C_3H_6. This result suggests that C_3H_8 is formed by a chain mechanism.

As demonstrated in γ-radiolysis,[2] the telomer formation may also be expected in the heavy-ion radiolysis of isobutyraldehyde at the early stage where C_3H_6 is produced. The accumulated telomer will then be radiolyzed (Reaction 1), and the chain mechanism may be explained in terms of a series of Reactions 2 — 5.

$$\text{Telomer} \longrightarrow C_3H_7\cdot + RCO\cdot \quad (1)$$

$$C_3H_7\cdot \xrightarrow{\Delta} C_3H_6 + H\cdot \quad (2)$$

$$C_3H_7\cdot + C_3H_7CHO \longrightarrow C_3H_8 + \dot{C}H_2(CH_3)CHCHO \quad (3)$$

$$\dot{C}H_2(CH_3)CHCHO \longrightarrow C_3H_6 + HCO\cdot \quad (4)$$

$$C_3H_6 + C_3H_7O\cdot \longrightarrow \text{Telomer} \quad (5)$$

References

1) M. Matsui and M. Imamura: Bull. Chem. Soc. Japan, 47, 1113 (1974).
2) C. E. Stoops and C. L. Furrow: J. Org. Chem., 26, 3264 (1961).

9-2. Emission Spectra of Alkali Halides under Heavy-Ion Irradiation at 4.2K

K. Kimura and M. Imamura

Ionizing radiations densely produce excited states, ions, and free radicals along their tracks in condensed matter. Interactions among these species, which exert substantial effects on the succeeding processes, are expected to be pronounced in heavy-ion irradiation than in X- or γ-irradiation.

Information on the interactions within radiation tracks could be obtained by measuring emission spectra or ESR spectra in some cases more directly than by other analytical methods. This report presents preliminary results on emission spectra of a KBr single crystal under He- and C-ion irradiation at 4.2 K. The results of ESR have been reported previously.[1)]

Two intrinsic emission bands at 280 and 545 nm from γ-irradiated KBr have been assigned to the transitions from a singlet exciton, $^1\Sigma_u \rightarrow {}^1\Sigma_g$, and from a triplet exciton, $^3\Sigma_u \rightarrow {}^1\Sigma_g$, respectively; the principal color centers formed at 4.2 K are F and H.

A single crystal of KBr was subjected to irradiation with 25-MeV He-ions and 85-MeV C-ions at 4.2 K, and emission spectra were recorded as shown in Fig. 1.

In comparison with the spectrum for γ irradiation, the bandwidth is broader by 0.07 eV for He-ion and by 0.18 eV for C-ion than that for γ-irradiated KBr. This broadening is presumably due to a superposition of the states split by the interaction between excitons densely formed by heavy-ion irradiation.

The ratio of emission intensity of the singlet exciton to that of the triplet exciton for He- and C-ion irradiation is 2 – 3 times the ratio for γ irradiation. This result is puzzling in view of the fact that the rate of radiationless relaxation of the singlet exciton increases with increasing temperature more rapidly than that of the triplet exciton does, because the temperature

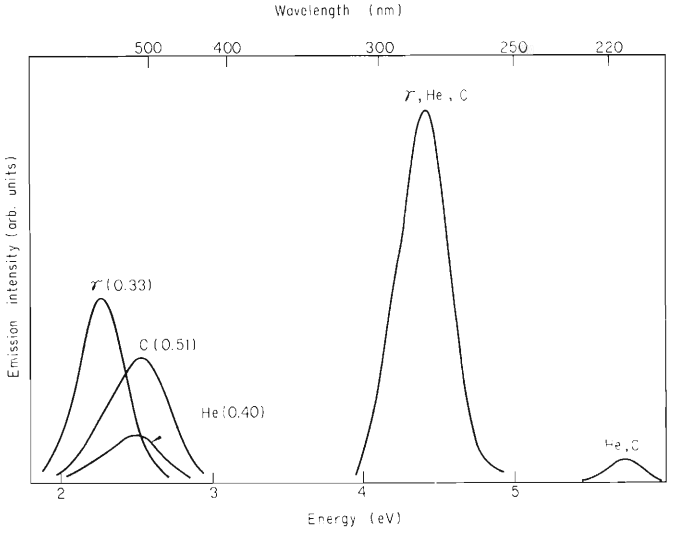

Fig. 1. Emission spectra of KBr under irradiation of γ-rays, He-, and C-ions at 4.2 K. Intensities are normalized at 280 nm. The values in parentheses show halfwidths in eV.

of heavy-ion tracks must be higher.

Prolonged irradiation or irradiation at high dose rates results in decrease in the intensity ratio and shift of the emission band of the triplet exciton to shorter wavelengths, as shown in Table 1. The spectra obtained cannot be ascribed to known color centers. These results suggest the formation of other color centers under these irradiation conditions or the deformation of the wavefunction of the triplet exciton due to dense formation of the color center.

Table 1. Ratio of emission intensities, I_{280}/I_{510}.

Dose (nA)	Dose (nC)	I_{280}/I_{510}
0.58		6
4.8	2200	7
0.3	3600	3
0.76	3840	3
1.1	4040	3

Reference

1) K. Kimura, M. Ogawa, M. Matsui, T. Karasawa, M. Imamura, Y. Tabata, and K. Oshima: J. Chem. Phys., 63, 1797 (1975); IPCR Cyclotron Progr. Rep., 8, 120 (1974).

9-3. Inactivation of Bacterial Cells with Different DNA Repair Capacity by He-, C-, and N-Ions

F. Yatagai, T. Takahashi, and A. Matsuyama

Many investigators have presented evidence for that DNA is an important target for the action of charged-particle radiation in affecting the viability of bacterial cells and that the efficiency of their DNA repair largely influences the cellular radiosensitivity. Therefore, it becomes important to determine the LET dependence of repair capacity for DNA lesions in order to elucidate the LET effect on bacterial cells.

E. coli k-12 AB 1157 (rec^+), AB 2470 (recB), and JC 1553 (recA) were bombarded with α-particles, C-ions, and N-ions from the cyclotron. These strains have already been known to have largely different repair capacity for DNA lesions caused by UV or X-irradiation. The preparation of bacterial cells and dosimetry were made in the same way as previously described.[1)]

All survival curves of these strains determined by the visible-colony counting method show an exponential type for the cyclotron beams as well as for ^{60}Co γ-rays. The values of $1/D_{37}$ for ^{60}Co γ-rays were found to be those in Table 2, and the decrease in $1/D_{37}$ with increase of LET_∞ was observed with all these strains bombarded by the cyclotron beams. As can be seen in Fig. 1, the $1/D_{37}$ values for recA were found to be almost the same as those for recB in the LET_∞ region greater than ~ 30 keV/μm (α-particles). The difference in $1/D_{37}$ values between the rec^+ wild type and the above two mutants diminishes as the LET_∞ of bombarding particles is increased.

Radiation sensitivity can also be expressed as an effective inactivation cross section, S_{eff}. Figure 2 shows the experimental results that S_{eff} for each strain increases with increasing LET_∞

Table 1. Values of best-fit parameters in Eqn. (1) determined by the method of least-squares.

Strain	S_0 (μm^2)	ℓ (nm)	j_0	ω_0 (keV)	X^2
rec^+	0.367	0.287	1	1.0	0.193
recB	0.557	2.23	2	1.0	0.0650
recA	0.549	2.42	2	1.0	0.397

Table 2. Values of best-fit parameters in Eqn. (2) determined by the method of least-squares.

Strain	S_0 (μm^2)	ℓ (nm)	j_0	ω_0 (keV)	X^2	b(μm/keV)	$1-\ell^{-bL}$(γ-rays)	$1/D_{37}$(krad^{-1}) (γ-rays)
rec^+	0.560	5.53	2	1.0	0.654	5.01×10^{-3}	1.00×10^{-3} (1.0)	8.47×10^{-2} (1.0)
recB	0.560	6.16	2	1.0	0.105	3.12×10^{-2}	6.24×10^{-3} (6.2)	5.18×10^{-1} (6.1)
recA	0.560	6.06	2	1.0	0.496	3.47×10^{-2}	6.94×10^{-3} (6.9)	7.75×10^{-1} (9.1)

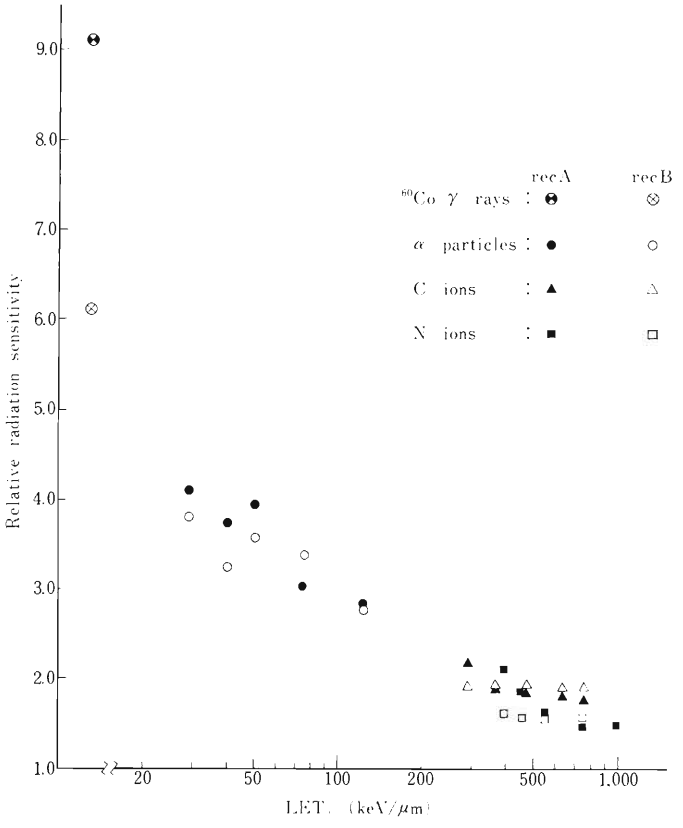

Fig. 1. Relative radiation sensitivities of the mutants, recA and recB to those of the wild type strain, rec$^+$ (see text).

of α-particles and that heavier charged particles give higher values of S_{eff} at the same beam energy per nucleon. However, changes in the beam energy or LET_∞ on C- or N-ions do not largely vary the values of S_{eff} except in the case of recA strain.

An attempt was made to interpret the characteristic LET dependence by the target theory based on the microdose concept proposed by Oda et al.[2] According to the theory, S_{eff} is expressed as the sum of the effects of the track core (S^c_{eff}) and δ-rays (S^δ_{eff}),

$$S_{eff} = S^c_{eff} + S^\delta_{eff} = S_0\left(1 - \sum_{j=0}^{j_0-1} f^c_j\right) + S_0\,\alpha\, Z_{eff}^2\left(1 - \sum_{j=0}^{j_0-1} f^\delta_j\right), \quad (1)$$

where $$f^c_j = \frac{(\ell L_{\omega<\omega_0})^j}{j!}\exp(-\ell L_{\omega<\omega_0}), \text{ and } f^\delta_j = \frac{(\ell L_{\omega>\omega_0})^j}{j!}\exp(-\ell L_{\omega>\omega_0}).$$

The quantity S_0 is the geometrical cross section of the target, ℓ the thickness of the target, W the primary activation energy (35 eV), j_0 the critical number of primary activations, $L_{\omega<\omega_0}$ the track core LET, $L_{\omega>\omega_0}$ the local LET of the secondary electron, and ω_0 the cutoff energy for δ-rays.

Calculation was made by the method of least-squares to fit the experimental data using Eqn. (1). The best-fit parameters are summarized in Table 1, and the theoretical curves including these parameters are shown in Fig. 2. Since the target size is expressed by the values of S_0 and ℓ, the three strains used here should have almost the same values for these two parameters. However, the calculation with these three strains gives different values of S_0 and ℓ as shown in Table 1. This result may suggest that S_0 and ℓ are affected by the DNA repair capacity characteristic of each strain.

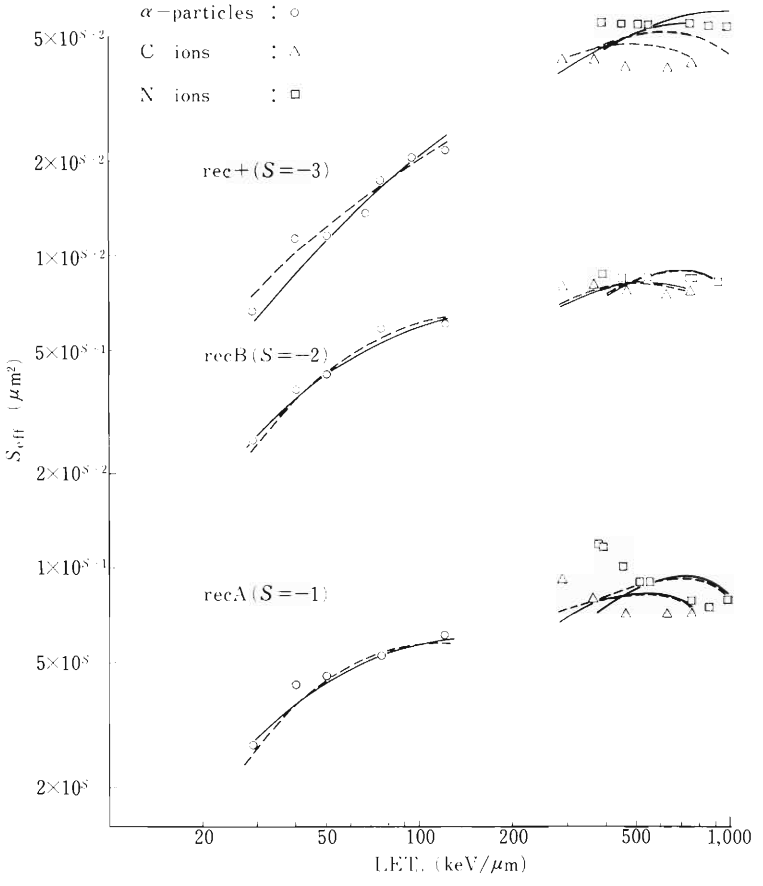

Fig. 2. LET dependence of S_{eff} for three strains. Solid and broken lines show the theoretical curves for each kind of charged particles calculated from Eqns. (2) and (1) respectively (see text).

Then, an analytical method to give almost the same target size to these strains by introducing a term of DNA repair capacity to Eqn. (1) was applied for the bacterial system like this. Parameter of DNA repair capacity, b, is defined to express the probability that the initial damage is repaired as exp(−bL). Since (1 − exp(−bL)) gives the probability that initial damage becomes lethal, Eqn. (1) can be modified as follows:

$$S_{eff} = S^{c}_{eff}\left(1 - \exp\left(-bL_{\omega,\omega_0}\right)\right) + S^{\delta}_{eff}\left(1 - \exp\left(-bL_{\omega,\omega_0}\right)\right). \quad (2)$$

Figure 2 also shows that the theoretical curves which were calculated from Eqn. (2) using the parameters in Table 2 explain the experimental data fairly well. According to the definition of parameter b, the value of (1 − exp(−bL)) for low LET radiation such as ^{60}Co γ-rays might be expected to reflect the radiation sensitivity of bacterial cells. As shown in Table 2, these values for each strain are found not to be contradict with the sensitivity for ^{60}Co γ-rays as expected. These results suggest that such an analytical method considering the DNA repair capacity would be powerful for understanding the LET effect on bacterial inactivation.

References

1) F. Yatagai, T. Takahashi, Y. Kitajima, and A. Matsuyama: J. Radiat. Res., 15, 90 (1974).
2) N. Oda, T. Numakunai, and S. Ohtani: Biophys. Aspects of Radia. Quality, IAEA-SM 145/47, Vienna, 99 (1971).

9-4. Effects of Heavy Ion on the DNA Synthesis in Bacterial Cells

S. Kitayama, F. Yatagai, and A. Matsuyama

We are interested in the difference between radiochemical lesions on DNA induced by low and high LET radiations. In case of low LET radiation such as ^{60}Co γ-rays, energy loss events occur independently each other and radiochemical lesions might be separated on the long DNA strand at least within low doses of irradiation. On the contrary, the energy loss events take place along the track of a heavy ion making ionization column. Traversal of such track core through the chromosome region in the cell may induce radiochemical lesions on both strand of duplex DNA. The double strand break of DNA is an example of such lesions and the ratio of double- to single-strand scissions increases with increasing LET.[1] On irradiation of DNA solution with γ-rays, the number of single-strand breaks is approximately 20 times larger than that of the double-strand breaks. About 30 % of single-breaks have free 3'-OH terminal and they become a priming site for DNA polymerase I.[2] As schematically illustrated in Fig. 1, unirradiated duplex DNA is a poor template for DNA polymerase I, since the enzyme requires free 3'-OH and the complementary strand (Fig. 1 (a)). Low-LET radiation such as γ-rays induces many single-strand breaks and some of them have free 3'-OH with the intact complementary strand as shown in Fig. 1 (b). Subsequently, DNA polymerase I can start DNA synthesis from these sites. On the other hand, it would be expected after high LET irradiation that both strands of duplex DNA have radiation

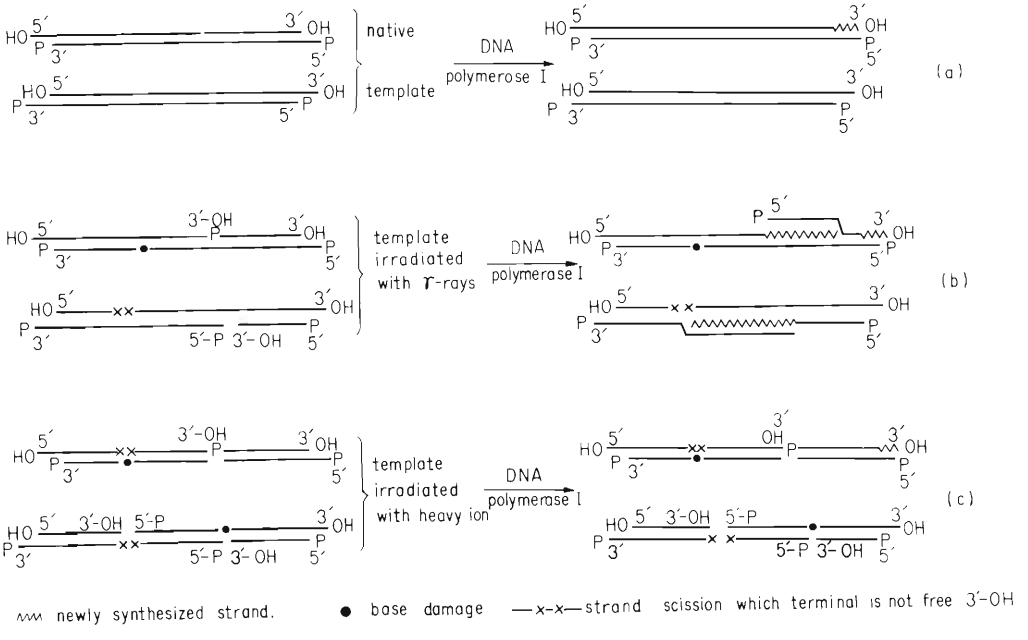

Fig. 1. Schematic representation of priming activity of DNA.

∿∿∿ newly synthesized strand.

● base damage

–× × strand scission which terminal is not free 3'-OH

damage at a complementary site, for example, a double-strand break or single-strand break plus base damage (Fig. 1 (c)). DNA which has these damages is a poor template for DNA polymerase I. If such explanation is applicable for the inactivation of living cells by radiations, unscheduled DNA synthesis would be observed clearly after irradiation with low LET radiations, but poorly or not after the bombardment with high-LET particles.

When the cells which are made permeable to deoxyribonucleoside triphosphate are irradiated with γ-rays, the rate of DNA synthesis is stimulated possibly by the increase in internal 3'-OH termini in duplex DNA as stated above.[3)-5)] DNA synthesis in the permeable cells of Micrococcus radiodurans, the preparation of which was recently succeeded in this laboratory, was found to be stimulated by irradiation with ^{60}Co γ-rays up to about three fold. Permeable cells of M. radiodurans is a suitable system for comparing the effect of low and high LET radiations, because this bacterium is very resistant to radiation and shows a shoulder on its dose-response curves. Within shoulder doses the radiation damages should be repaired irrespective of the type of damage or of the type of repair system. In addition to the damage on DNA, a damage on the cell membrane might be plausible after heavy-ion bombardment. When heavy ion traversed it, the destruction of the transport barrier of the cell membrane could take place more or less. However, intact cells of M. radiodurans (not permeable to dXTP) did not incorporate dXTP into DNA after irradiation of N-ions with a dose which corresponds to several hundred traversals of heavy ions through the cell membrane (Fig. 2). Irradiation of the permeable cells with N-ions stimulated the rate of DNA synthesis similarly to the irradiation with γ-rays. The extent of stimulation by N-ions was 2 – 3 fold, which was the same as the stimulation by γ-rays. This result indicates that free 3'-OH termini are produced directly or by enzymatic reaction after irradiation with N-ions, but the complementary strands are intact. This is somewhat different from the expectation shown in Fig. 1. Some explanations would be possible why the

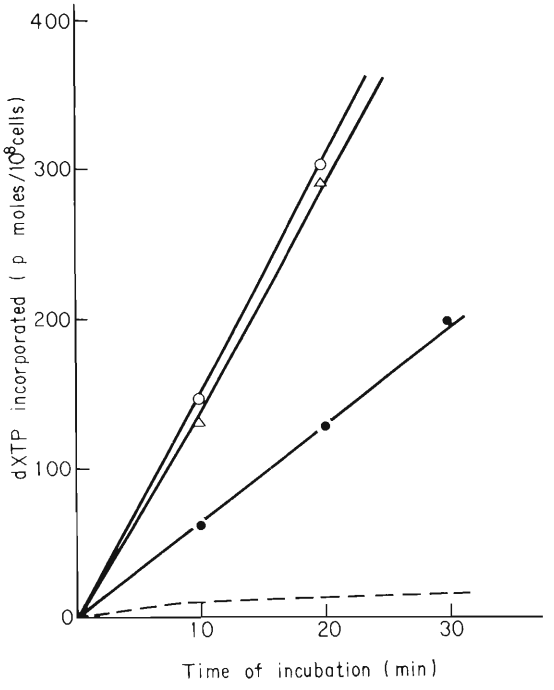

Fig. 2. Stimulation of (^{3}H)-TTP incorporation by irradiation with ^{60}Co γ-rays and N-ions.
Permeable cells (straight line) or intact cells (broken line) were irradiated with γ-rays (200 krad) or N-ions (2.9 MeV, 25 nC) and incubated at 37°C in the complete reaction mixture for DNA synthesis.
● — ●, unirradiated control; ○ — ○, irradiated with γ-rays; △ — △, irradiated with N-ions.

experimental results did not coincide with the expectation stated above. For example, δ-rays might induce single-strand breaks at a very distant position from the track core on the folded chromosome in bacterial cells. An alternative explanation would be that duplex DNA in living cells is protected from damages produced simultaneously on both complementary strand. These possibilities could be studied in more details using charged particles with different LET and the biochemical system as stated above.

References

1) R. C. Christensen and C. A. Tobias: Int. J. Radiat. Biol., 22, 457 (1972).
2) R. B. Kelly, M. Atkinson, J. Huberman, and A. Kornberg: Nature, 224, 495 (1969).
3) W. E. Masker and P. C. Hanawalt: Proc. Natl. Acad. Sci. U.S.A., 70, 129 (1973).
4) D. Billen and G. Hellermann: Biochim. Biophys. Acta, 361, 166 (1974).
5) S. Kitayama and A. Matsuyama: ibid., in press.

10. PREPARATION OF RADIOISOTOPES AND LABELED COMPOUNDS

10-1. Production of Radioisotopes and Preparation of Labeled Compounds for Medical Use

T. Nozaki, S. Ambe, M. Iwamoto, T. Ohsawa,
T. Karasawa, M. Okano, Y. Kasida, T. Ido, K. Suzuki,
K. Fukushi, L. Iwata, T. Irie, T. Hara, and K. Taki

The production of ^{18}F, ^{43}K, and ^{123}I has been continued to meet the needs mainly of medical use. The following process was found to be convenient for the production of ^{43}K: (1) drench the inside wall of a glass bombardment vessel (6 cm in diameter, 70 cm in length) with dilute phosphoric acid (1 : 4) and keep the vessel standing vertically for several hours; (2) bombard argon streaming slowly (1 ℓ/min) in the bombardment vessel with α-particles of 20 – 21 MeV incident energy; (3) set the vessel vertical, joint a reflux condenser and a quartz flask containing $CaCO_3$ (1 g) and water (20 mℓ) to the top and the bottom of the vessel, respectively, and heat the flask strongly with a direct flame for about 10 min; (4) leave the flask to cool and transfer the water in it into a vial through a millipore filter. The water in the vial contains usually about 90 % of the total ^{43}K formed and is ready for intravenous injection.

A new cyclotron for producing exclusively ^{11}C, ^{13}N, and ^{18}F will be installed at the National Nakano Chest Hospital, Tokyo, next year. For the purpose of routine production of $^{13}N_2$ and carrier-free $^{13}NH_3$ by this cyclotron, the chemical form of ^{13}N formed by proton bombardment of water was studied under various conditions, together with possible methods for its conversion into the desired compounds by remote operation. As for the excitation function of the $^{16}O(p, \alpha)^{13}N$ reaction, various different curves have been reported. We re-examined it and obtained a curve agreeing fairly well with that reported by Whitehead.[1)]

Studies have been continued on the preparation of ^{18}F-labeled compounds and the measurement of their behavior in mouse. Similarly to 6-fluoro-9-benzylpurine-^{18}F (Compd 1),[2)] 2-fluoro-9-benzylpurine-^{18}F (Compd 2) was synthesized and their behavior in vivo was intercompared. The following two differences were found: (1) the C-F bond of Compd 1 is ruptured gradually in the animal body, but that of Compd 2 is stable; and (2) a fairly high concentration of Compd 1 is observed in the brain soon after its injection, but Compd 2 is not accumulated in the brain. The preparation of 8-fluoro-9-benzylpurine is now under way, though this compound seems to be rather unstable.

By the Schiemann reaction, m- and p-fluorophenyl-alanine-^{18}F were synthesized and their distribution in mouse and rat after intravenous injection was measured. The effect of prior injection of some hormones on their distribution is now under

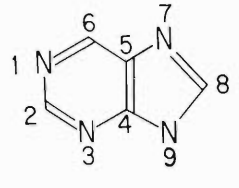

Fig. 1. Purine molecule.

examination.

We intend to obtain 19-halogenocholesterol and 6-halogenomethyl-19-norcholesterol labeled with various radio-halogens in order to compare the effect of substitution with different halogen atoms on the behavior of substituted steroids in vivo. The preparation of the labeled compounds is now under study; a mixture of the labeled products will be injected into animals.

The synthesis of selenomethionine-^{72,73}Se was achieved by a pure chemical method. Biosynthesis, however, is regarded as clearly superior to this method especially for the preparation in optically active state, and is now being attempted. Since ^{72}Se and ^{73}Se decay into radio-arsenic, the labeled selenomethionine would be an interesting compound for the study of the behavior of radio-arsenic formed in vivo.

References

1) A. B. Whitehead and J. S. Foster: Can. J. Phys., 36, 1276 (1958).
2) T. Nozaki, Y. Ohtsuka, A. Tahara, S. Ambe, T. Ido, K. Fukushi, and Y. Kasida: IPCR Cyclotron Progr. Rep., 7, 129 (1973).

11. RADIATION MONITORING

11-1. Gamma-Ray Exposure from Cyclotron Operation at the Monitoring Station

T. Hamada, M. Okano, M. Nishida, and I. Sakamoto

Measurements of gamma-ray exposure have been continued at the monitoring station built at a location ca. 85 m SSE from the cyclotron by using a scintillation detector with a specially designed shield for energy compensation.[1)]

The small contribution of the cyclotron to the exposure was identified and separated from others on the pattern of continuous monitoring data by taking the meteorological record and the machine operation record into consideration. Actually, a number of short-term increases in 15 minutes' counts of the detector were able to be correlated with conditions of machine operation, and the speed and direction of wind, and decided to be the contribution of the cyclotron.

The incremental values above the fairly constant background were summed for each machine operation and converted into exposure dose. Table 1 shows the result of such analysis based on the monitoring data during the period from 1970 to 1973, which yielded the annual dose of ca. 30 μR.

A major dose contribution was found to be due to ^{18}F production for medical use where a part of the beam passes through free air and produces radioactive gases such as ^{13}N and ^{15}O. In early 1973 the target system in the ^{18}F production was improved so that no radioactive gases were produced in the atmosphere. Since then no significant short-term increase of exposure from cyclotron has been observed until Oct. 1975.

Reference

1) T. Hamada, M. Okano, and M. Ota: IPCR Cyclotron Progr. Rep., 1, 81 (1967).

Table 1. Gamma ray dose at the monitoring station due to cyclotron operations.

Date	Time (h)	Wind directions	Speeds (m/s)	Integrated doses (μR)	Machine operations		
					Time (h)	Subjects	Accelerated particles
1970				9.4			
4/24	0.5 – 09			6.4	21 – 09	RC	d
7/23	3 – 06			1.0	18 – 05	RC	d
10/29	10 – 14			2.0	09 – 14	F	h
1971				35.6			
2/3	10 – 14	N		0.9	09 – 14	F	h
2/8	09 – 15			1.8	09 – 14	F	h
2/9	17 – 22			0.8	16 – 22	RC	p
3/17	09 – 16			0.1	07 – 12	F	h
5/25	09 – 17	NW – E	0 – 3	1.2	08 – 13	F	h
6/21	10 – 14	NW – NNW	1 – 3	4.1	09 – 13	F	h
7/15	09 – 15	N	1 – 3	2.2	09 – 14	F	h
10/1	14 – 19	NW	1 – 5	3.5	12 – 18	F	h *
11/4	10 – 14	NNW	1 – 6	5.2	09 – 13	RC	h
11/10	10 – 15	NNW – ENE	0 – 3	4.7	09 – 13	RC	h
11/30	16 – 06	NW – W	8 – 0	3.5	09 –	NP	d
12/1	19 – 24	N – NW	0 – 2	3.4	15 – 21	RC	h
12/8	11 – 16	W – N – NE	0 – 5	4.1	09 – 15	RC	h
1972				30.5			
2/22	13 – 16	NNW	4 – 10	2.7	09 – 15	RC	h
2/24	11 – 18	N–W-SW–NW	2–4–1–8	3.3	09 – 18	RC	h
4/18	21 – 24	N – NW	3 – 4	1.6	16 – 24	RC	p
5/30	12 – 21	NW	1 – 5	5.4	09 – 21	RC	p
7/12	0 – 08	NNW – NW	0 – 3	2.7	0 – 08	RC	p *
7/31	12 – 15	N – E	1 – 6	1.0	09 – 15	RC	h
12/12	02 – 07	NW ?	0 – 2	8.8	08 – 11	F	h
12/15	05 – 08	W – NW	0 – 2	0.2	06 – 10	F	h
12/26	11 – 13	NNW – NE	0 – 3	1.8	09 – 15	RC	p
12/27	14 – 16	N–E–S–SW	0 – 2	3.0	09 – 22	RI	α
1973				3.0			
2/8	14 – 17	NNW	12 – 3	1.1	12 – 16	RC	h
3/14	14 – 17	NNW	4 – 15	1.9	09 –	NP	

RC: radiochemistry, F: F-18 production, NP: nuclear physics, RI: radioisotope production. p: proton, d: deutron, h: helium-3, α: helium-4. * Include rainfall

11-2. Routine Monitoring

K. Koda, I. Sakamoto, and I. Usuba

Results of routine monitoring on the cyclotron from April 1973 to March 1974 are described.

No remarkable change in leakage radiation and residual activities was observed during this period.

(1) Surface and air contamination

The surface contamination of the floor of cyclotron room, where the highest level of contamination had usually been detected in the cyclotron building, has been kept as low as about 10^{-7} $\mu Ci/cm^2$, owing to wiping-off of the floor twice a year.

When the accelerating chamber was opened, slight contamination of the air in the cyclotron room was observed. The value of radioactive concentration (beta-gamma) was 10^{-12} $\mu Ci/cm^3$.

Tritium still remained in the accelerating chamber since the last triton acceleration in December 1970. On the inner surface of the accelerating chamber a contamination of 10^{-3} – 10^{-4} $\mu Ci/cm^2$ of tritium and 10^{-5} – 10^{-6} $\mu Ci/cm^2$ of other beta- and gamma-emitters was found.

The tritium concentration of the air in the chamber ranges 10^{-4} – 10^{-5} $\mu Ci/cm^3$. Before overhauling work begins the air in the chamber is removed completely. Afterward, air contamination is not found in the cyclotron room.

(2) Drainage

The concentration of radioactivities in the drain water of the cyclotron building was found

Table 1. Annual exposure dose distribution and average dose for the workers from 1967 to 1974.
(Dose accumulated from April to next March)

Year	Total number of workers	Dose distribution (mrem)					Average dose per person (mrem)
		Un-detectable	10 ~ 100	101 ~ 300	301 ~ 1000	>1000	
1967	42	9	9	15	8	1	212
1968	46	0	8	13	18	7	507
1969	46	0	11	17	16	2	318
1970	49	0	19	12	15	3	299
1971	50	7	15	15	12	1	261
1972	47	10	17	12	7	1	199
1973	48	14	22	11	1	0	79
1974	52	30	18	3	1	0	32

to be of the order of 10^{-7} μCi/cm^3.

The total quantity of activities in the aqueous release in this period was about 24 μCi, and the radioisotopes found by the gamma-ray spectrometry were mainly ^{58}Co and ^{60}Co.

(3) Personnel monitoring

Since the enforcement of the rule in 1973 that enough interval for "cooling" should be taken before entering the cyclotron room after deuteron acceleration, the exposure of the workers to radiation decreased remarkably as shown in Table 1. Namely, the average annual dose per person has been decreased down to 32 mrem as compared to several hundred mrems for before 1973.

In this period the accumulated dose of external exposure of the cyclotron operators was 850 man-mrem, which was 50.6 % of the accumulated dose of all cyclotron workers, and the maximum personnel dose was 320 mrem. The dose to the cyclotron workers is decreasing year by year.

11-3. Neutron Measurement in the Cyclotron Room and the Experimental Area

K. Koda, I. Sakamoto, and I. Usuba

The leakage radiation was measured at various points in the cyclotron building when a ^{13}C target placed in a large experimental area was bombarded with a ^{3}He beam of 30 MeV; the beam current was 6 – 7 nA.

The flux of fast neutrons and thermal neutrons, was measured by the activation method using the reactions $^{32}S(n, p)^{32}P$ and $^{23}Na(n, \gamma)^{24}Na$ and dose of gamma-rays with gamma-ray pocket dosimeters, respectively. The minimum levels detected by the above measurements were about 120 n/cm^2 sec, 15 n/cm^2 sec, and 0.01 mR/h, respectively.

The neutron dose rate was calculated using the conversion factor given in NBS Handbook 63, and the results are shown in Table 1.

Fast neutrons were predominantly observed at the following points: the septum (No. 1 point in Table 1), the beam exit of the machine (No. 3), and the slit boxes (No. 4 and No. 5), and the flux at these points was larger than that at other points. The ratio of fast neutron flux to thermal one at the No. 1 point was 1.3, while that at the No. 2 point which was 3 m apart from the septum was 0.15.

Table 1. Neutron fluxes and dose equivalent rates at various points in the cyclotron building.

Radiation \ Point of observation*		1	2	3	4	5	6	7	8	9	10	11
N_f	Flux (n/cm^2 sec)	1.6×10^4	570	4.2×10^4	1.6×10^4	4.0×10^3	230	–**	180	–	130	–
	Dose rate (mrem/h)	2.9×10^3	110	7.9×10^3	2.9×10^3	740	42		34		24	
N_{th}	Flux (n/cm^2 sec)	1.2×10^4	3.9×10^3	4.8×10^3	2.0×10^3	2.9×10^3	–	26	37	–	490	–
	Dose rate (mrem/h)	44	15	18	7.3	11		0.1	0.1		1.9	
N_f/N_{th}		1.3	0.15	8.7	8.0	1.4			4.9		0.26	
γ (mR/h)						120	0.4	0.5	7	–	3.8	0.1

* See the figure shown below, ** Undetectable.

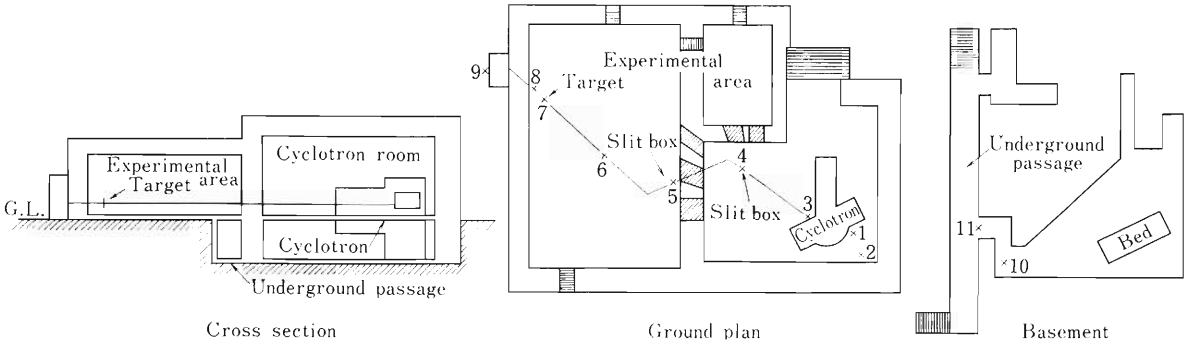

11-4. Measurement of Residual Tritium

S. Fujita and I. Sakamoto

Tritium gas was supplied to the ion source in order to accelerate tritium ions by the cyclotron in 1970[1]. The residual tritium is decreasing since then, but it is still detected in the air in the accelerating chamber (Fig. 1). Since the values of these data were dispersing, it was suspected that the tritium concentration would vary with time after the vacuum of the chamber was broken.

In summer and winter of 1975, measurements were made on the desorption rate of tritium from the inner surface of the chamber wall during the period of overhauling. Samples of air were collected in a can in the stem tank at about 20cm inside from the inspection port adjacent to the accelerating chamber and measured by a collection-type ionization chamber.[1]

First sampling was made just after purging the air in the tank and the accelerating chamber by a fan which is permanently equipped for this purpose. Then sampling was continued intermittently for 9 days, during which the tank and the chamber were normally closed. As shown in Fig. 2, the tritium concentration increases with time and the rate of growth is faster in summer than in winter; the time required for reaching a maximum permissible concentratior

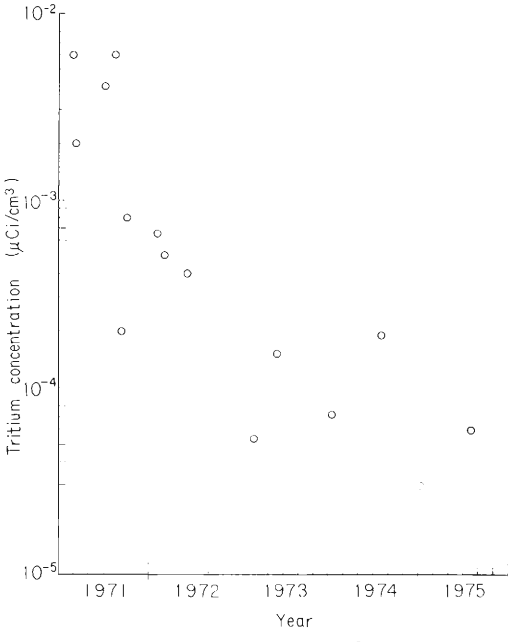

Fig. 1. Monitoring data for tritium concentration in the accelerating chamber.

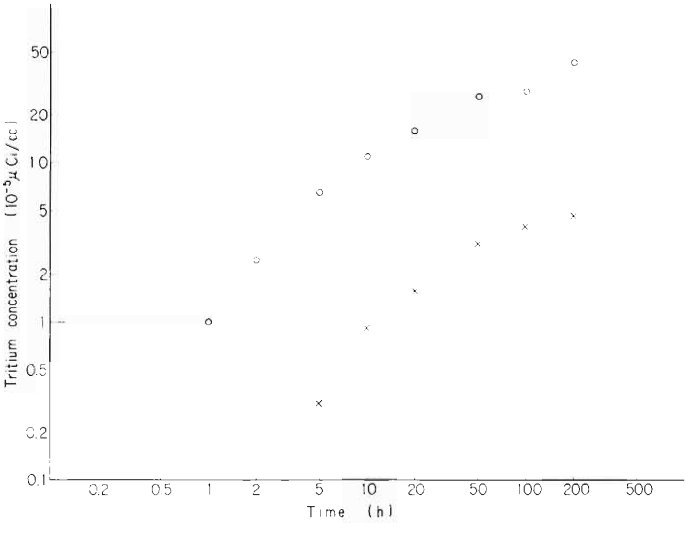

Fig. 2. Increase of tritium concentration with time after purging air in the chamber.
- ・ : data obtained during the period of Aug. 5-13, 1975
- × : data obtained during the period of Jan. 9-18, 1975

for tritium is only 2 hours in summer compared with 30 hours in winter. It suggests the effect of ambient temperature on the desorption rate of tritium from the chamber wall.

Reference

1) I. Kohno, A. Shimamura, I. Sakamoto, T. Tonuma, S. Takeda, N. Nakanishi, K. Matsuda, K. Koda, and T. Hamada: IPCR Cyclotron Progr. Rep., 4, 11 (1970).

12. HEAVY ION LINEAR ACCELERATOR PROJECT

12-1. Status of Constructional Work of the Linear Accelerator in December, 1975

M. Odera

A contract for fabrication of the first cavity was made with the Sumitomo Heavy Industries, Ltd. The contract also includes construction of drift tubes loaded with quadrupole magnets and the precise alignment of their axes within the accuracy of 0.1 mm for the full length of the cavity. The resonator will be completed at the factory in March 1976, and installed as soon as the accelerator building becomes ready to accept it in the next summer, because we wish to make a radiofrequency power test of the cavity as early as possible, though constructional work of the building will continue, till autumn.

Two quadrupole magnets made at the machine shop of the Institute and the one made by the Sumitomo Co. are being tested as to the extent of deviation of mechanical and magnetic axes under the different manufacturing processes, the maximum field gradient obtainable, field harmonics, flood cooling of coils, etc. A final design of the drift tubes will be frozen according to the results of the tests.

Orders were placed for a 500 kV power supply, an ion source housing at high voltage potential, an insulated-shaft-driven generator system for supply of power to the terminal and an accelerating column. They will be installed next summer in the injector room.

A commercially available cryogenic pump having capacity of 5000 ℓ/sec at high vacuum was bought and tested. It's operation was found very simple and satisfactory. It is planned to use a cryo-pump in parallel with a molecular pump for each cavity.

A synthesized signal generator was purchased together with a wideband solid state amplifier. The former has a frequency range up to 110 MHz with a stability of 3×10^{-8}/day and the latter has 50 db gain between 250 kHz and 105 MHz with power rating at 50 W. As a final-stage power tube, an RCA 4648 tetrode was chosen and a proto-type high power amplifer chain system is being constructed. The first unit will be tested and evaluated for a period between April 1976 and March 1977 to decide a final detailed design of the high power system.

12-2. Status of the Injector System

M. Hemmi and M. Odera

Figure 1 is a plan of the injector system. The high voltage terminal in which a heavy ion source and its power supply are to be installed has a large floor area to provide for the future development of the heavy ion accelerator technology. The housing is supported on porcelain insulators 3.39 m high from the basement floor. The supporting structure is designed to be sturdy enough against earthquakes up to 0.3 G acceleration in the horizontal direction.

Rating of the high voltage unit is 500 kV and 10 mA and the stability of voltage is 10^{-4} against 10 % line voltage change. A 50 kVA, 50 Hz generator at the high voltage terminal is driven via a fiberglass reinforced epoxy rod by an alternator at ground potential. Capacity of the generator is sufficient for ion sources of any type available at present.

A prototype frequency-modulated light communication system between the high voltage terminal and a local control panel was made. Light is transmitted through thin-fiber light conductors covered with an opaque insulator. Tuning forks having high Q-values are used to discriminate the frequency of modulation and to secure high selectivity against error signals such as corona discharge noise. Figure 2 shows a block diagram of the system.

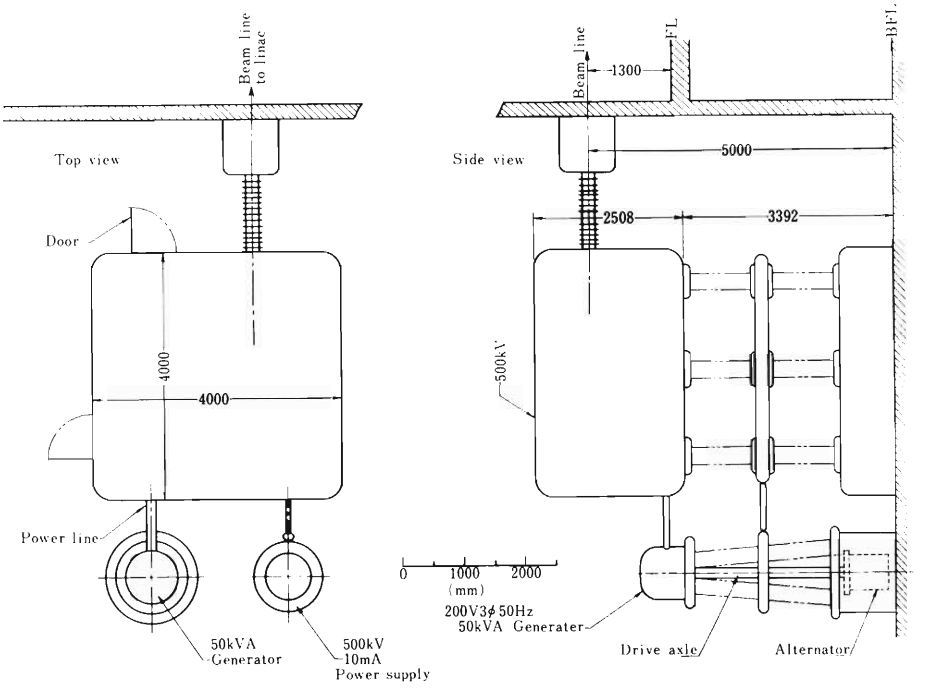

Fig. 1. Top and side views of the injector system.

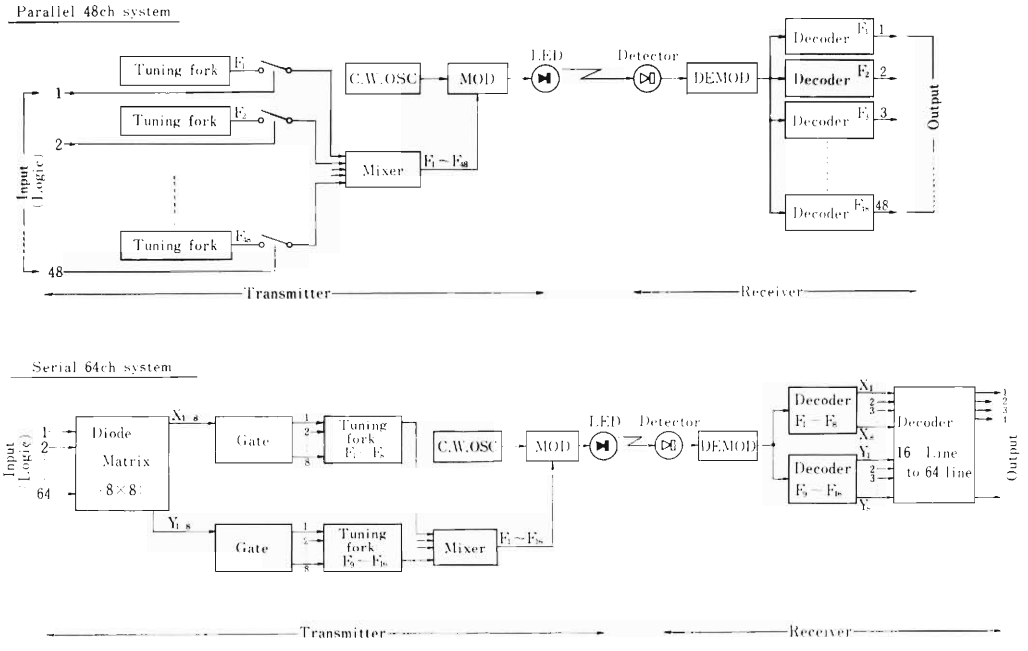

Fig. 2. Block diagram of the frequency modulated light communication system.

12-3. Structure of the Drift-Tube Magnet

Y. Miyazawa, T. Inoue, and M. Odera

A coil of a quadrupole magnet in a drift tube made by using the tape coil technique[1] is shown in Fig. 1. Though it looks much simpler than the plate stacking coil reported before,[2] careful fabrication procedure and skill are required. Thickness of the copper tape is 0.5 mm and that of insulator is 0.18 mm. The insulator is made of a glass cloth impregnated with semi-cured epoxy resin. The coil consists of 52 layers of copper and insulator tape glued and heat-treated. Holes are machined to accept pole pieces. Etching by a ferric chloride or nitric acid solution removes metal bits induced by the machining process and bridging the insulator layer. The effective number of turns is 26. A photograph of the yoke shown in Fig. 2 indicates the path of cooling liquid cut on the surface. The yoke is inserted into a shell and sealed by electron beam welding and a coolant flows in the slots to cool the shell heated by radiofrequency loss. Figure 3 shows an apparatus for circulating Freon 113 through the tube and a heat exchanger for cooling.

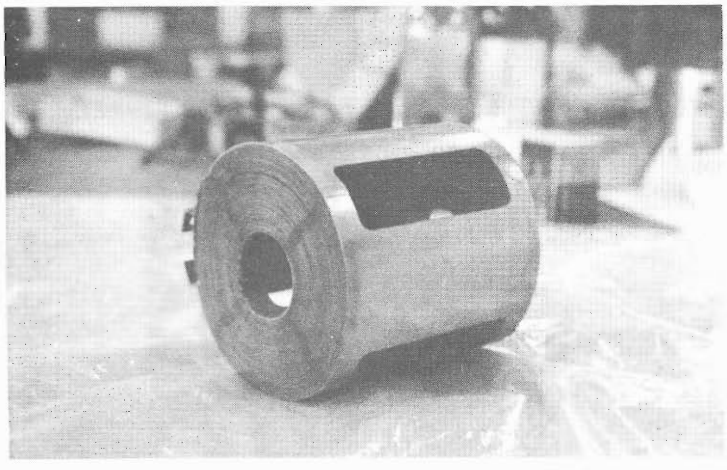

Fig. 1.
Photograph of Berkeley-type tape coil.

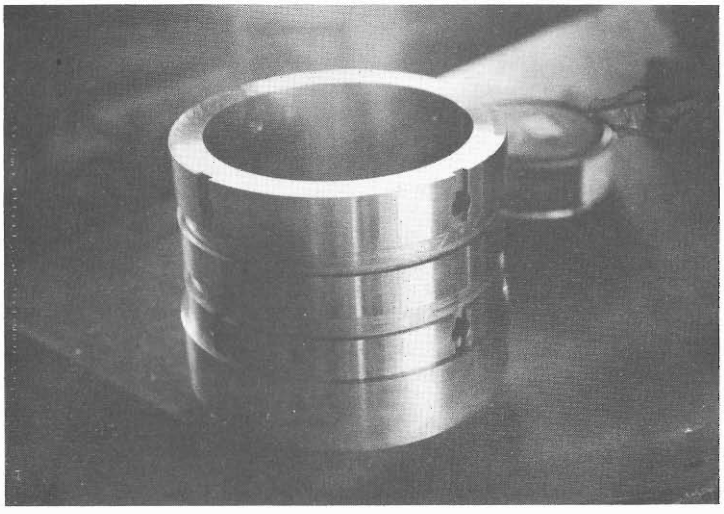

Fig. 2.
Photograph of quadrupole magnet yoke.

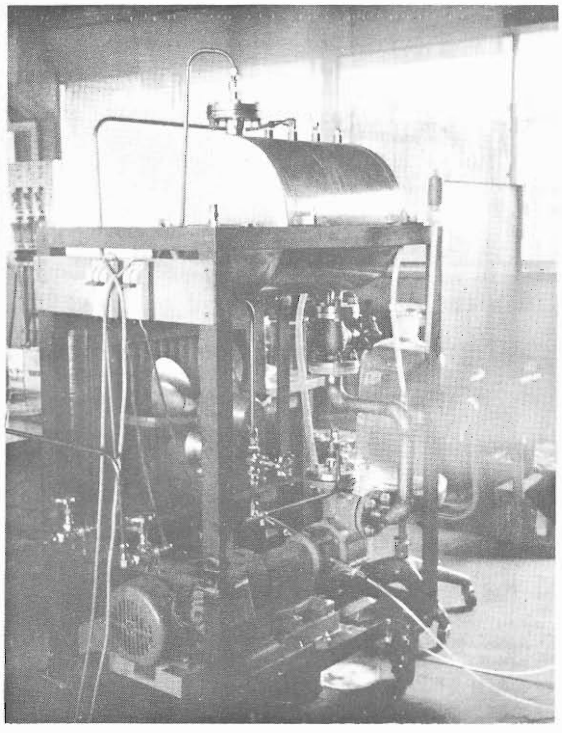

Fig. 3. Freon-113 circulation system for flood cooling of the drift tube magnets.

References

1) R. M. Main and R. Yourd: Proc. Fourth Intern. Conf. on Magnet Tech., p. 349 (1972).
2) T. Inoue and M. Odera: IPCR Cyclotron Progr. Rep., 8, 159 (1974).

12-4. Beam Acceptance of the Drift Tube Focusing System

T. Tonuma, F. Yoshida, and M. Odera

In the linac cavities, there are 36 whole length drift tubes and a half length input section in which focusing elements are contained.[1] Theoretically, the best beam profile will be obtained by tuning the exciting current of each quadrupole magnet separately and adopting different axial length for each magnet in proportion to the length of the drift tube. However, for practical purposes, it is not necessary to make such fine individual adjustments of exciting current or axial length of magnet to obtain a well-focused beam tolerable for experiments. The tuning procedure may be made much simpler by using the same value for field gradients of several quadrupoles and permitting excitation of their coils connected in series. This simplification causes no substantial loss of beam quality by suitably choosing combination of the quadrupole magnets. Moreover, an orbit analysis has shown it possible to make the magnets divided into 9 groups and to keep the geometrical parameters constant in each group.

Figure 1 shows acceptance and emittance diagrams of the drift tube focusing system designed on the basis of the above method of grouping of currents and magnet dimensions. The solid line represents acceptance and the dotted line emittance of the beam at the entrance of each cavity. It is assumed that the beam fills completely the acceptance diagram when injected into

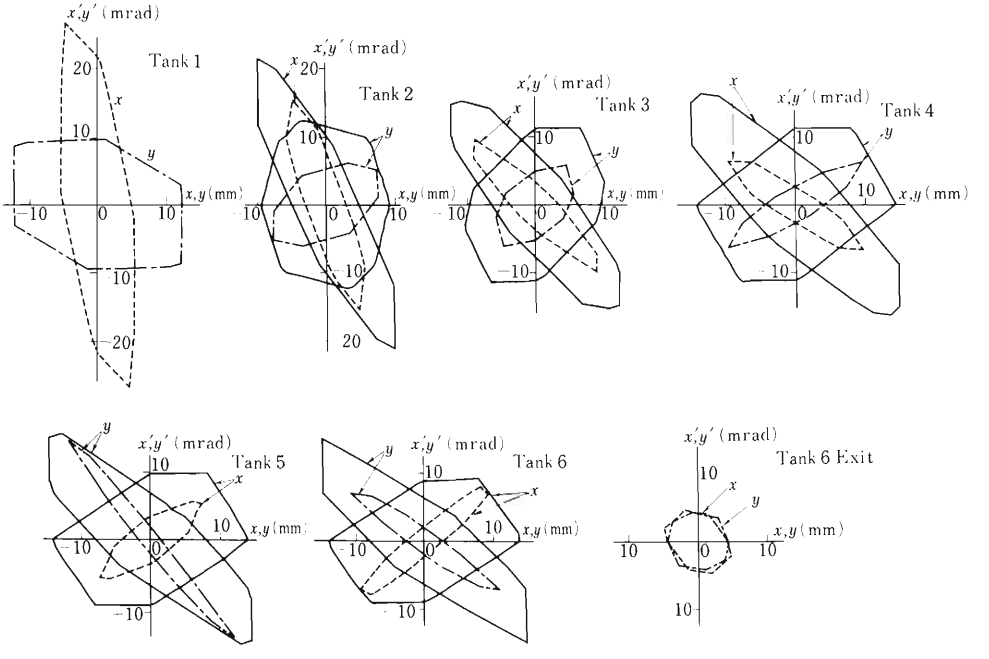

Fig. 1. Acceptance and emittance diagrams for beam at entrance of cavities. X and Y denote vertical and horizontal directions respectively. Lens sequence is vertically focusing and horizontally defocusing at the entrance of the first cavity. The solid line represents acceptance and the dotted line emittance and the two lines coincide in the first tank.

the first cavity. Therefore, the single line of tank 1 has two meanings of acceptance and emittance in the phase diagram. There are one or two singlet quadrupole magnets between cavities to transform emittance at the exit of each cavity into a shape fitted to the next cavity's acceptance. With this combination of the quadrupoles, a large transparency through the focusing system for the injected beam can be expected if enough precaution is paid for alignment of the focusing elements.

Reference

1) T. Tonuma, F. Yoshida, and M. Odera: IPCR Cyclotron Progr. Rep., 6, 18 (1972);
M. Odera: ibid., 7, 140 (1973);
T. Tonuma, F. Yoshida, and M. Odera: ibid., 7, 147 (1973); ibid., 7, 149 (1973); Reports I.P.C.R., (in Japanese), 51, 53 (1975).

12-5. Effect of Misalignment of Focusing Elements on Beam Acceptance

T. Tonuma, F. Yoshida, and M. Odera

Beam trajectory was computed for various misalignments and probable manufacturing errors. Figure 1 shows how the acceptance diagrams in the transversal phase space will change when the magnetic axis of focusing elements deviates from the beam axis. Calculation was made assuming a combined error of several types such as parallel shift in x-and y-directions, tilt of axis, and rotation around the symmetry axis of magnets. The detailed explanation of the computation procedure is given in reference 1. It is found that the coincidence of axis of magnets with that of acceleration within 0.1 mm for the first cavity is sufficient to guarantee good transparency. The tolerance in the alignment can be progressively relaxed for down-stream cavities.

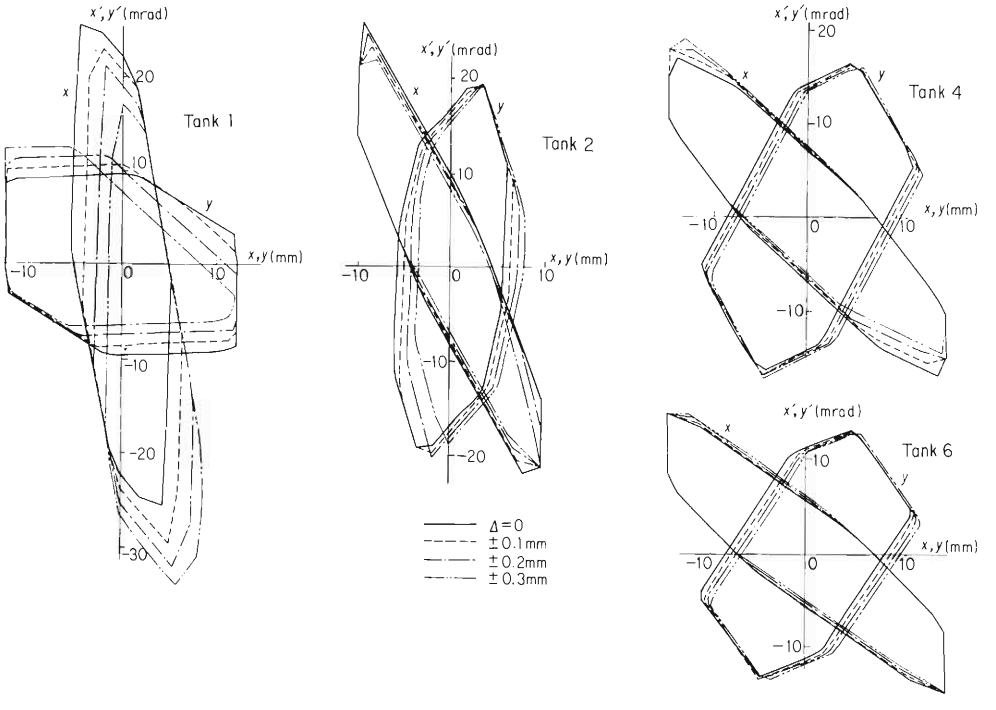

Fig. 1. Calculated beam acceptance of the cavities when the axes of focusing elements deviate from the acceleration axis. Deviations are distributed among the quadrupole elements such as to give maximum change in acceptance values.

Reference

1) T. Tonuma, F. Yoshida, and M. Odera: Reports I.P.C.R., (in Japanese), 51, 53 (1975).

12-6. Precise Measurement of the Symmetry Axis of Quadrupole Magnetic Field

I. Takeshita, I. Yokoyama, and M. Odera

For alignment of drift tubes it is required to determine to a certain allowable extent the axis of each quadrupole magnet which is to be installed in a drift tube shell. Coincidence of the axis of field with the geometical center of the tube within 50 μm is desirable in order to secure good transparency of the beam through a combination of many such quadrupoles. Centering apparatus for this purpose was devised and constructed using a Hall-effect probe. By rotating the probe by 180 degrees around the axis of symmetry, exactly the same voltage would be observed from the Hall element if the axis of rotation coincides with the axis of the magnetic field.

Figure 1 is a photograph of the apparatus. A magnet to be measured is fixed on a turn-table, which is an accessory of an instrument-microscope and is provided with a two-dimensional fine positioning mechanism to bring an object on the table in the center of the microscope field. The mechanism is useful for determination of center of the magnet. In addition, a guide is provided on the table to make the center of the magnet automatically coincide closely with the axis of rotation of the table. Temperature of the Hall element was kept constant by attaching a thermister on the back of the element which controls a heater to warm air flowing around the probe. Figure 2 shows the circuit for measurement.

Reproducibility of reading of Hall voltage was found satisfactory and the center of field

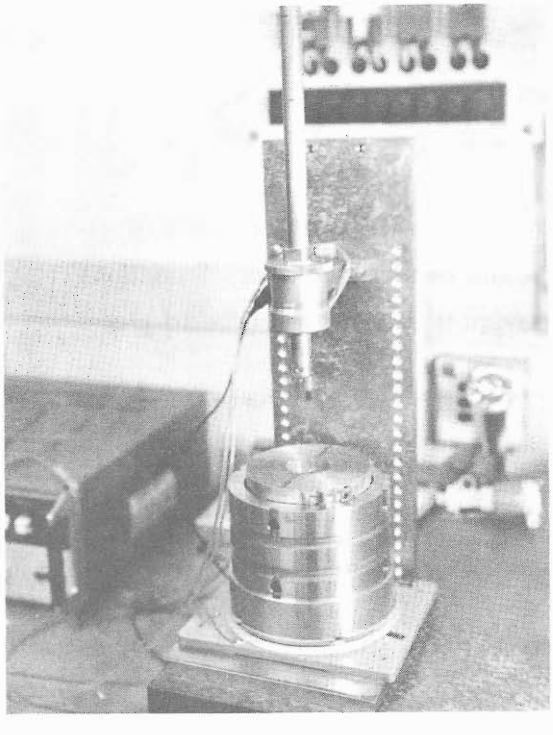

Fig. 1. Photograph of the magnetic-field centering apparatus.

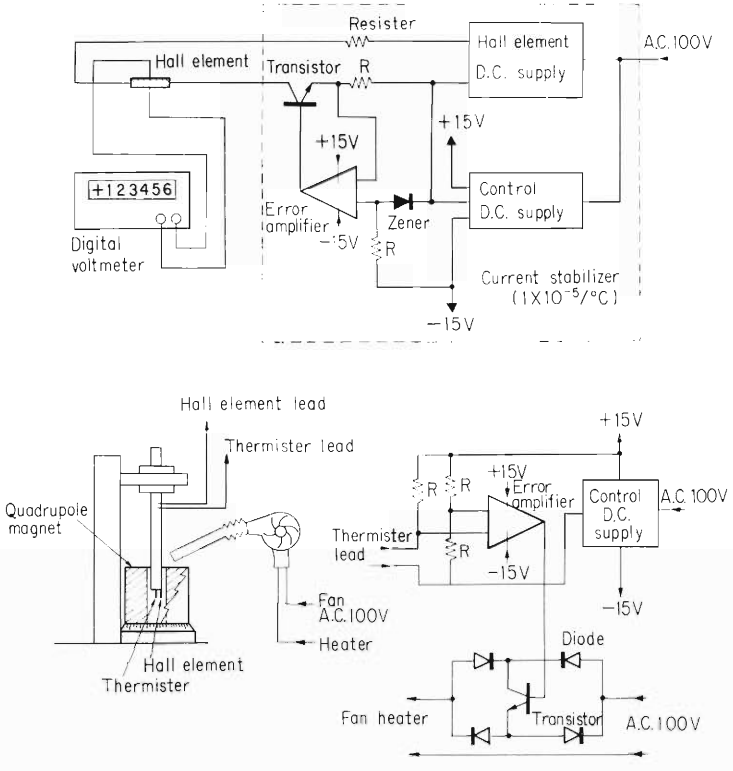

Fig. 2. Block diagram of measuring circuit.

can be determined within a few μm by a suitable conversion procedure. By the magnet shown in Fig. 1 the deviation of the field center from that of geometrical symmetry was 9 μm in x- and 4 μm in y-directions. This deviation can be attributed to the remanent field effect caused by a slight asymmetry in the magnetic property of some poles. The difference is less than the earth's magnetism. Such a small asymmetry may be generated by the difference of mechanical stress that each pole has experienced during machining, or by the difference in stress of bolts which fix poles to the yoke of magnet. Since measurements were made at a low field strength, the effect of remanent field seems more manifest than would be in the real use. The field of 5 kG is expected in the real use, and the strength at the radius where the probe is placed in the present measurements was 500 G.

13. LIST OF PUBLICATIONS

1) T. Tonuma, F. Yoshida, and M. Odera: "Beam Dynamics of the RIKEN Heavy Ion Linear Accelarator", Reports I.P.C.R., (in Japanese), 51, 53 (1975).
2) H. Kumagai, M. Okano, and A. Hashizume: "A Simple Data Recorder and Its Applications to the Radiation Measurement", Reports I.P.C.R., (in Japanese), 51, 120 (1975).
3) B. Imanishi, H. Onishi, and O. Tanimura: "The Multi-Step Effects in the $^{16}O - {}^{17}O$ Elastic and Inelastic Core-Exchange Scattering", Phys. Lett., 57B, 309 (1975).
4) T. Nomura, K. Hiruta, M. Yoshie, H. Ikezoe, T. Fukuda, and O. Hashimoto: "In-beam α- and γ-ray Spectroscopy for ^{216}Ra", Phys. Lett., 58B, 273 (1975).
5) T. Motobayashi, I. Yamane, Y. Nogami, N. Takahashi, M. Hara, K. Sagara, M. Katoh, H. Yamashita, and B. Imanishi: "Full Recoil Analysis of the Elastic Scattering of ^{16}O on ^{19}F by the Core-Exchange Model", Phys. Lett., 59B, 421 (1975)
6) W. Kutschera, B. A. Brown, H. Ikezoe, G. D. Sprouse, Y. Yamazaki, Y. Yoshida, T. Nomura, and H. Ohnuma: "Lifetimes of the 6^+ States in ^{42}Ti and ^{46}Ca and E2 Effective Charges in $(1f_{7/2})^{\pm 2}$Nuclei", Phys. Rev., C12, 813 (1975).
7) N. Bendjaballah, J. Delaunay, T. Nomura, A. Jaffrin, and H. J. Kim: "Shape Transition in the Yrast Band of ^{56}Fe", Phys. Rev. Lett., (in press).
8) N. Shiotani, T. Okada, T. Mizoguchi, and H. Sekizawa: "Angular Distribution of Positron Annihilation Radiation in Vanadium and Niobium-Experiment", J. Phys. Soc. Japan, 38, 423 (1975).
9) H. Ohnuma, S. Takeda, N. Nakanishi, S. Yamada, M. Sekiguchi, and H. Toyama: "Study of the ^{58}Ni(d, t)^{57}Ni Reaction at 24 MeV", J. Phys. Soc. Japan, 38, 1557 (1975).
10) K. Kimura, M. Ogawa, M. Matsui, T. Karasawa, M. Imamura, Y. Tabata, and K. Oshima: "ESR Study of the Spatial Distribution of Radicals Trapped in the Heavy Ion-Irradiated n-Eicosane Single Crystal", J. Chem. Phys., 63, 1797 (1975).
11) S. Ambe and F. Ambe: "Mossvauer Emission Spectrum of ^{121}Sb after the $\bar{B}$ Decay of ^{121m}Sn in SnS_2: Nuclear Decay Synthesis of Antimony (V) Sulfide", J. Chem. Phys., 63, 4077 (1975).
12) T. Nozaki, M. Iwamoto, and T. Ido: "Yield of ^{18}F for Various Reactions from Oxygen and Neon", Intern. J. Appl. Radiat. Isotopes, 25, 339 (1974).
13) T. Nozaki, M. Furukawa, S. Kume, and R. Seki: "Production of ^{28}Mg by Triton and α-Particle Induced Reactions", Intern. J. Appl. Radiat. Isotopes, 26, 17 (1975).
14) T. Nozaki, Y. Yatsurugi, and Y. Endo: "Charged Particle Activation Analysis, Studies on Carbon, Nitrogen and Oxygen Mainly in Semiconductor Silicon", J. Radioanal. Chem., (in press).
15) F. Yatagai, T. Takahashi, and A. Matsuyama: "Inactivation of Bacterial Cells by Cyclotron Beam", J. Radiat, Res., 16, 99 (1975).

16) M. Matsui and M. Imamura: "Radiation Chemical Studies with Cyclotron Beams. IV, The Effect of Water in the Heavy-Ion Radiolysis of Liquid Acetone", Bull. Chem. Soc. Japan, 48, 2346 (1975).

17) H. Shiraishi, H. Sakairi, E. Yagi, T. Karasawa, R. R. Hasiguti, and R. Watanabe: "Growth Process of Helium Bubbles in Aluminum", Nippon Kinzoku Gakkaishi (in Japanese), 39, 233 (1975).

18) T. Kammuri and T. Kishimoto: "Boson Description of Nuclear Collective Motion (1)", Z. Physik, (in press).

19) T. Nomura: "On the Alpha Decay from the Excited State of Heavy Nuclei", Genshikaku Kenkyu, 20, 467 (1975).

20) G. B. Hagemann, R. Broda, B. Herskind, M. Ishihara, S. Ogaza, and H. Ryde: "Gamma Decay after Heavy Ion Reactions Studied by First and Higher Order Multiplicity Measurements", Nucl. Phys., A245, 166 (1975).

21) S. Kusuno and T. Wada: "Microscopic Theory for Proton, Deutron, Helion, and Alpha Scattering from Collective Levels in Doubly Even Spherical Nuclei", Sci. Papers I.P.C.R., 69, 147 (1975).

22) T. Motobayashi, I. Kohno, K. Katori, M. Yoshie, T. Ooi, and H. Kamitsubo: "Anomalous Angular Distribution in the Transition to the Sy_2 State in ^{17}O", Phys. Rev. Lett., 36, 391 (1976).

(Papers presented at meetings)

1) T. Inamura: "Lifetimes of High Spin Rotational States in ^{181}Ta", Symp. on Structure of Medium Mass Nuclei and pf-shell Nuclei, Osaka, Jan. 1975, RCNP-P-2 (1975).
2) B. Imanishi: "Coupled Channel Analysis for Elastic and Inelastic Core-Exchange Scattering", The INS-IPCR Symp. on Cluster Structure of Nuclei and Transfer Reactions Induced by Heavy-Ions, Tokyo, March (1975).
3) O. Tanimura, H. Ohnishi, and B. Imanishi: "The Coupled Channel Analysis for the Core-Exchange Scattering", The INS-IPCR Symp. on Cluster Structure of Nuclei and Transfer Reactions Induced by Heavy-Ions, Tokyo, March (1975).
4) T. Motobayashi, I. Yamane, Y. Nogami, N. Takahashi, K. Sagara, M. Mihara, M. Katoh, H. Yamashita, and B. Imanishi: "Elastic and Inelastic Scattering of ^{16}O and ^{19}F", The INS-IPCR Symp. on Cluster Structure of Nuclei and Transfer Reactions Induced by Heavy-Ions, Tokyo, March (1975).
5) B. Imanishi, H. Ohnishi, and O. Tanimura: "The Multi-Step Effects in the ^{16}O–^{17}O Core-Exchange Elastic and Inelastic Scattering", The INS-IPCR Symp. on Cluster Structure of Nuclei and Transfer Reactions Induced by Heavy-Ions, Tokyo, March (1975).
6) K.-I. Kubo and B. Imanishi: "The Recoil Effects in the Core-Exchange Scattering of ^{16}O–^{18}O", The INS-IPCR Symp. on Cluster Structure of Nuclei and Transfer Reactions Induced by Heavy-Ions, Tokyo, March (1975).
7) T. Motobayashi, I. Kohno, S. Nakajima, M. Yoshie, K. Katori, T. Mikumo, and H. Kamitsubo: "Transfer Reactions Induced by ^{14}N on ^{12}C at 79 MeV", The INS-IPCR Symp. on Cluster Structure of Nuclei and Transfer Reactions Induced by Heavy Ions, Tokyo, March (1975).
8) T. Motobayashi: "Elastic and Inelastic Scattering of ^{16}O on ^{19}F", The INS-IPCR Symp. on Cluster Structure of Nuclei and Transfer Reactions Induced by Heavy Ions, Tokyo, March (1975).
9) T. Suzuki, T. Matsuura, and K.-I. Kubo: "The DWIA Analysis of ^{20}Ne$(\alpha, 2\alpha)^{16}$O Reactions at E_α = 78.6 MeV", The INS-IPCR Symp. on Cluster Structure of Nuclei and Transfer Reactions Induced by Heavy Ions, Tokyo, March (1975).
10) T. Matsuura, K.-I. Kubo, A. Arima, and M. Ichimura: "Do Excited Alpha-Clusters Play a Role in Four-Nucleon Transfer Reaction?", The INS-IPCR Symp. on Cluster Structure of Nuclei and Transfer Reactions Induced by Heavy Ions, Tokyo, March (1975).
11) H. Kamitsubo: "Optimum Q-valves in the Multinucleon Transfer Reactions and Determination of the Moment of Inertias", The INS-IPCR Symp. on Cluster Structure of Nuclei and Transfer Reactions Induced by Heavy-Ions, Tokyo, March (1975).
12) S. Nakajima, I. Kohno, M. Yoshie, K. Katori, T. Mikumo, T. Motobayashi, and H. Kamitsubo: "DWBA Analysis of the Single Proton Transfer Reactions Induced by Heavy Ions on the f-p Nuclei", The INS-IPCR Symp. on Cluster Structure of Nuclei and Transfer Reactions Induced by Heavy Ions, Tokyo, March (1975).

13) T. Kammuri and T. Wada: "Folding Model for the Nucleus-Nucleus Interaction", The INS-IPCR Symp. on Cluster Structure of Nuclei and Transfer Reactions Induced by Heavy Ions, Tokyo, March (1975).

14) T. Kammuri, H. Yoshida, and S. Yamaji: "Sequential Process in the Two-Nucleon Transfer between Heavy Ions-Numerical Analysis", The INS-IPCR Symp. on Cluster Structure of Nuclei and Transfer Reactions Induced by Heavy-Ions, Tokyo, March (1975).

15) S. Ambe and F. Ambe: "^{121}Sb-Mössbauer Emission Spectrum of $^{121m}Sns_2$", 32th Ann. Meeting of the Chem. Soc. of Japan, Tokyo, April (1975).

16) T. Inamura: "Nuclear Lifetimes of the Recoils", 30th Ann. Meeting of Phys. Soc. of Japan, Kyoto, April (1975).

17) A. Hashizume, Y. Tendow, T. Katou, and H. Kumagai: "The Cross Sections to Produce ^{88m}Y and ^{90m}Nb via ^{89}Y + α Reaction", 30th Ann. Meeting of Phys. Soc. of Japan, Kyoto, April (1975).

18) M. Yambe, M. Hirasawa, M. Fujioka, M. Oshima, J. Katakura, S. Hayashibe, and T. Ishimatsu: "The Decay of ^{119m}Te", 30th Ann. Meeting of Phys. Soc. of Japan, Kyoto, April (1975).

19) A. Koyama, E. Yagi, and H. Sakairi: "Secondary Electron Emission from Al and Ni by Fast-Proton and α-Particle Bombardment", Ann. Meeting of the Japan Soc. of Appl. Phys. Narashino, April (1975).

20) F. Yatagai, J. Ohi, K. Suzuki, T. Takahashi, and A. Matsuyama: "LET Dependence of Inactivation of Bacterial Cells with Different DNA Repair Capacity", Ann. Meeting of Agr. Chem. Soc. of Japan, Sapporo, July (1975).

21) S. Motonaga, T. Fujisawa, M. Hemmi, H. Takebe, K. Ikegami, and Y. Yamazaki: "Performance of the IPCR Polarized Ion Source", 4th Int. Symp. on Polarization Phonomena in Nuclear Reactions, Zurich, Aug. (1975).

22) T. Fujisawa, H. Kamitsubo, T. Wada, M. Koike, Y. Tagishi, and T. Kanai: "Angular Correlation Measurement for ^{13}C(^{3}He, α)^{12}C (4.43 MeV) Reaction", 4th Int. Symp. on Polarization Phenomena in Nuclear Reactions, Zurich, Aug. (1975).

23) T. Takemasa: "Exact Finite-Range DWBA Calculations for the Reaction ^{60}Ni(^{18}O, ^{16}O)^{62}Ni$_{g.s.}$", Ann. Meeting of Phys. Soc. of Japan Hirosaki, Sept. (1975).

24) T. Ooi, T. Motobayashi, I. Kohno, M. Ishihara, T. Numao, T. Fukuda, and S. M. Lee: "Role of Critical Angular Momentum in the ^{12}C(^{14}N, ^{6}Li)^{20}Ne Reaction", Ann. Meeting of Phys. Soc. of Japan, Hirosaki, Sept. (1975).

25) F. Kakimoto, N. Nakanishi, and H. Ohnuma: "^{24}Mg(d, p)^{25}Mg at $E_d \sim 21$ MeV," Ann. Meeting of Phys. Soc. of Japan, Hirosaki, Sept. (1975).

26) H. Sakairi, E. Yagi, A. Koyama, T. Karasawa, and R. R. Hasiguti: "Cyclotron Irradiation Damage in Copper and Copper Alloys", U.S.-Japan Seminar on Radiation-Produced Defects and Defects Clusters and Their Effects in Metals, Aimes, Sept. (1975).

27) K. Matsumoto, T. Kataoka, M. Terasawa, M. Shimada, S. Nakahigashi, H. Sakairi, and E. Yagi: "Embrittlement of Austenitic Stainless Steel Irradiated with α-Particles", U.S.–Japan

Seminar on Radiation-Produced Defects and Defects Clusters and Their Effects in Metals, Aimes, Sept. (1975).

28) N. Bendjaballah, J. Delaunay, and T. Nomura: "The Quasi-Band Structure in ^{57}Co", Symp. on Nuclear Structure, Balatonfürrd, Sept. (1975).

29) T. Nomura, T. Fukuda, K. Hiruta, and W. Kutschera: "Complete Determination of the Nuclear Alignment of the 8^+ State in ^{216}Ra Populated in the ^{207}Pb(^{12}C, 3n) Reaction", Symp. on Highly Excited States in Nuclei, Jülich, Sept. (1975).

30) T. Tonuma and M. Odera: "Orbit Analysis of the Riken Heavy Ion Linear Accelerator", Ann. Meeting of Phys. Soc. of Japan, Hirosaki, Sept. (1975).

31) H. Sakairi, E. Yagi, A. Koyama, T. Karasawa, and R. R. Hasiguti: "Cyclotron Irradiation of Cu_3Au Alloys at Low Temperature", Int. Conf. on Fundamental Aspects of Radiation Damage in Metals, Gatlinberg, Oct. (1975).

32) T. Nozaki: "Charged Particle Activation Analysis. Studies on Carbon, Nitrogen and Oxygen Mainly in Semiconductor Silicon", Int. Nucl. and Atomic Activ. Anal. Conf., Gatlinburg, USA, Oct. (1975).

33) F. Ambe and S. Ambe: "Mössbauer Spectroscopic Studies of Recoil ^{119}Sb and ^{119m}Te Atoms in SnSb and SnTe", 19th Symp. on Radiochem., Fukuoka, Oct. (1975)

34) M. Matsui and M. Imamura: "Heavy-Ion Radiolysis of Liquid Isobutyraldehyde. Formation of Hydrocarbon by Chain Mechanism", 18th Conf. on Radiation Chem., Tokyo, Oct. (1975).

35) K. Kimura, M. Matsui, and M. Imamura: "Color Center Formation in Alkali Halides by Heavy-Ion Irradiation", 18th Conf. on Radiation Chem., Tokyo, Oct. (1975).

36) F. Yatagai, K. Takeda, K. Shiratori, T. Takahashi, and A. Matsuyama: "LET Effects on Bacterial Inactivation and Its Repair Capacity", Ann. Meeting of the Japan Radiation Research Soc., Tokyo, Oct. (1975).

37) S. Kitayama, F. Yatagai, and A. Matsuyama: "Effect of N-Ion Irradiation on DNA Synthesis in the Permeable Cells of M. Radiodurans", Ann. Meeting of Radiation Research Soc. of Japan, Tokyo, Oct. (1975).

38) T. Tonuma, F. Yoshida, and M. Odera: "Beam Dynamics of IPCR (RIKEN) Heavy Ion Linac", Int. Conf. on Heavy Ion Sources, Gatlingburg, Tennessee, Oct. (1975).

14. LIST OF PERSONNEL

Members of the Board

HAGIHARA Hitosi 萩原 仁 (Chairman)
KAMITSUBO Hiromichi 上坪宏道
NOZAKI Tadashi 野崎 正
HAMADA Tatsuji 浜田達二
NAKANE Ryohei 中根良平
ODERA Masatoshi 小寺正俊

Users Committee

HAMADA Tatsuji 浜田達二 (Chairman)
KAMITSUBO Hiromichi 上坪宏道
MATSUYAMA Akira 松山 晃
ODERA Masatoshi 小寺正俊
SEKIZAWA Hisashi 関沢 尚
IMAMURA Masashi 今村 昌
KOHNO Isao 河野 功
NOZAKI Tadashi 野崎 正
SAKAIRI Hideo 坂入英雄

Operation and Machine Maintenance Group

FUJITA Shin 藤田 新
KAGEYAMA Tadashi 影山 正
KOHNO Isao 河野 功
OGIWARA Kiyoshi 荻原 清
IKEGAMI Kumio 池上九三男
KOHARA Shigeo 小原重夫
NAKAJIMA Hisao 中嶋尚雄
TAKEBE Hideki 武部英樹

Scientific and Engineering Personnel

Cyclotron Laboratory

FUJISAWA Takashi 藤沢高志
INAMURA Takashi 稲村 卓
KAMITSUBO Hiromichi 上坪宏道
KOHNO Isao 河野 功
MOTONAGA Shoshichi 元永昭七
NAKANISHI Noriyoshi 中西紀喜
SUZUKI Toshio 鈴木敏男
YAMAJI Shuhei 山路修平**
FUJITA Jiro 藤田二郎
ISHIHARA Masayasu 石原正泰
KARASAWA Takashi 唐沢 孝
MATSUURA Toshihiko 松浦俊彦
NAKAJIMA Shunji 中島諄二
NOMURA Toru 野村 亨*
WADA Takeshi 和田 雄

(Visitors)

ICHIMURA Munetake 市村宗武 (Univ. of Tokyo)
FUJINO Takeo 藤野武夫 (Univ. of Tokyo)
HANAZONO Sakae 花園 栄 (Univ. of Tokyo)
HIRUTA Kotaro 蛭田幸太郎 (Tokyo Inst. Tech.)
IMANISHI Bunryu 今西文竜 (Nihon Univ.)
KAMMURI Tetsuo 冠 哲夫 (Univ. of Osaka)
KATORI Kenji 鹿取謙二 (Tokyo Univ. of Educ.)
KAWAI Mitsuji 河合光路 (Tokyo Inst. Tech.)
KOIKE Masahiro 小池正宏 (Univ. of Tokyo)
MIKUMO Takashi 三雲 昂 (Tokyo Univ. of Educ.)
OHNUMA Hajime 大沼 甫 (Univ. of Tokyo)
SAKAGUCHI Harutaka 坂口治隆 (Kyoto Univ.)

* On leave of absence to : DPHNBE, CEN Saclay, B.P. 2, 91190 Gif/Yvette, France
** On leave of absence to : Institut für Theoretische Physik der Universität Frankfurt/M 6 Frankfurt/M.I, Robert-Mayer-Strasse 8-10, West Germany.

TAKEMASA Tadashi 武政尹士 (Univ. of Osaka)
WAKAI Masamichi 若井正道 (Univ. of Osaka)
YOSHIDA Hiroshi 吉田 弘 (Tokyo Inst. Tech.)
YOSHIE Morio 吉江森男 (Tokyo Univ. of Educ.)

Linac Laboratory (Electronics Laboratory)

CHIBA Yoshiaki 千葉好明
INOUE Toshihiko 井上敏彦
ODERA Masatoshi 小寺正俊
TONUMA Tadao 戸沼正雄
HEMMI Masatake 逸見政武
MIYAZAWA Yoshitoshi 宮沢佳敏
SHIMAMURA Akira 島村 曼
YOSHIDA Fusako 吉田房子

(Students)

FUKUDA Tomokazu 福田共和 (Univ. of Tokyo)
MOTOBAYASHI Tohru 本林 透 (Univ. of Tokyo)
NUMAO Toshio 沼尾登志男 (Univ. of Tokyo)
OOI Takao 大井孝雄 (Tokyo Univ. of Educ.)
TANAKA Koichiro 田中耕一郎 (Univ. of Tokyo)

Radiation Laboratory

AWAYA Yohko 粟屋容子
HASHIZUME Akira 橋爪 朗
KATOU Takeo 加藤武雄
KUMAGAI Hidekazu 熊谷秀和
TAKAHASHI Tan 高橋 旦
HAMADA Tatsuji 浜田達二
IZUMO Koichi 出雲光一
KONNO Satoshi 金野 智
OKANO Masaharu 岡野真治
TENDOW Yoshihiko 天道芳彦

(Visitors)

DOKE Tadayoshi 道家忠義 (Waseda Univ.)
FUJIOKA Manabu 藤岡 学 (Tohoku Univ.)
HAYASHIBE Shogo 林部昭吾 (Tohoku Univ.)
IIO Masahiro 飯尾正宏 (Tokyo Metropol. Jeriatric Hosp.)
NAGAHARA Teruaki 永原照明 (Rikkyo Univ.)
SUZUKI Kazuaki 鈴木一明 (Japan Anal. Chem. Res. Inst.)

Nuclear Analytical Chemistry Laboratory

AMBE Fumitoshi 安部文敏
ARATANI Michi 荒谷美智
IWAMOTO Masako 岩本正子
SAITO Nobufusa 斎藤信房
AMBE Shizuko 安部静子
ITO Yoshiko 伊東芳子
NOZAKI Tadashi 野崎 正

(Visitors)

FUKUSHI Kiyoshi 福士 清 (Nat. Inst. of Radiological Sciences)
HARA Toshihiko 原 敏彦 (Nat. Nakano Chest Hosp.)
IDO Tatsuo 井戸達雄 (Nat. Inst. of Radiological Sciences)
KASIDA Yoshihiko 樫田義彦 (Nat. Inst. of Radiological Sciences)
TAKI Koh 滝 幸 (Kitazato Univ.)
YATSURUGI Yoshifumi 八剣吉文 (Komatsu Electronic Metals Co., Ltd.)

Synthetic Organic Chemistry Laboratory

OSAWA Tomihiko 大沢富彦

Radiobiology Laboratory

KITAYAMA Shigeru 北山 滋
MATSUYAMA Akira 松山 晃
YATAGAI Fumio 谷田貝文夫

Radiation Chemistry Laboratory

IMAMURA Masashi 今村 昌
KIMURA Kazuie 木村一宇
MATSUI Masao 松井正夫

Metal Physics Laboratory

KOYAMA Akio 小山昭雄
SAKAIRI Hideo 坂入英雄
SHIOTANI Nobuhiro 塩谷亘弘
YAGI Eiichi 八木栄一

Magnetic Materials Laboratory

OKADA Takuya 岡田卓也
SEKIZAWA Hisashi 関沢 尚

(Visitor)

MIZOGUCHI Tadashi 溝口 正 (Gakushuin Univ.)

Work Shop

TAKESHITA Isao 竹下勇夫
YOKOYAMA Ichiro 横山一郎

Radiation Monitoring and Safety Office

IGARASHI Kazui 五十嵐一戊
KODA Kugao 甲田陸男
SAKAMOTO Ichiro 坂本一郎
USUBA Isao 薄葉 勲

15. LIST OF OUTSIDE USERS AND THEIR THEMES

(Jan. – Dec. 1975)

1) M. Nakamura, Kyushu Univ.
"Production of ^{43}Kr for Heart Scanning"

2) Y. Homma, Tokyo Metropolitan Univ.
"Production of ^{61}Cu, ^{123}I and ^{123}I"

3) K. Shiraishi, A. Hishinuma, and K. Kazuho, Japan Atomic Energy Research Inst.
"Radiation Damage of Stainless Steel by Alpha Particles"

4) T. Katou, S. Kawasaki, and T. Furuta, Japan Atomic Energy Research Inst.
"Study of Effect of Helium Bubbles on the Mechanical Behavior of Stainless Steel"

5) M. Terasawa, M. Shimada, and M. Iimura, Toshiba R. & D. Center
"Cyclotron Irradiation for Study of FBR Material Embrittlment"

6) A. Furusawa and S. Tamaki, Niigata Univ.
"Production of ^{124}I for Perturbed Angular Correlation Measurement"

7) S. Shikata, Kyushu Univ.
"Production of ^{53}Mn"

8) K. Komura, M. Sakamoto,* and A. Ando,** Inst. for Nuclear Study, Tokyo Univ., *Kanazawa Univ., and **Junior College of Medical Technology
"Production of ^{167}Tm for Medical Use"

9) I. Kuze, Japan Radioisotope Association
"Production of ^{56}Co."

10) H. Nakahara and M. Yanokura, Tokyo Metropolitan Univ.
"Measurement of the Excitation Function for ^{121}Sb (^{3}He, α) ^{122}Sb and ^{123}Sb(α, ^{3}He)^{122}Sb Reactions"

11) T. Furusawa, M. Hishinuma, and K. Fukai, Japan Atomic Research Inst.
"Study of Stainless Steel Swelling by Helium Injection"

12) Y. Murakami and Y. Homma, Tokyo Metropolitan Univ.
"Production of ^{61}Co"

13) Y. Murakami, E. Shirai, and M. Unno, Tokyo Metropolitan Univ.
"Production of ^{61}Cu, ^{67}Ga, and ^{68}Ge"

14) M. Honda, O. Nitou, and R. Genshou, Inst. for Solid State Physics, Tokyo Univ.
"Production of Mg Isotopes"

15) K. Shiraishi, A. Hishinuma, and K. Fukai, Japan Atomic Research Inst.
"Helium Effect on the Formation of Void in SUS316 by Electron Bombardment"

16) H. Nakahara, Tokyo Metropolitan Univ.
"Study of Direct Process in the Nuclear Reaction"

AUTHOR INDEX

IPCR Cyclotron Progress Report

理化学研究所サイクロトロン年次報告 第9巻(1975)

印　刷　昭和51年（1976）3月25日
発　行　昭和51年（1976）3月30日
発行者　理化学研究所
代表者　福　井　伸　二
〒351　埼玉県和光市広沢2番1号
電話（0484）62－1111
編集者　理化学研究所サイクロトロン運営委員会
委員長　浜　田　達　二
印刷所　丸　星　印　刷　株　式　会　社
〒101　東京都千代田区神田神保町1丁目42番地

定価 3,000円

理化学研究所

埼玉県　和光市　広沢